in collaboration with

Nuclear Energy Research Initiative
Project 01-124

Reactor Physics and Criticality Benchmark Evaluations for Advanced Nuclear Fuel

Final Technical Report

September 10, 2008

Prepared for the U.S. Department of Energy
Under the Idaho Operations Office
Contract DE-FG07-01SF22330

Record of Revisions

Revision	Date	Page/Sections Changed	Brief Description
000	September 2008	N/A	Initial Release

Table of Contents

List of Tables

List of Figures

Executive Summary

The nuclear industry interest in advanced fuel and reactor design often drives towards fuel with uranium enrichments greater than 5 wt% ^{235}U. Unfortunately, little data exists, in the form of reactor physics and criticality benchmarks, for uranium enrichments ranging between 5 and 10 wt% ^{235}U. The primary purpose of this project is to provide benchmarks for fuel similar to what may be required for advanced light water reactors (LWRs). These experiments will ultimately provide additional information for application to the criticality-safety bases for commercial fuel facilities handling greater than 5 wt% ^{235}U fuel.

Because these experiments are designed primarily to be reactor physics benchmarks, and not just criticality benchmarks, it is desired to include measurements of critical boron concentration, relative pin powers, relative assembly flux, burnable absorber worth, and isothermal temperature coefficients, for each configuration. Guidelines for developing an appropriate experimental configuration include bounding current pressurized water and boiling water reactor (PWR and BWR, respectively) fuel-to-water and metal-to-water ratios and maintaining consistency between experiment geometry and current PWR and BWR analysis tools used for reload designs (e.g., CASMO/SIMULATE).

To demonstrate the ability of computer codes to handle the geometry and spectrum of the experiments, various codes are used to calculate k_{eff} of the materials and critical boron concentration for the proposed experiments. Comparison of the isotopic compositions demonstrates good agreement. For the most part, the significance of the variations was observed to be minimal by comparing the k_{inf} values calculated for the assemblies. Comparison of the calculated critical boron concentrations indicates reasonable agreement between the NEMO, KENO and MCNP calculations, but the SIMULATE calculations for the smaller pitch case resulted in significantly lower predicted boron concentrations.

Due to the nature of the nodal methodology, it was expected that the nodal codes, NEMO and SIMULATE, might exhibit difficulties with the small core configurations. NEMO uses reflector data generated by APOLLO2-F. The reflector methodology used in APOLLO2-F is more rigorous than that used in CASMO3. This may explain why NEMO appears to produce results more in-line with KENO and MCNP than those produced by SIMULATE.

The S/U analysis of the proposed experiment designs found that the experiments would serve as excellent benchmarks for the low temperature configurations of the design systems studied. However, they would provide little data for the validation of codes at reactor operating conditions. The experiments will provide

reasonable benchmarks for commercial assembly configurations containing soluble boron and for ^{235}U capture. With the limitations placed on this experiment design, such as fuel enrichment and dimensions, amount of fuel pellets, finite size open core tank and symmetric arrays, the series is likely as close to commercial assemblies as can be achieved.

The fuel cycle evaluation discussed in Section 5 indicates that increasing enrichments to 10.0-wt% ^{235}U is a viable option for most of today's equipment. The economic model indicates that there is little incentive for plants using an 18-month cycle to increase enrichments. For the base case models, the 24-month cycle is the most competitive. Up to 6.5-wt% is an economically attractive option for the 24-month cycle with interest rates up to 9.5%.

1. Introduction

The nuclear industry interest in advanced fuel and reactor design often drives towards fuel with uranium enrichments greater than 5 wt% ^{235}U. Unfortunately, little data exists, in the form of reactor physics and criticality benchmarks, for uranium enrichments ranging between 5 and 10 wt% ^{235}U. The primary purpose of this project is to provide benchmarks for fuel similar to what may be required for advanced light water reactors (LWRs). These experiments will ultimately provide additional information for application to the criticality-safety bases for commercial fuel facilities handling greater than 5 wt% ^{235}U fuel.

Because these experiments are designed primarily to be reactor physics benchmarks, and not just criticality benchmarks, it is desired to include measurements of critical boron concentration, relative pin powers, relative assembly flux, burnable absorber worth, and isothermal temperature coefficients, for each configuration. Guidelines for developing an appropriate experimental configuration include bounding current pressurized water and boiling water reactor (PWR and BWR, respectively) fuel-to-water and metal-to-water ratios and maintaining consistency between experiment geometry and current PWR and BWR analysis tools used for reload designs (e.g., CASMO/SIMULATE).

1.1 Objective

The objective of the NERI project is to design, perform, and analyze critical benchmark experiments for validating reactor physics methods and models for fuel enrichments greater than 5-wt% ^{235}U. The proposed experiments are designed as reactor physics benchmarks, to include measurements of critical boron concentration, burnable absorber worth, relative pin powers, and relative average powers, and to provide additional information for application to the criticality-safety bases for commercial fuel facilities handling greater than 5-wt% ^{235}U fuel.

To demonstrate the ability of the computer codes to handle the geometry and spectrum of the experiments, the codes are used to calculate k_{inf} of the materials and critical boron concentration for the experiments. The calculated parameters and calculated number densities are compared to evaluate the effectiveness of the computer codes on a code-to-code basis. These comparisons are documented in subsequent sections.

1.2 Background

This project began in September of 2001. Phase 1, which included the period of time from September 1, 2001 through August 31, 2002, focused primarily on designing the experiments using available fuel, preparing the necessary plans, procedures and authorization basis for performing the experiments, and preparing for the transportation, receipt, and storage of the unirradiated Pathfinder fuel formerly stored at the Pennsylvania State University (PSU).

In Phase 1, the project team designed the proposed experiments and prepared the safety authorization to perform these experiments at the criticals facility. The proposed experiments were documented in September of 2002. These were the basis for the initial evaluation and as-built design for the program.

Work in Phase 1 also included the development and submittal of a license application for a shipping package in support of the transportation of fuel. On February 10, 2003, the Nuclear Regulatory Commission (NRC) issued the WE-1 Shipping Container Safety Evaluation Report and Certificate of Compliance.[1]

Phase 2, September 1, 2002 through August 31, 2003, began the manufacturing and application phase. This phase focused primarily on the actual experiments. The tasks addressed in Phase 2 included analyzing the proposed experiments using current industry computer codes and shipping the fuel. A code-to-code comparison report analyzing the proposed experiments was issued in February 2003 and was included in the project's Quarterly Status Report for Quarter 6.

Phase 3 involved transporting the fuel, downloading the fuel from the existing elements, reinserting the fuel into aluminum cladding for use in the experiments, and installing hardware for the experiments. The final Pathfinder Fuel shipment was completed on November 21, 2003. A total of ten shipments were necessary to move the entire inventory of Pathfinder fuel.

From the downloaded Pathfinder Fuel, the project fabricated 2,200 fuel rods. That same year, the project completed procurement of all of the experiment hardware and mated the new hardware with the existing critical assembly. The project also developed all of the necessary procedures and completed all of the reactor operator training, in preparation for the actual experimental program.

In 2005, the team procured assays of samples from the Pathfinder fuel inventory. These assays helped to quantify the isotopics, impurities, and their uncertainties in the Pathfinder fuel. Ten samples were shipped to a laboratory for analysis using a high-resolution, inductively coupled plasma mass spectroscopy process. The analysis team incorporated the results of these assays, along with as-built dimensions, into the preliminary computer models. Using these revised models, the team completed calculations of the proposed experiments. These calculations are discussed later in this report.

To date, the team has yet to perform the actual experiments. Delays at the criticals facility resulted in project delays beyond the available budget. Although the project did not complete these experiments, the laboratory still plans to run these experiments under other Department of Energy funding. The results are expected to be published by the end of calendar year 2009.

1.3 Process

The project is organized into 5 tasks:

Task 1: Design the experiments and procure fuel

Task 2: Analyze the proposed experiments

Task 3: Transport and fabricate the fuel, procure and install the hardware, perform the experiments

Task 4: Analyze the actual experiments and compare calculated values of physics parameters with the measured values

Task 5: Evaluate typical fuel-processing operations to establish the limits and restrictions required for fabricating higher-enriched fuel.

Unfortunately, the team did not perform the actual experiments prior to the end of this project. For Task 4, the team did revise the physics models to reflect as-built dimensions and incorporate the results of the fuel assays. The results of these as-built calculations are documented in subsequent sections.

2. Description of Experiments

This series of experiments involves water-moderated, square-pitched lattices with low-enriched (6.93 wt% ^{235}U) cylindrical fuel rods. These arrays consist of fully-flooded, uniform lattices of aluminum-clad fuel rods in an aluminum tank. Figure 2-1 shows the layout of the experiment hardware. However, the lattice shown in the figure is a triangular pitch lattice. The proposed NERI array is a 3x3 array of 15x15, square-pitched, fuel assemblies. Figure 2-2 shows the lattice design for these experiments.

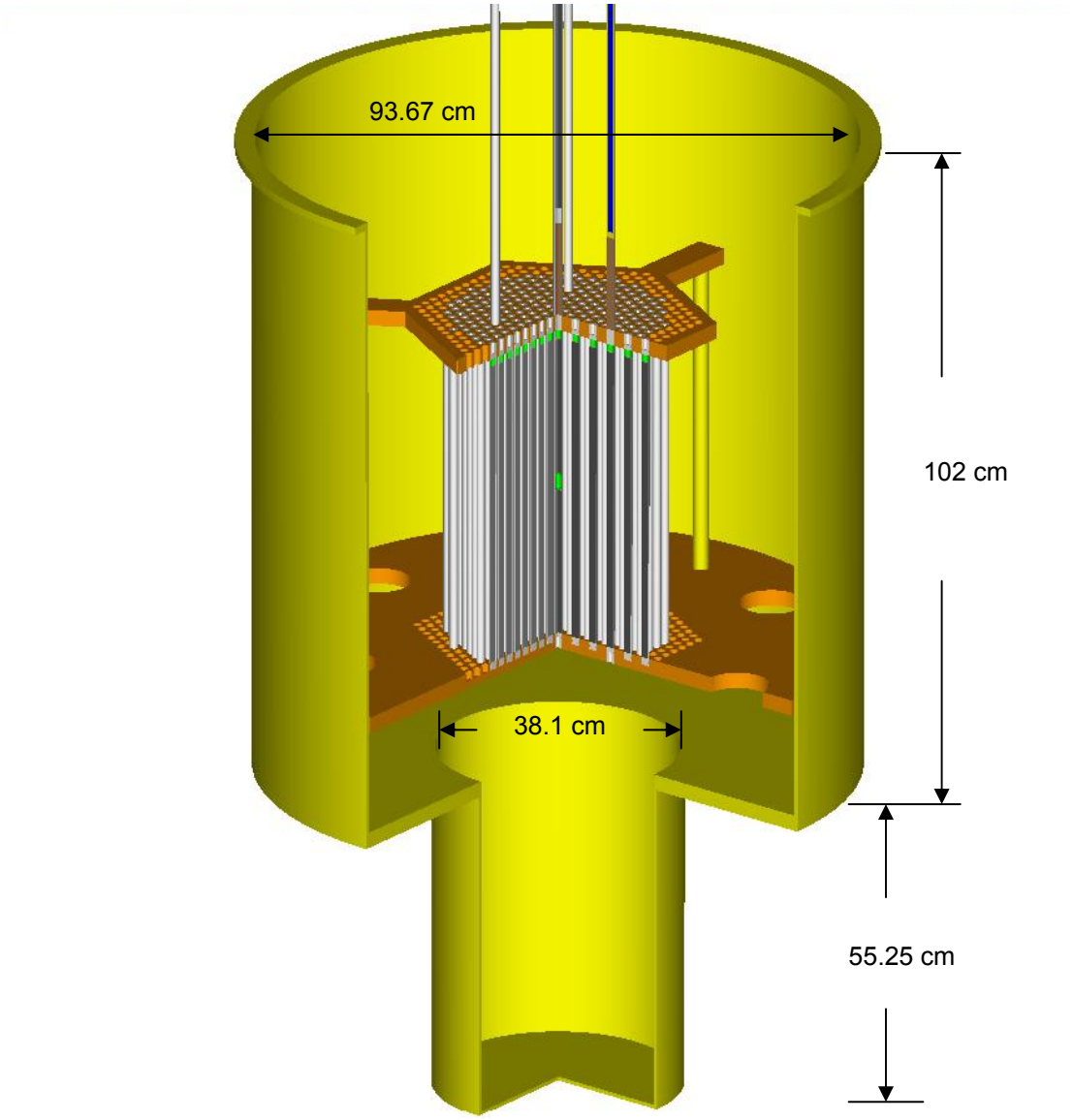

Figure 2-1: Configuration of the BUC-CX Critical Assembly with Water Tank

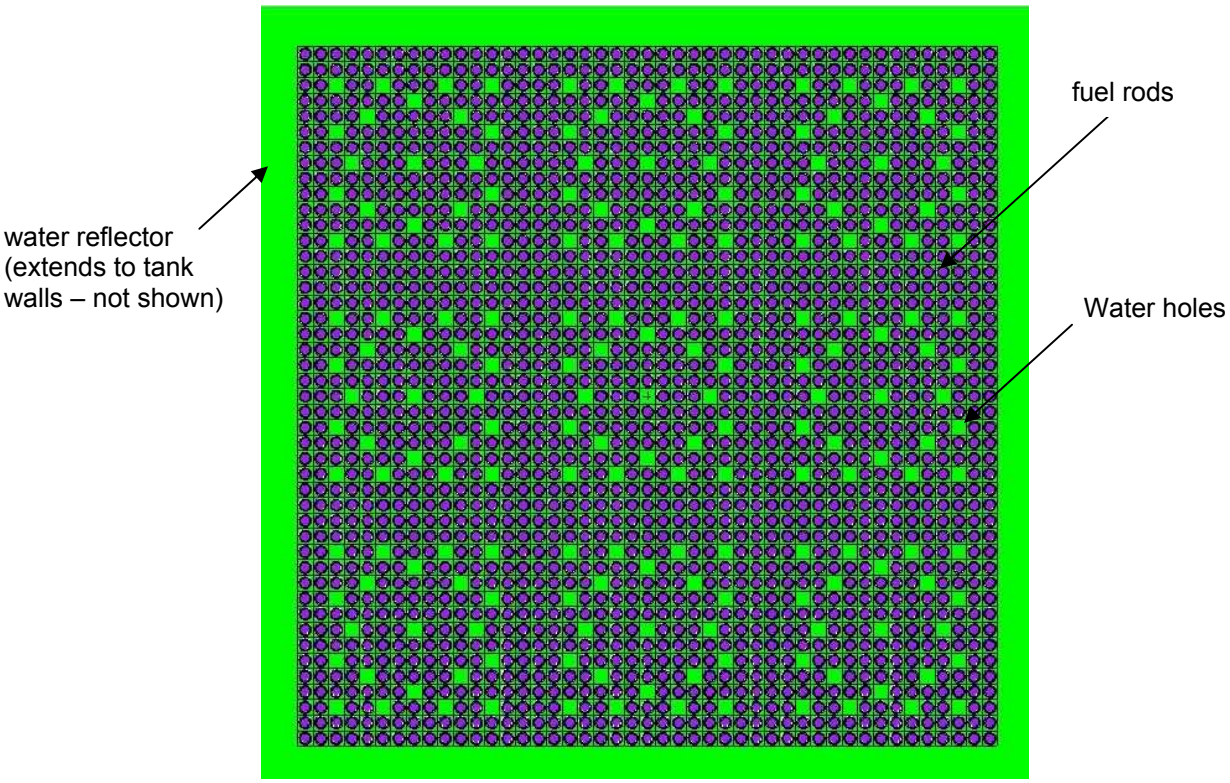

Figure 2-2: 3x3 Array of 15x15 Assemblies

2.1 Preliminary Design

The initially proposed experiments considered two pitch values and two moderator temperature values. The pitch values were chosen to "book-end" the range of water-to-fuel ratios currently found in American commercial Pressurized Water Reactors (PWRs). The temperatures were chosen based on the range of temperatures that the experimental facility can support. The low value (20 °C) is the effective ambient temperature in the facility. The high value (60 °C) is the maximum temperature that the system can sustain without modifications to the hardware.

In addition to varying the temperature and pitch, the experiments also initially included the use of integral absorber rods. This involved replacing fuel rods with UO_2-Gd_2O_3 rods. Figure 2-3 shows the proposed locations of the absorber rods.

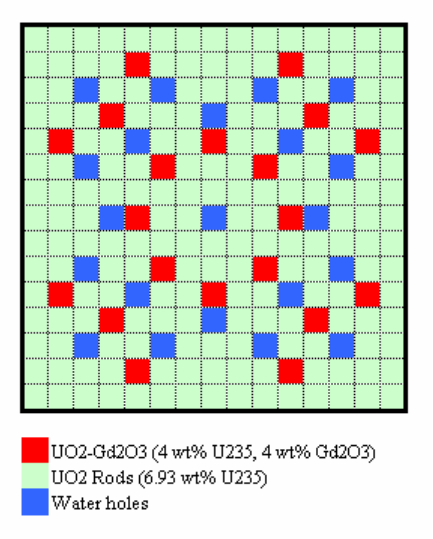

Figure 2-3: Burnable Absorber Pattern for Center Assembly.

Table 2-1 displays a list of the originally planned experiments. These are the experiments that were originally analyzed using the various reactor physics tools.

Table 2-1: Initially Proposed Experiments

Experiment	Pitch (cm)	Absorber	T_{mod} (C)
1	0.800	None	20
2	0.800	20 UO_2-Gd_2O_3 rods	20
3	0.800	None	60
4	0.800	20 UO_2-Gd_2O_3 rods	60
5	0.855	None	20
6	0.855	20 UO_2-Gd_2O_3 rods	20
7	0.855	None	60
8	0.855	20 UO_2-Gd_2O_3 rods	60

2.2 As-built Design

The final “as-built” experiments still involve water-moderated, square-pitched lattices with low-enriched (6.9 wt% ^{235}U) cylindrical fuel rods. These arrays consist of fully flooded, uniform lattices of aluminum-clad fuel rods in an aluminum tank. The proposed NERI array is a 3x3 array of 15x15, square-pitched, fuel assemblies. The hardware layout and the lattice design are also consistent with Figures 2-1 and 2-2. Consistent with the preliminary design, although the lattice shown in Figure 2-1 is a triangular pitch lattice, the actual built lattice is square pitch, as shown in Figure 2-2. Figure 2-4 displays an axial view of one assembly including the details of the fuel rods.

The as-built experiments also consider two pitch values: 0.800 cm and 0.855 cm. The pitch values are chosen to "book-end" the range of water-to-fuel ratios currently found in American commercial PWRs. However, due to the cost increases for gadolinia over the duration of this project, the gadolinia cases were dropped from the final experiment list. Also, in an attempt to keep this program cost-effective, the higher temperature experiments were also removed from the list of planned experiments. Table 2-2 displays the list of the planned experiments. These experiments are analyzed in the following discussion of the as-built calculations.

Table 2-2: Final Planned Experiments

Pitch (cm)	Absorber	T_{mod} (C)
0.800	None	20
0.855	None	20

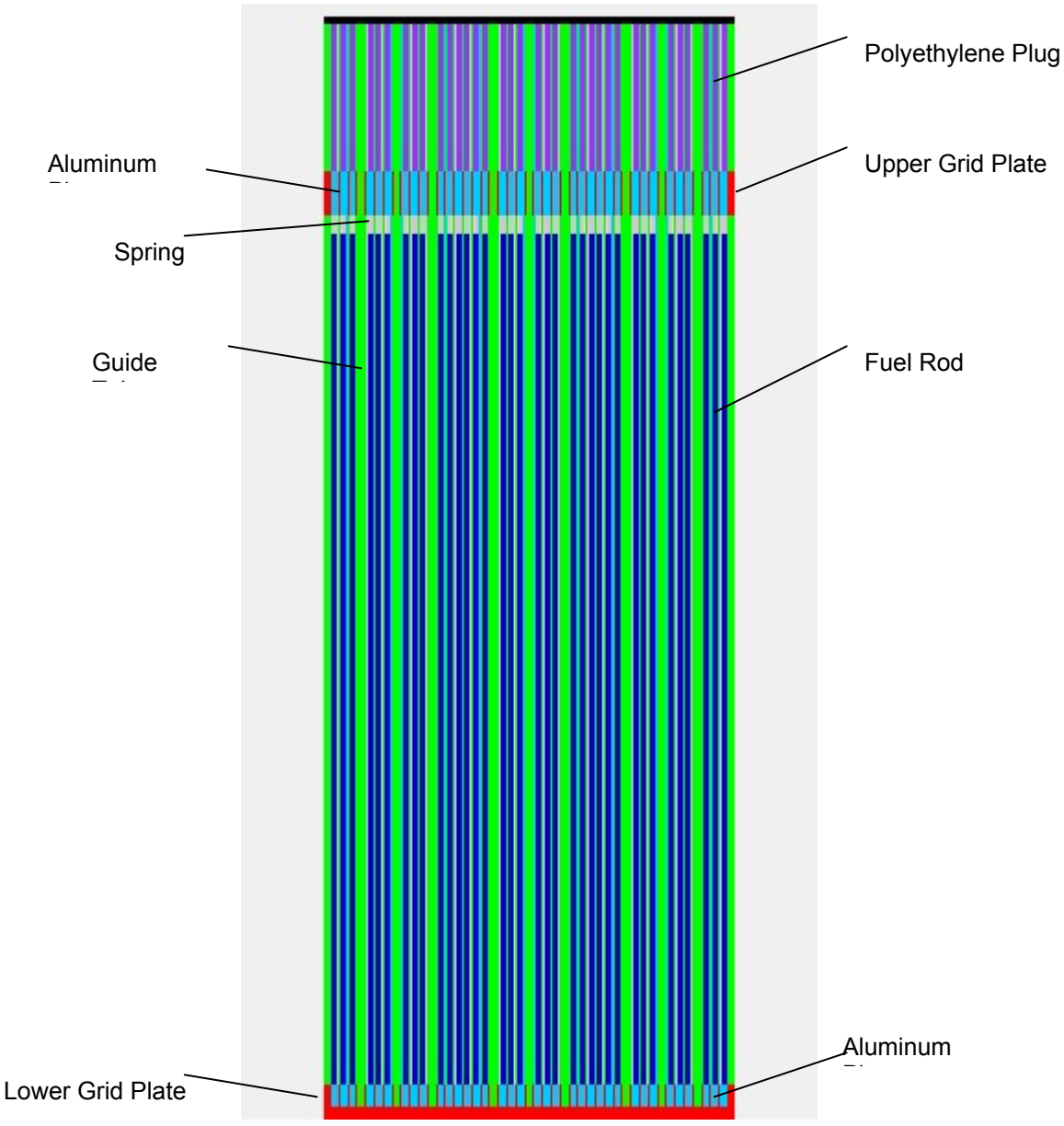

Figure 2-4: Axial View of Center Assembly

3. Analysis of Experiments

3.1 Computer Codes

Table 3-1 contains a list of the codes and cross section libraries used by the participating organizations.

Table 3-1: Analysis Tools

Analysis Tools	Cross Section Library
APOLLO2-F / NEMO	JEF-2, 99-Group
KENO V.a (CSAS25 analysis sequence)	ENDF/B-V, 238-Group (SCALE)
NEWT	ENDF/B-V, 44-Group (SCALE)
HELIOS	ENDF/B-VI, 190-Group
CASMO3 / SIMULATE-3	ENDF/B-4[1] 40-Group
MCNP	ENDF.B-VI, continuous Energy

1. CASMO3's neutron data library is based on data from ENDF/B-4, but contains some data from other sources.

APOLLO2-F, version 2.4.10 is an assembly lattice code developed by the Commissariat B l'Energie Atomique (CEA) and modified for its design needs. APOLLO2-F solves the 99-group transport equation for the assembly geometry using the discretized integral differential form based on the collision probability method. APOLLO2-F uses a heterogeneous/homogeneous equivalence calculation to obtain the homogenized, six-group cell properties used for the assembly calculation. The assembly calculations can be carried out on various geometries such as eighth assembly and quarter assembly. A sophisticated self-shielding model is applied to the cross sections to correctly account for resonances. APOLLO2-F furnishes the homogenized two-group cross section that will be used in NEMO.

NEMO is a proprietary reactor physics analysis tool. NEMO uses an optimized nodal expansion method, to calculate reactivity and power distributions for PWRs in either steady state or transient conditions. NEMO uses a two-energy group structure and employs the nodal expansion method to determine the currents and fluxes at the surface of each node in the core. Multidimensional problems

may be analyzed with thermal-hydraulic feedback and isotopic depletion. Pin power reconstruction is accomplished based on either a full assembly or an assembly quadrant.

HELIOS is a 2-D collision probability coupled neutron-gamma transport code with burnup capabilities. Scandpower, Inc developed HELIOS primarily for lattice depletion calculations. HELIOS's general 2-D geometry allows for great flexibility in defining system models. HELIOS performs resonance self-shielding calculations internally. HELIOS allows for the input of an axial buckling factor to simulate a finite height for a system. The ZENITH post processor allows for easy calculation and output of pin powers and neutron flux spectra. The AURORA viewer generates graphical representations of the 2-D system geometry.

KENO V.a is a multigroup Monte Carlo criticality program that operates within the SCALE code system. KENO V.a is used to calculate the k_{eff} and neutron flux of a 3-D system. Resonance self-shielding calculations are performed by the BONAMI-II code for the unresolved resonance region and by NITAWL-III for the resolved resonance region. A criticality analysis is performed within the SCALE code system in the CSAS25 criticality safety analysis sequence. This analysis sequence automatically generates resonance-shielded cross sections and performs the criticality analysis. The KMART utility module enables the calculation of reaction rates and the output of neutron flux spectra.

NEWT is a prototypic 2-D deterministic neutron transport code that allows for the input of arbitrary geometry and uses an automated flexible meshing scheme. NEWT was developed to operate within the SCALE code system and uses the same resonance self-shielding techniques as are used with KENO V.a. NEWT allows for the input of an axial height, which it uses to generate a geometric buckling correction to simulate a system with a finite height.

CASMO3 is a multigroup two-dimensional transport theory code for burnup calculations on boiling water reactor (BWR) and PWR assemblies or simple pin cells. The code handles a geometry consisting of cylindrical fuel rods of varying composition in a square pitch array and can model fuel rods loaded with gadolinium.

SIMULATE-3 is an advanced two-group nodal code for the analysis of BWRs and PWRs. The SIMULATE-3 data library contains two-group cross sections, microscopic cross sections, fission product data, discontinuity factors and kinetic data. This data is generated for every fuel type.

MCNP is a general-purpose Monte Carlo N-Particle code that can be used for neutron, photon, electron, or coupled neutron/photon/electron transport. This analysis uses the code's capability to calculate eigenvalues for critical systems. MCNP used point-wise cross section data. For neutrons, MCNP accounts for all

reactions given in a particular cross section evaluation. The code uses both the free gas and S(α,β) models.

3.2 Preliminary Calculations Model

3.1.1. Assumptions

For the preliminary calculations, although the conceptual design for these experiments had been finalized, a number of issues had not been resolved in regards to as-built fuel, absorbers, and measurement techniques. As a result, a number of assumptions were necessary for these calculations. The following assumptions were used consistently in all of the models for preliminary calculations.

- UO_2 Fuel Densities: 10.29 g UO_2/cm^3 (~94% TD)
- UO_2-Gd_2O_3 Fuel Densities: 10.11 g UO_2-Gd_2O_3/cm^3
- UO_2-Gd_2O_3 Weight percents: 4.0% Gd_2O_3 in UO_2-Gd_2O_3
4.0% ^{235}U in U
- Instrumentation Tube: Wet (same dimensions as the Guide Tube)

The UO_2 fuel density was based on the median value of the range provided in the fuel specification sheets. This value was later corrected on the basis of chemical assay results. However, at the time of the preliminary calculations, the fuel had not yet been shipped to the laboratory, so no confirmatory analysis was available.

The UO_2-Gd_2O_3 fuel density and weight percents were based on commercial norms. However, the actual fuel density and weight percent depends on the run that the actual material is taken from. At the time of the analysis, the material had not been procured. Therefore, the values for UO_2-Gd_2O_3 fuel density and weight percents could only be assumed at that time. Over the course of the project, it became apparent that the project did not have adequate funding to include the gadolinia cases. The analysis of the design is included here, but these were not repeated for the as-built evaluation.

The instrument tube may be wet or dry, depending upon what method of measurement for assembly power used. Because this detail had not been finalized, the instrument tube was assumed to be wet (e.g. full of water).

All of the models included these assumptions to ensure consistency.

3.1.2. General Model Parameters

Table 3-2 identifies the model parameters used consistently for all of the preliminary calculations. These parameters define the analyzed configurations. The consistent use of these values ensures a like-kind comparison between the analysts.

Table 3-2: General Model Parameters for the Preliminary Critical Configurations

Assembly Parameters	
Assembly Layout	15x 15
Pin Pitch (cm)	0.8 or 0.855
Pin radius (cm)	0.263
Clad Material	Al
Clad Internal radius (cm)	0.2815
Clad External radius (cm)	0.3175
Operation Parameters	
Number of Assemblies in Reactor	9
Cold Fuel Height (cm)	50
Fuel Temperature (°C)	20 or 60
Clad Temperature (°C)	20 or 60
Coolant Temperature at Entrance (°C)	20 or 60
Coolant Temperature at Entrance (°C)	20 or 60

3.2 As-built Calculations Model

3.2.1. Assumptions

For the as-built calculations, more actual information was available. The revised models use “as-built” dimensions provided in References 1 and material information provided by ORNL (Section 8). There were no significant assumptions necessary for these calculations.

3.2.2. General Model Parameters

Tables 3-3 and 3-4 identify the model parameters used for the as-built calculations. The parameters listed in Tables 3-3 and 3-4 define the as-built configurations analyzed. Because the tank itself is a minimum of 6 inches from the fuel, the tank was not included in the models. Therefore, these tables do not contain any tank data.

Table 3-3: Fuel Rod Parameters for the As-built Critical Configurations

Component	Dimension	SI	English
Fuel	Diameter	0.5258	0.2070
	Active Fuel Length	48.9128	19.2570
Cladding	Outside Diameter	0.635	0.250
	Inside Diameter	0.564	0.222
	Height	75.565	29.750
Top Plug	Diameter	0.635	0.250
	Height	3.106	1.223
Poly Plug	Diameter	0.526	0.207
	Height	21.2725	8.375
6061 Al Plug	Diameter	0.526	0.207
	Height	2.54	1.00
Spring	Diameter	0.4572	0.180
	Height	1.069	0.421
Bottom Plug	Diameter	0.635	0.250
	Height	1.27	0.50

Table 3-4: Hardware Parameters for the As-built Critical Configurations

Component	Dimension	SI (cm)	English (in.)
Upper Grid Plate (Square)[1]	Side Length	41.91	16.50
	Hole Diameter	0.6604	0.260
	Height	2.54	1.00
	Pitch[2]	0.800/0.855	0.3150/0.3366
Lower Grid Plate (Circular)[3]	Diameter	46.355	18.250
	Hole Diameter	0.6604	0.260
	Height	2.54	1.00
	Pitch[2]	0.800/0.855	0.3150/0.3366
Upper Tank (not modeled)	Outside Diameter	94.945	37.380
	Inside Diameter	93.675	36.880
	Height (w/o floor)	95.250	37.50
	Floor Thickness[4]	2.54	1.00
Lower Tank (not modeled)	Outside Diameter	39.37	15.50
	Inside Diameter	38.10	15.00
	Height (w/o floor)	957.705	20.750
	Floor Thickness	2.54	1.00

Notes:
1. Upper grid plate is located such that the plate aligns with the aluminum plugs in the fuel rods and the bottom of the grid plate is level with the top of the spring region.
2. Two sets of plates with different pitches are used.
3. Lower grid plate is located such that the plate aligns with the aluminum bottom end-plugs in the fuel rods and the top of the grid plate is level with the bottom of the fuel region.
4. The floor of the upper tank has a 38.10 cm (15 inch) “hole” that aligns with the inner diameter of the lower tank.

The sensitivity and uncertainty analysis performed on the preliminary experiments indicated that performing the temperatures at 60 °C provided little value added (see Section 4.4.4). In an effort to keep this program cost-effective, the original list of planned experiments was limited to only the 20 °C cases. Table 3-5 lists the operating parameters for the final planned experiments.

Table 3-5: Operation Parameters for As-built Calculations

Operation Parameter	Value
Number of Assemblies in Core	9
Fuel Temperature (°C)	20
Clad Temperature (°C)	20
Coolant Temperature at Entrance (°C)	20
Coolant Temperature at Entrance (°C)	20

In addition to adjusting the list of planned experiments and the as-built dimensions, the as-built calculations also addressed additional information available regarding the fuel. The following tables provide the results of the assay analysis of the fuel. These data presented in the tables were used in the as-built models.

Table 3-6: Fuel Enrichment

Run#	Sample ID	$^{234}U/^{238}U^{*}$	2σ	$^{235}U/^{238}U^{*}$	2σ	$^{236}U/^{238}U^{*}$	2σ
8683	13527-1	0.000308	0.000007	0.07525	0.00015	0.000688	0.000014
8686	13527-2	0.000309	0.000005	0.07521	0.00015	0.000688	0.000014
8701	13527-3	0.000309	0.000003	0.07522	0.00015	0.000687	0.000014
8704	13527-4	0.000309	0.000002	0.07511	0.00015	0.000685	0.000014
8710	13527-5	0.000308	0.000002	0.07523	0.00015	0.000687	0.000014
8713	13527-6	0.000307	0.000002	0.07515	0.00015	0.000689	0.000014
8728	13527-7	0.000307	0.000002	0.07509	0.00015	0.000686	0.000014
8731	13527-8	0.000307	0.000002	0.07516	0.00015	0.000685	0.000014
8737	13527-9	0.000307	0.000002	0.07514	0.00015	0.000686	0.000014
8740	13527-10	0.000306	0.000002	0.07519	0.00015	0.000688	0.000014
Average		0.000308		0.07518		0.000687	
Std Dev		0.000001		0.00005		0.000001	

* **Ratios represent atom ratios.**

Table 3-7: Impurities in the Fuel (Section 8)

Element	Average	Maximum	Minimum
B (ng/g)	3.76E+02	1.56E+03	2.24E+01
V (ng/g)	1.22E+02	1.56E+02	9.71E+01
Cr (ng/g)	2.11E+04	4.03E+04	1.31E+04
Mn (ng/g)	2.52E+03	4.51E+03	1.50E+03
Fe (ng/g)	9.33E+04	1.79E+05	5.27E+04
Co (ng/g)	2.06E+02	3.13E+02	1.27E+02
Ni (ng/g)	3.33E+04	5.73E+04	2.31E+04
Cu (ng/g)	1.99E+03	4.95E+03	2.26E+02
Mo (ng/g)	1.93E+03	5.19E+03	6.34E+02
Ag (ng/g)	1.47E+02	6.67E+02	2.24E+01
Cd (ng/g)	1.23E+02	9.36E+02	2.21E+01
Sm (ng/g)	2.55E+01	5.31E+01	2.21E+01
Eu (ng/g)	2.25E+01	2.27E+01	2.21E+01
Gd (ng/g)	2.25E+01	2.27E+01	2.21E+01
Dy (ng/g)	2.25E+01	2.27E+01	2.21E+01
W (ng/g)	1.07E+02	1.23E+02	8.53E+01
SAMPLE WT.	2.22E+00	2.26E+00	2.20E+00

4. Results of Analysis

The project team performed evaluations of the proposed experiments using various industry tools. In addition, the team performed a sensitivity and uncertainty analysis (S/U) using the SEN3/KENO option available in scale. The following subsections discuss the results of these evaluations.

4.1 Results of the Preliminary Calculations

For the purpose of the preliminary comparison, two basic areas were chosen: cross sections and calculated critical boron concentration. The cross sections data, which includes number densities and material k_{inf} calculations, represent the results of the cross section generation. Generation of the cross sections is the first step in the calculations. The comparisons of the number densities and k_{inf} values provide a check of an essential input into the critical boron calculations. Significant differences in the number densities or k_{inf} values would indicate that any calculated critical boron would likely be suspect.

The comparison of the critical boron calculation results is a comparison of the final results of the preliminary analysis. Assuming good agreement in the previous comparisons of the number densities and k_{inf} values, a significant systematic difference in the calculated critical boron concentration may indicate a problem in the model or the methodology.

4.1.1 Cross Sections

For comparison of the cross sections, the two parameters chosen to represent the models are material number densities and k_{inf}. Table 4-1 lists the material number densities used by each of the organizations for the preliminary calculations.

Table 4-1: Fuel Material Isotopic Compositions (given in atm/b*cm)

Fuel Type	Isotope[1]	Organization 1	Organization 2	Organization 3
UO_2	^{235}U	1.6107E-03	1.6104E-03	1.6104E-03
	^{238}U	2.1341E-02	2.1344E-02	2.1342E-02
	O	4.5938E-02	4.5931E-02	4.5928E-02
UO_2-Gd_2O_3	^{235}U	8.8140E-04	8.7679E-04	8.7675E-04
	^{238}U	2.0886E-02	2.0777E-02	2.0770E-02
	O	4.5564E-02	4.5324E-02	4.5321E-02
	^{154}Gd	2.9443E-05	2.8217E-05	2.8826E-05
	^{155}Gd	1.9988E-04	1.9887E-04	2.0184E-04
	^{156}Gd	2.7645E-04	2.7680E-04	2.7914E-04
	^{157}Gd	2.1136E-04	2.1096E-04	2.1139E-04
	^{158}Gd	3.3546E-04	3.3323E-04	3.3180E-04
	^{160}Gd	2.9522E-04	2.9292E-04	2.8801E-04

1. Only the isotopes common to all three calculations are reported. Isotopes ^{234}U, ^{236}U, and ^{152}Gd appear in at least one of the models, but they represent less than significant quantities (<2x10-5 atm/b*cm).

The isotopic compositions show good agreement, particularly for the fuel without gadolinia. The comparison of the isotopic compositions of the fuel with gadolinia does show some variation between the three models. To some degree, this is a result of inclusion of other isotopes not shown in the table, but identified in the footnote to the table. The significance of the variations shown in the table can be evaluated by comparing the k_{inf} values listed in Table 4-2.

Table 4-2: Calculated k_{inf} Values for Fuel Materials for the Preliminary Calculations

Case	APOLLO2-F	KENO V.a[1]	HELIOS	NEWT	MCNP[2]	CASMO3	Average
1	1.519	1.527	1.522	1.531	1.528	1.521	1.525
2	1.254	1.255	1.254	1.253	1.254	1.249	1.253
3	1.515	1.522	1.517	1.527	1.524	1.516	1.520
4	1.254	1.248	1.247	1.248	1.252	1.243	1.249
5	1.551	1.556	1.552	1.559	1.557	1.550	1.554
6	1.274	1.276	1.275	1.271	1.276	1.270	1.274
7	1.546	1.552	1.549	1.556	1.554	1.546	1.550
8	1.269	1.268	1.268	1.265	1.274	1.263	1.268

1. All KENO V.a results had a σ ranging between 0.00020 and 0.00025.
2. All MCNP results had a σ ranging between 0.00050 and 0.00083.

The values reported in Table 4-2 are based on an infinite array of water-moderated fuel assemblies with no boron in the water. For the "no gadolinia" cases, the results from KENO and MCNP agree exceptionally well with each other, while APOLLO2-F, HELIOS and CASMO3 show good agreement for these same cases. HELIOS and APOLLO2-F show markedly good agreement (<0.2% difference) in all cases except for case 4, for which the difference in calculated k_{inf} is 0.5%.

To further evaluate the degree of agreement amongst all of the codes, Table 4-2 includes a calculated average value of the six calculations for each case. The calculated values for each case are compared with this calculated average value, and the percent-differences are reported in Table 4-3.

Interesting points noted in reviewing the data in Table 4-3 include:

- APOLLO2-F, KENO, and HELIOS, on average, are within 0.1% of the calculated average k_{inf}, but APOLLO2-F has a much greater variation about the average value.
- APOLLO2-F, HELIOS, and CASMO3 consistently under-predicts the average value for k_{inf} for non-gadolinia cases.
- APOLLO2-F and HELIOS consistently over-predicts the average value for k_{inf} for cases that include gadolinia.
- MCNP consistently over-predicts the average value for k_{inf}
- CASMO3 consistently under-predicts the average value for k_{inf}

Table 4-3: Variance of Calculated k_{inf} Values for the Preliminary Calculations

Case	APOLLO2-F	KENO V.a[1]	HELIOS	NEWT	MCNP[2]	CASMO3
1	0.36%	-0.13%	0.18%	-0.45%	-0.22%	0.25%
2	-0.08%	-0.12%	-0.04%	-0.01%	-0.05%	0.31%
3	0.37%	-0.10%	0.18%	-0.43%	-0.27%	0.25%
4	-0.39%	0.05%	0.12%	0.08%	-0.31%	0.45%
5	0.23%	-0.11%	0.13%	-0.35%	-0.16%	0.26%
6	-0.05%	-0.16%	-0.10%	0.22%	-0.20%	0.30%
7	0.27%	-0.08%	0.12%	-0.34%	-0.23%	0.26%
8	-0.05%	-0.04%	-0.02%	0.25%	-0.51%	0.38%
Max.	0.37%	0.05%	0.18%	0.25%	-0.05%	0.45%
Min.	-0.39%	-0.16%	-0.10%	-0.45%	-0.51%	0.25%
Avg.	0.08%	-0.09%	0.07%	-0.13%	-0.24%	0.31%

The results indicate that data provided to SIMULATE from CASMO3 should result in an over-prediction the calculated boron concentration by SIMULATE, relative to the other methodologies. MCNP should under-predict the boron concentrations, relative to the other methodologies. Of course, these conclusions assume equivalent methodologies. The next step is to assess the methodologies used by the various codes for calculating critical boron concentration, in light of the relative k_{inf} presented in Table 4-2.

4.2 Critical Boron for the Preliminary Calculations

The critical boron concentrations for the preliminary designs were calculated using:

- APOLLO2-F / NEMO
- ENDF/B-V / KENO
- ENDF/B-VI / MCNP
- CASMO3 / SIMULATE

The results of these calculations are documented in Table 4-4, and plotted in Figure 4-1. The data indicates reasonable agreement between the NEMO, KENO and MCNP calculations, but the SIMULATE calculations result in considerably higher boron concentrations.

Table 4-4: Calculated Critical Boron Concentrations for the Preliminary Calculations

	Boron Concentration (ppm B)			
Case	**APOLLO2-F[1]/ NEMO**	**ENDF/B-V[2]/ KENO**	**ENDF/B-VI[3]/ MCNP**	**CASMO3[4]/ SIMULATE**
1	586	721	680	973
2	263	388	350	665
3	583	656	620	919
4	258	334	295	617
5	1059	1135	1105	1246
6	674	752	725	909
7	1056	1105	1059	1204
8	671	739	680	867

1. APOLLO2-F uses the JEF-2 cross section library.
2. KENO V.a calculations used the 238-group cross section library available in SCALE.
3. MCNP calculations used the continuous-energy cross section library available in MCNP.
4. CASMO3/SIMULATE calculations used data from the ENDF/B-4 library, modified with some data from other sources.

Due to the nature of the nodal methodology, it was expected that the nodal codes, NEMO and SIMULATE, might exhibit difficulties with the small core configurations. NEMO uses reflector data generated by APOLLO2-F. The reflector methodology used in APOLLO2-F is more rigorous than that used in CASMO3. This may explain why NEMO appears to produce results more in-line with KENO and MCNP than those produced by SIMULATE.

Consistent with the conclusion discussed under Table 4-3, CASMO3/SIMULATE over-predicted the critical boron concentrations relative to the other methodologies. However, although MCNP did under-predict the boron concentration relative to KENO, it over-predicted the boron concentrations relative to NEMO.

4.2.1 Additional Analysis

To assess the significance of the differences noted in Table 4-4, and illustrated in Figure 4-1, additional calculations were performed using the critical boron concentration calculated by KENO. The eight critical configurations were

analyzed to calculate the system k_{eff}. The results of these calculations are shown in Table 4-5.

Table 4-5: Calculated Critical Boron Concentrations for the Preliminary Calculations

Case	Boron Concentration (ppm B)	NEMO	KENO V.a[1]	NEWT	HELIOS	MCNP[2]	SIMULATE
1	721	0.988	1.000	1.009	0.954	0.996	1.024
2	388	0.987	0.998	1.010	0.949	0.995	1.031
3	656	0.994	1.001	1.013	0.953	0.996	1.026
4	334	0.992	1.000	1.011	0.947	0.997	1.033
5	1135	0.993	0.999	1.014	0.958	0.998	1.011
6	752	0.993	1.001	1.014	0.956	0.998	1.017
7	1105	0.996	0.999	1.013	0.955	0.996	1.009
8	739	0.993	0.997	1.010	0.951	0.994	1.014

1. All KENO V.a results had a σ = 0.00013, except for Case 3 with had a σ = 0.00014
2. All MCNP results had a σ ranging from 0.00072 to 0.00078.

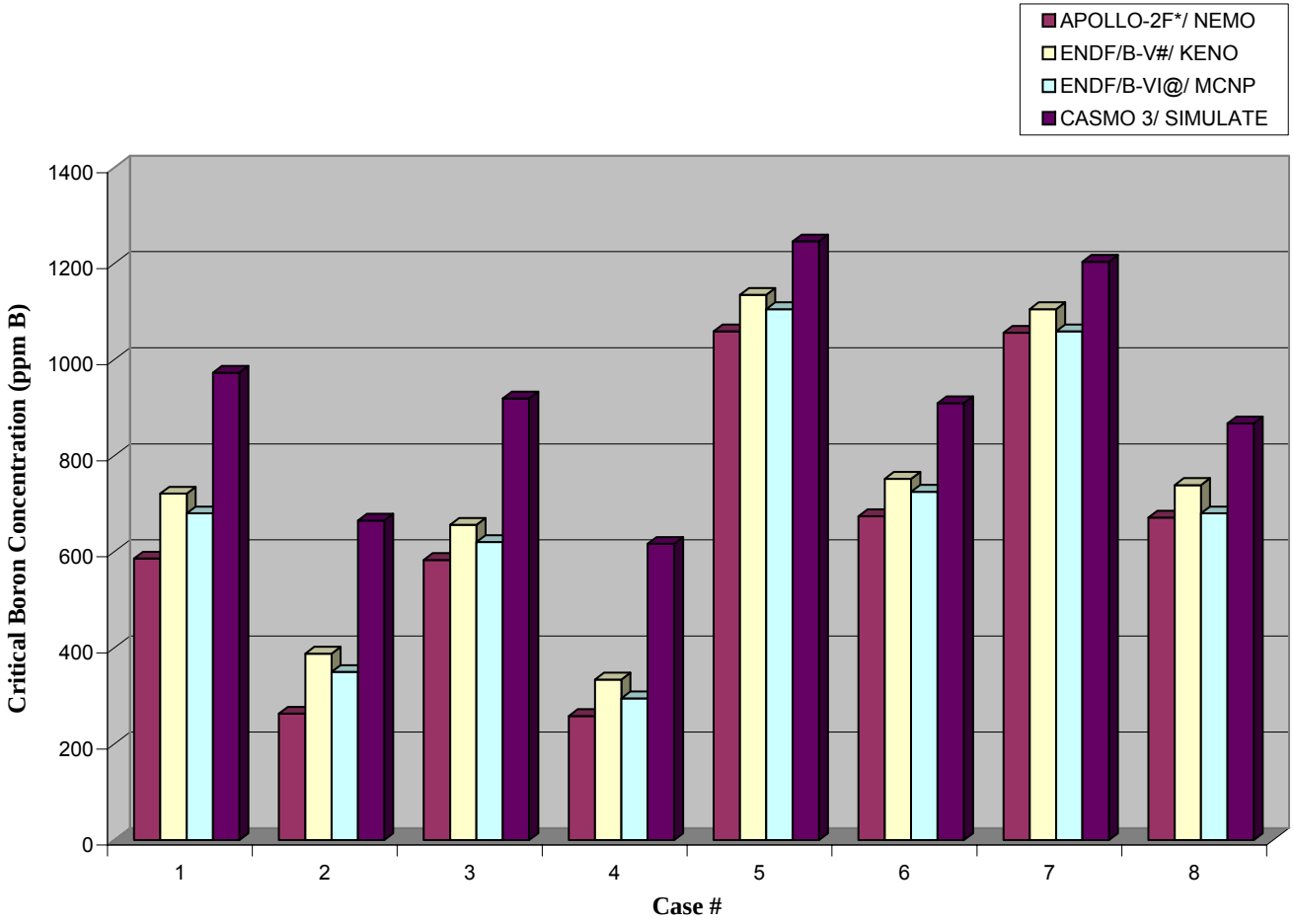

Figure 4-1: Comparison of Calculated Critical Boron Concentrations

The data reported in Table 4-5 indicates that KENO and MCNP demonstrate very good agreement. The difference in calculated k_{eff} for these two codes is less than 0.5% for all eight cases. These differences are likely primarily related to differences in the cross sections used. The KENO calculations use the 238-Group library with ENDF/B-V cross sections. The MCNP calculations using a continuous energy structure with ENDF/B-VI cross sections.

Going into this analysis, there was little doubt that MCNP and KENO could effectively analyze the proposed experiments, and the agreement between the MCNP and KENO calculations certainly does support that supposition.

As discussed previously, NEMO does calculate k_{eff} more consistent with KENO and NEWT, than does HELIOS or SIMULATE. NEMO tends to underestimate k_{eff}, compared to KENO, by about 0.7%, with the worst case being about 1.3 below the k_{eff} calculated by KENO. NEWT tends to overestimate k_{eff} by about 1 to 1.4%. HELIOS tends to underestimate k_{eff}, compared to KENO, by on the order of 4 or 5%. SIMULATE tends to overestimate k_{eff}, compared to KENO, by about 1 to 3.5%.

Using the NEMO results reported in Table 4-4 and Table 4-5, a ppmB/%Δk value can be calculated. For the non-gad cases (Cases 1, 3, 5, and 7) the minimum value is approximately 110 ppmB/%Δk. For the gadolinia cases, this value decreases to 100 ppmB/%Δk. These values are consistent with what is typically observed in commercial PWRs. This provides some assurance that the results reported are not spurious.

4.3 Results of the As-built Calculations

Using “as-built” dimensions and chemical assay data, and eliminating differences between the models used in the preliminary calculations, the configurations included in final list of proposed experiments were evaluated. Table 4-6 displays the results of these as-built calculations.

As expected, this additional information resulted in minor changes in the predicted critical boron concentrations. The comparison of the results show markedly better agreement than seen in the earlier analyses, although the APOLLO/NEMO and CASMO/SIMULATE calculations are still showing significant deviations in critical boron, particularly for the 0.800 cm pitch.

The concern remains that these experiments may be too small to be adequately evaluated using a nodal computer code.

Table 4-6: Calculated Critical Boron Concentrations for the As-built Calculations

Calculation Tools	Pitch	
	0.800 cm	0.855 cm
APOLLO2-F[1]/NEMO (Organization 1)	701	1,142
CASMO-3/SIMULATE (Organization 3)	427	1,057
ENDF/B-V/KENO (Organization 1)	636	1,048
ENDF/B-V/KENO (Organization 2)	640	1,050
ENDF/B-VI/MCNP (Organization 1)	632	1,051
ENDF/B-VI/MCNP (Organization 3)	635	1,055

Extensive time was spent trying to understand why the 0.855 cm pitch case would show excellent agreement between all of the codes, but the 0.800 cm pitch case would show such differences, particularly for the CASMO calculations. The lower ppm indicates that the CASMO code may have been calculating that the assembly had a higher leakage than really occurred from the critical array with the smaller (tighter) pin pitch. The buckling was calculated with 6 cm reflector.

Additionally, at the conclusion of the study, to ensure that there was no CASMO code version problem, the input was run using CASMO 4 code to ensure that the later version of the code would not give a different answer. The calculations were shown to be identical between both CASMO-3 and CASMO-4 for this set of problems.

4.4 Results of the Sensitivity Study

The team used the Tools for Sensitivity and Uncertainty Analysis Methodology Implementation (TSUNAMI), from the SCALE code system to assess the similarity of conceptual experiment designs to the intended commercial applications. The evaluation was documented in Reference 3.

TSUNAMI includes one-dimensional and three-dimensional sensitivity analysis sequences that compute the sensitivity of k_{eff} to perturbations in the neutron cross-section data. These sensitivity data can be used to compute relational integral indices that assess the similarity of two systems based on the nuclide-reaction-specific and energy-dependent sensitivity data. TSUNAMI has been demonstrated as an effective method for determining the applicability of benchmark experiments for use in code validation.[4]

4.4.1 Commercial Fuel Designs

Representative fuel assemblies of widely used commercial power reactor fuels were selected for analysis in this study. These representative assemblies are not the results of a comprehensive review of all nuclear fuel designs that could eventually be produced with higher enrichments, but are only selected to show trends in the data with regard to the applicability of the experimental data. Additional fuel designs may be considered in future analyses as needed.

Three commercial fuel designs were considered in this study: the Babcock and Wilcox (B&W) 15×15 fuel assembly, the Westinghouse 17×17 fuel assembly and the General Electric (GE) 8×8 fuel assembly. Some design properties of these assemblies are shown in Table 8. In each assembly, the fuel is UO_2 at 96% of theoretical density or 10.5216 g/cm^3.

Table 4-7: Design Properties of Commercial Fuel Assemblies Considered

Assembly	Fuel O.D. (cm)	Clad O.D. (cm)	Pitch (cm)	Clad Material
B&W 15×15	0.9505	1.0871	1.4427	Zr
Westinghouse 17×17	0.7844	0.9144	1.2598	Zr
GE 8×8	1.04394	1.2268	1.6256	Zircalloy-2

Each of the assemblies shown in Table 4-7 was modeled with ^{235}U enrichments of 4, 6, 7, and 10 wt %. Furthermore, each configuration was modeled under various conditions that could be encountered throughout the fuel cycle, excluding burnup. Each design was modeled at two temperatures. Shipping, storage and initial core loading conditions were simulated with models at 20°C. Average properties at operating conditions were modeled at higher temperatures. The same conditions were used for all low temperature models of the various fuel types. At the high temperature, the same average properties were used for the pressurized water reactor (PWR) fuel types (B&W and Westinghouse) and different conditions were considered for the boiling water reactor (BWR) fuel (GE). For the BWR, the uniform average moderator density was used for the entire length of the fuel assembly. The temperature and moderator density conditions used in the models are shown in Table 4-8.

Table 4-8: Temperature and Moderator Density Conditions for Commercial Fuel

Assembly Type/ Condition	T_{fuel} (°C)	T_{clad} (°C)	T_{mod} (°C)	ρ_{mod} (g/cm^3)
All – (Low Temp)	20	20	20	0.99821
PWR – (High Temp)	577	322	284	0.75760
BWR – (High Temp)	567	347	285	0.51510

Burnable poison (BP) rods were also considered in the commercial fuel models. For all fuel types and enrichments, the BP rods were composed of Gd_2O_3 in UO_2 with 4 wt-% Gd_2O_3 and a ^{235}U enrichment of 4 wt%. The BP rods have the same dimensions as the fuel rods they replace in each model. They were also modeled at the same temperatures as the fuel rods. The number of poison rods for each assembly type was as follows: B&W 15×15 has 20 BPs, Westinghouse 17×17 has 24 BPs, and GE 8×8 has 8 BPs. The loadings of the BP rods in these assembly designs are shown in Figures 4-2 through 4-4, respectively.

All commercial fuel assembly models were reflected on the x and y boundaries to create infinite arrays. Most models consist of one assembly with the appropriate interstitial assembly spacing and reflective boundary conditions. In some cases, a simulated core loading was produced with 9 assemblies in a 3×3 array with 3 assemblies containing BPs and the other 6 with no BPs. This arrangement is shown in Figure 4-5. The 3×3 array is reflected along the x and y boundaries to produce an infinite core with a 1/3 loading of BP assemblies. It is acknowledged that, in an actual core design, the non-BP assemblies would be burned fuel. However, the goal of the 1/3 loading is to test the magnitude of the sensitivity of the core to the BP rods, and this simplified model should adequately sample the BPs. The configurations modeled for each fuel assembly type are presented in Table 4-9. Each of these configurations was modeled for enrichments of 4, 6, 7, and 10 wt-% ^{235}U. Some of the PWR cases were modeled with 500-ppm natural boron in the moderator. The soluble boron was included in the Low Temperature-1/3 BP case and all High Temperature cases. Each model of the commercial fuel design systems was analyzed with the SEN3/KENO sequence to generate sensitivity data.

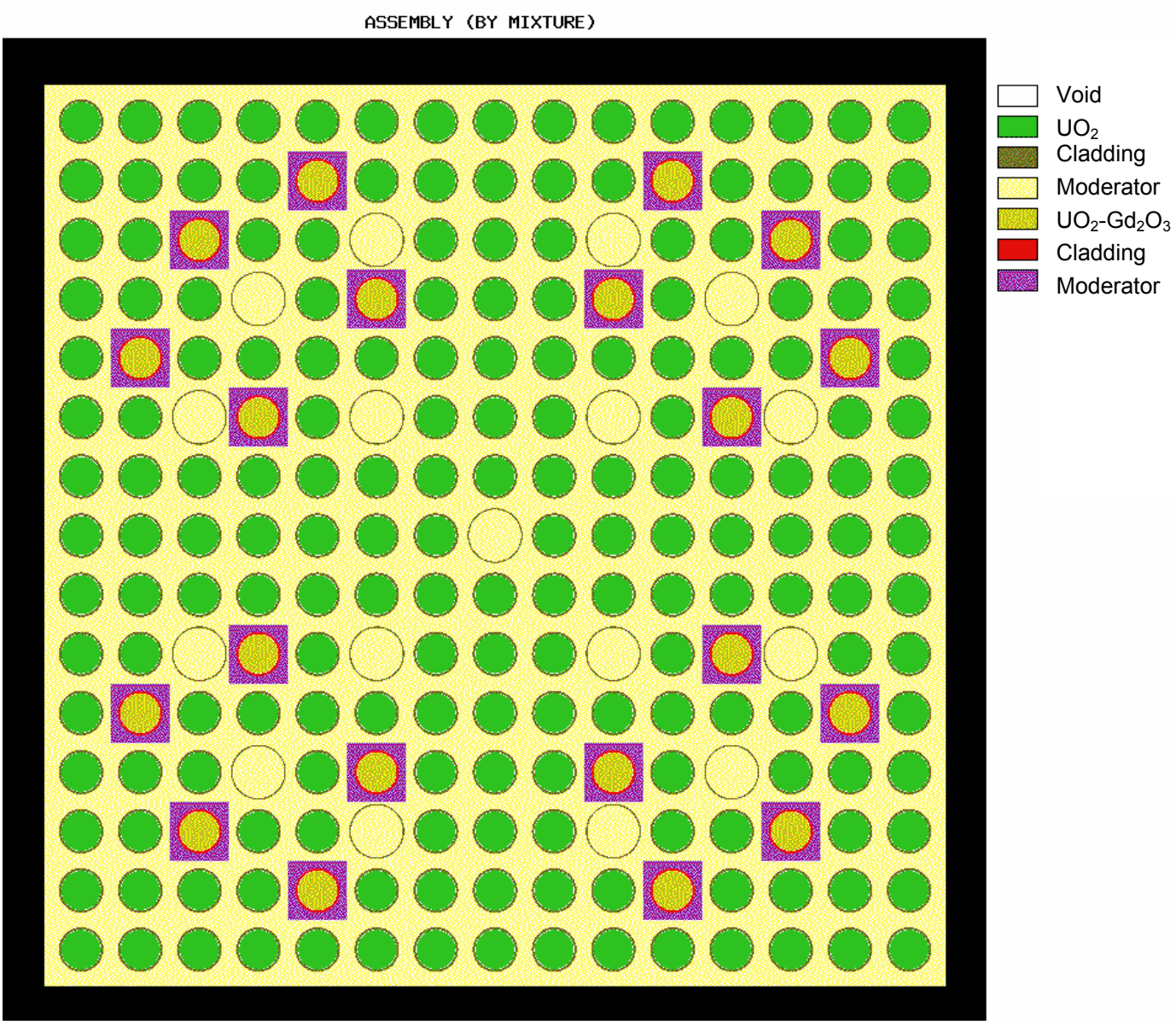

Figure 4-2: Geometric Arrangement of B&W 15x15 Assembly with 20 BP Rods

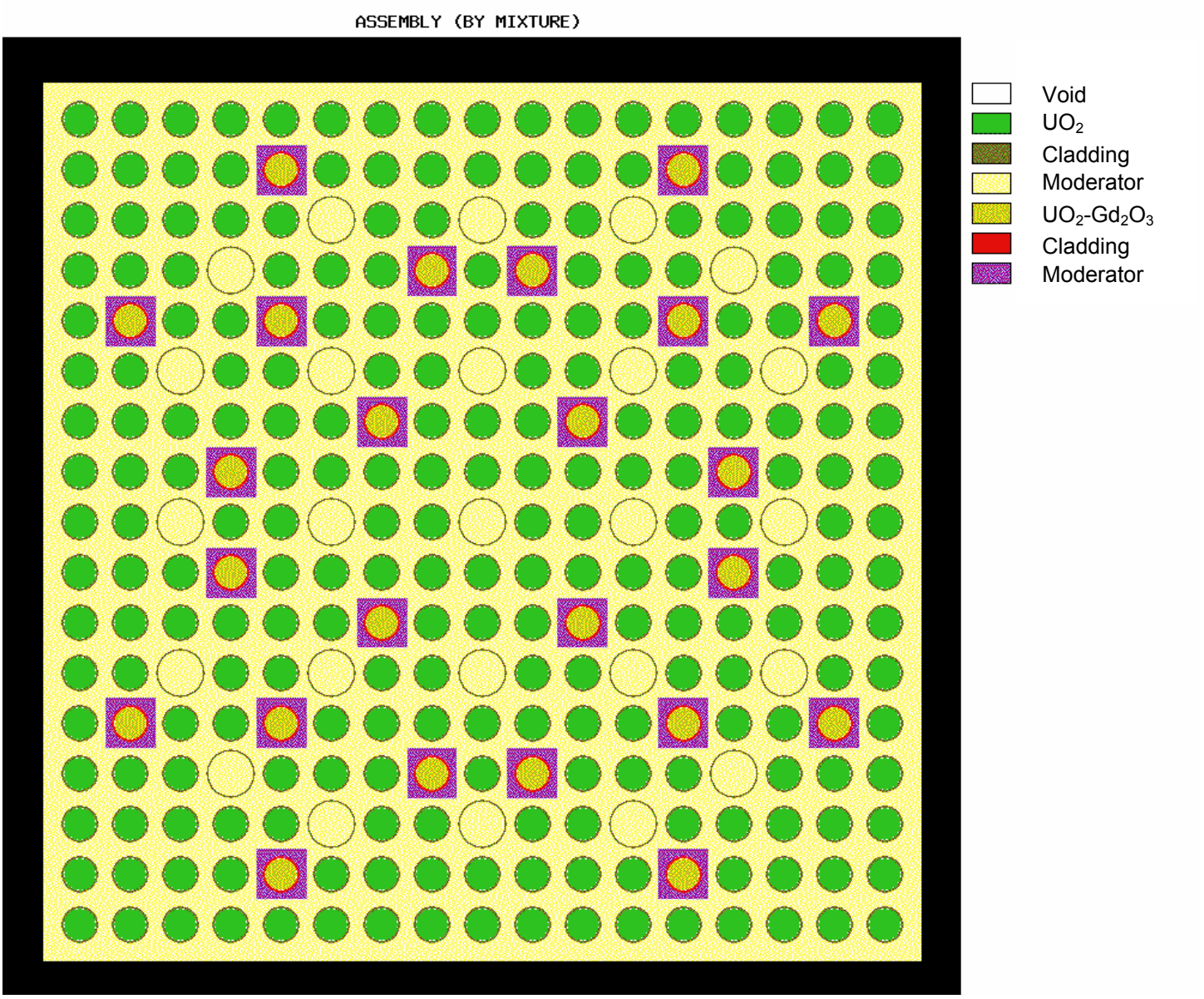

Figure 4-3: Geometric Arrangement of Westinghouse 17x17 Assembly with 24 BP Rods

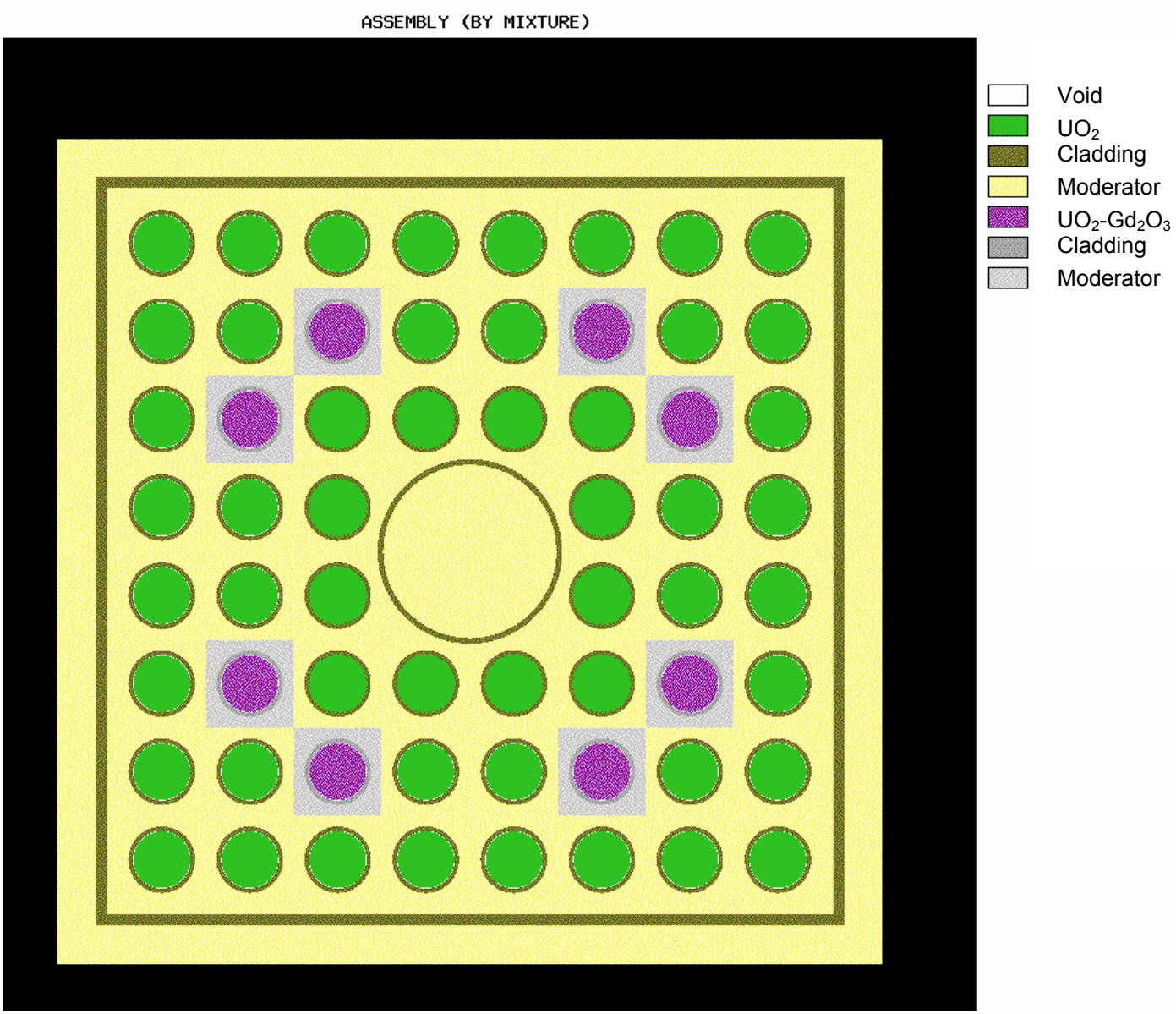

Figure 4-4: Geometric Arrangement for BWR 8x8 Fuel Assembly with 8 BP Rods

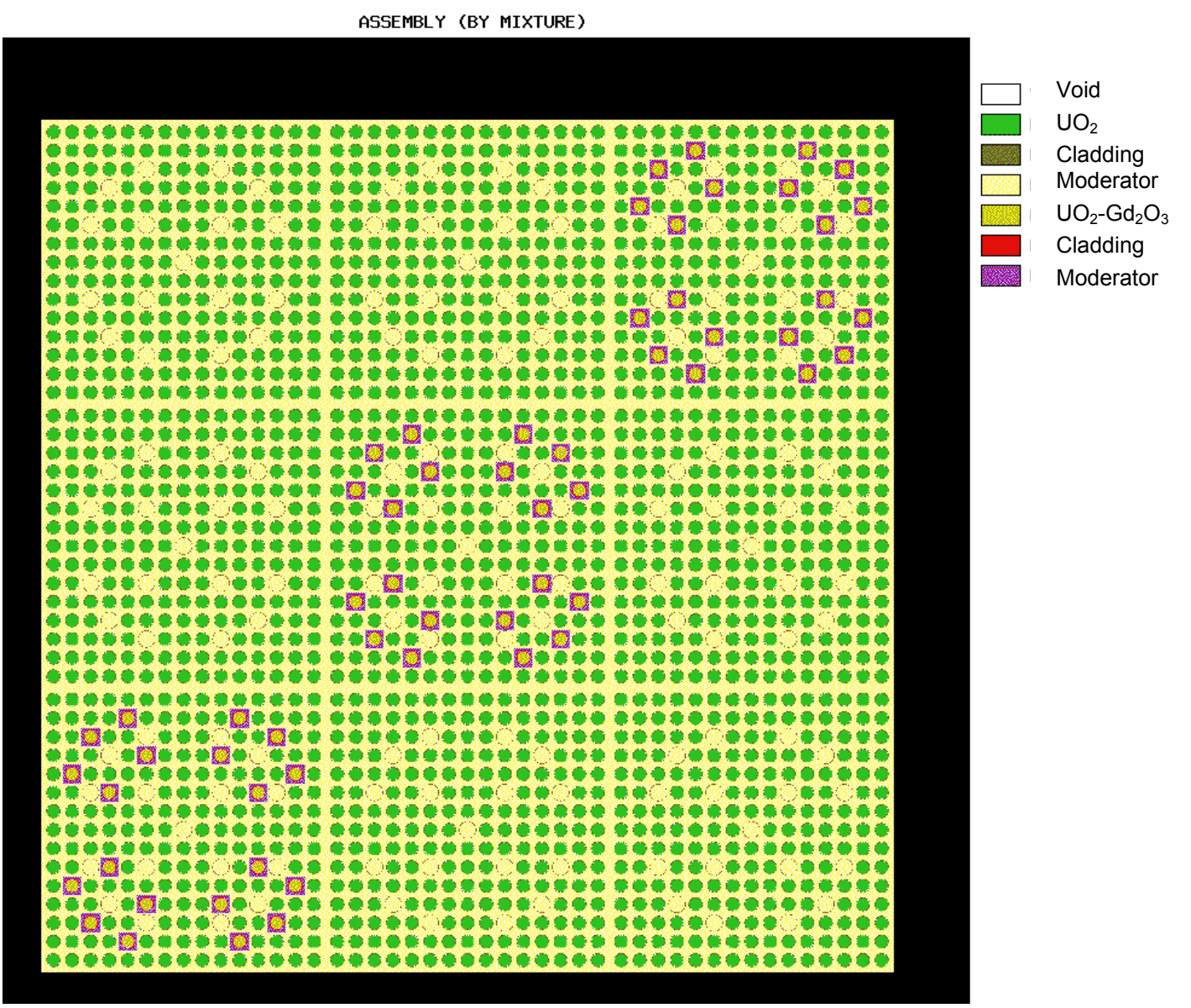

Figure 4-5: Geometric Arrangement of B&W 15□15 Assemblies with 1/3 Loading of 20 BP Rods

Table 4-9: Assembly Configurations Modeled

Temperature	**Low Temperature**			**High Temperature**		
Poisoned Assembly Arrangement → ***Assembly Type*** **↓**	**All BP**	**1/3 BP**	**No BP**	**All BP**	**1/3 BP**	**No BP**
B&W 15×15	✓	✓	✓	✓	✓	✓
Westinghouse 17×17			✓	✓		✓
GE 8×8	✓			✓		

4.4.2 Existing Experiments

The team performed a review of existing critical benchmark experiments with ^{235}U enrichments in the range of 5–10 wt-%. A total of 154 experimental configurations meeting this criterion have been identified, and sensitivity data for 142 of these experiments have been generated with the SEN3/KENO analysis sequence. Each of these experiments was obtained from the *International Handbook of Evaluated Criticality Safety Benchmark Experiments*. Summaries of the analyzed compound and solution experiments are provided in Tables 4-10 and 4-11.

Table 4-10: Compound Benchmark Critical Experiments Included in S/U Analysis

Identification	Type	Enrichment (wt %)	Lattice Pitch (cm)
IEU-MET-FAST-007-001	Metal Alloy	9.9	
LEU-COMP-THERM-018-001	Square-Pitched Arrays	7.0	1.32
LEU-COMP-THERM-019-001	Hexagonally-Pitched Arrays	5.19	0.7
LEU-COMP-THERM-019-002	Hexagonally-Pitched Arrays	5.19	0.8
LEU-COMP-THERM-019-003	Hexagonally-Pitched Arrays	5.19	1.4
LEU-COMP-THERM-020-001	Hexagonally-Pitched Arrays	5.0	1.3
LEU-COMP-THERM-020-002	Hexagonally-Pitched Arrays	5.0	1.3
LEU-COMP-THERM-020-003	Hexagonally-Pitched Arrays	5.0	1.3
LEU-COMP-THERM-020-004	Hexagonally-Pitched Arrays	5.0	1.3
LEU-COMP-THERM-020-005	Hexagonally-Pitched Arrays	5.0	1.3
LEU-COMP-THERM-020-006	Hexagonally-Pitched Arrays	5.0	1.3
LEU-COMP-THERM-020-007	Hexagonally-Pitched Arrays	5.0	1.3
LEU-COMP-THERM-021-001	Hexagonally-Pitched Arrays + Soluble Boron	5.0	1.0
LEU-COMP-THERM-021-002	Hexagonally-Pitched Arrays + Soluble Boron	5.0	1.0
LEU-COMP-THERM-021-003	Hexagonally-Pitched Arrays + Soluble Boron	5.0	1.0
LEU-COMP-THERM-021-004	Hexagonally-Pitched Arrays + Soluble Boron	5.0	1.3
LEU-COMP-THERM-021-005	Hexagonally-Pitched Arrays + Soluble Boron	5.0	1.3
LEU-COMP-THERM-021-006	Hexagonally-Pitched Arrays + Soluble Boron	5.0	1.3
LEU-COMP-THERM-022-001	Hexagonally-Pitched Arrays	9.83	0.7
LEU-COMP-THERM-022-002	Hexagonally-Pitched Arrays	9.83	0.8
LEU-COMP-THERM-022-003	Hexagonally-Pitched Arrays	9.83	1.0
LEU-COMP-THERM-022-004	Hexagonally-Pitched Arrays	9.83	1.22

Table 4-10 (continued)

Identification	Type	Enrichment (wt %)	Lattice Pitch (cm)
LEU-COMP-THERM-022-005	Hexagonally-Pitched Arrays	9.83	1.4
LEU-COMP-THERM-022-006	Hexagonally-Pitched Arrays	9.83	1.83
LEU-COMP-THERM-022-007	Hexagonally-Pitched Arrays	9.83	1.85
LEU-COMP-THERM-023-001	Hexagonally-Pitched Arrays	9.83	1.4
LEU-COMP-THERM-023-002	Hexagonally-Pitched Arrays	9.83	1.4
LEU-COMP-THERM-023-003	Hexagonally-Pitched Arrays	9.83	1.4
LEU-COMP-THERM-023-004	Hexagonally-Pitched Arrays	9.83	1.4
LEU-COMP-THERM-023-005	Hexagonally-Pitched Arrays	9.83	1.4
LEU-COMP-THERM-023-006	Hexagonally-Pitched Arrays	9.83	1.4
LEU-COMP-THERM-024-001	Square-Pitched Arrays	9.83	0.62
LEU-COMP-THERM-024-002	Square-Pitched Arrays	9.83	0.88
LEU-COMP-THERM-025-001	Hexagonally-Pitched Arrays	7.41	0.7
LEU-COMP-THERM-025-002	Hexagonally-Pitched Arrays	7.41	0.8
LEU-COMP-THERM-025-003	Hexagonally-Pitched Arrays	7.41	1.0
LEU-COMP-THERM-025-004	Hexagonally-Pitched Arrays	7.41	1.22
LEU-COMP-THERM-026-001	Hexagonally-Pitched Arrays	4.92	1.29
LEU-COMP-THERM-026-002	Hexagonally-Pitched Arrays	4.92	1.29
LEU-COMP-THERM-026-003	Hexagonally-Pitched Arrays	4.92	1.09
LEU-COMP-THERM-026-004	Hexagonally-Pitched Arrays	4.92	1.09
LEU-COMP-THERM-032-001	Hexagonally-Pitched Arrays	9.83	0.7
LEU-COMP-THERM-032-002	Hexagonally-Pitched Arrays	9.83	0.7
LEU-COMP-THERM-032-003	Hexagonally-Pitched Arrays	9.83	0.7
LEU-COMP-THERM-032-004	Hexagonally-Pitched Arrays	9.83	1.4
LEU-COMP-THERM-032-005	Hexagonally-Pitched Arrays	9.83	1.4
LEU-COMP-THERM-032-006	Hexagonally-Pitched Arrays	9.83	1.4
LEU-COMP-THERM-032-007	Hexagonally-Pitched Arrays	9.83	1.85
LEU-COMP-THERM-032-008	Hexagonally-Pitched Arrays	9.83	1.85

Table 4-10 (continued)

Identification	Type	Enrichment (wt %)	Lattice Pitch (cm)
LEU-COMP-THERM-032-009	Hexagonally-Pitched Arrays	9.83	1.85
LEU-COMP-THERM-049-001	Array of homogeneous units	4.98	
LEU-COMP-THERM-049-002	Array of homogeneous units	4.98	
LEU-COMP-THERM-049-003	Array of homogeneous units	4.98	
LEU-COMP-THERM-049-004	Array of homogeneous units	4.98	
LEU-COMP-THERM-049-005	Array of homogeneous units	4.98	
LEU-COMP-THERM-049-006	Array of homogeneous units	4.98	
LEU-COMP-THERM-049-007	Array of homogeneous units	4.98	
LEU-COMP-THERM-049-008	Array of homogeneous units	4.98	
LEU-COMP-THERM-049-009	Array of homogeneous units	4.98	
LEU-COMP-THERM-049-010	Array of homogeneous units	4.98	
LEU-COMP-THERM-049-011	Array of homogeneous units	4.98	
LEU-COMP-THERM-049-012	Array of homogeneous units	4.98	
LEU-COMP-THERM-049-013	Array of homogeneous units	4.98	
LEU-COMP-THERM-049-014	Array of homogeneous units	4.98	
LEU-COMP-THERM-049-015	Array of homogeneous units	4.98	
LEU-COMP-THERM-049-016	Array of homogeneous units	4.98	
LEU-COMP-THERM-049-017	Array of homogeneous units	4.98	
LEU-COMP-THERM-049-018	Array of homogeneous units	4.98	

Table 4-11: Solution Benchmark Critical Experiments Included in S/U Analysis

Identification	Type	Enrichment (wt %)	Uranium concentration (g/l)
LEU-SOL-THERM-001-001	Cylindrical solution tank	4.94	978.3
LEU-SOL-THERM-003-001	Spherical solution tank	10.07	296.0
LEU-SOL-THERM-003-002	Spherical solution tank	10.07	264.0
LEU-SOL-THERM-003-003	Spherical solution tank	10.07	260.0
LEU-SOL-THERM-003-004	Spherical solution tank	10.07	255.0
LEU-SOL-THERM-003-005	Spherical solution tank	10.07	203.0
LEU-SOL-THERM-003-006	Spherical solution tank	10.07	197.0
LEU-SOL-THERM-003-007	Spherical solution tank	10.07	193.0
LEU-SOL-THERM-003-008	Spherical solution tank	10.07	171.0
LEU-SOL-THERM-003-009	Spherical solution tank	10.07	168.0
LEU-SOL-THERM-004-001	Cylindrical solution tank	9.97	310.1
LEU-SOL-THERM-004-002	Cylindrical solution tank	9.97	290.4
LEU-SOL-THERM-004-003	Cylindrical solution tank	9.97	270.0
LEU-SOL-THERM-004-004	Cylindrical solution tank	9.97	253.6
LEU-SOL-THERM-004-005	Cylindrical solution tank	9.97	241.9
LEU-SOL-THERM-004-006	Cylindrical solution tank	9.97	233.2
LEU-SOL-THERM-004-007	Cylindrical solution tank	9.97	225.3
LEU-SOL-THERM-005-001	Cylindrical solution tank	5.64	400.2
LEU-SOL-THERM-005-002	Cylindrical solution tank	5.64	400.2
LEU-SOL-THERM-005-003	Cylindrical solution tank	5.64	400.2
LEU-SOL-THERM-006-001	Cylindrical solution tank	10.07	420.5
LEU-SOL-THERM-006-002	Cylindrical solution tank	10.07	420.5
LEU-SOL-THERM-006-003	Cylindrical solution tank	10.07	420.5
LEU-SOL-THERM-006-004	Cylindrical solution tank	10.07	420.5
LEU-SOL-THERM-006-005	Cylindrical solution tank	10.07	420.5
LEU-SOL-THERM-007-001	Cylindrical solution tank	9.97	313.0
LEU-SOL-THERM-007-002	Cylindrical solution tank	9.97	290.7
LEU-SOL-THERM-007-003	Cylindrical solution tank	9.97	270.0
LEU-SOL-THERM-007-004	Cylindrical solution tank	9.97	253.9
LEU-SOL-THERM-007-005	Cylindrical solution tank	9.97	241.9
LEU-SOL-THERM-008-001	Spherical solution tank	9.97	240.2
LEU-SOL-THERM-008-002	Spherical solution tank	9.97	240.7
LEU-SOL-THERM-008-003	Spherical solution tank	9.97	241.1
LEU-SOL-THERM-008-004	Spherical solution tank	9.97	239.8
LEU-SOL-THERM-009-001	Spherical solution tank	9.97	244.7
LEU-SOL-THERM-009-002	Spherical solution tank	9.97	245.0
LEU-SOL-THERM-009-003	Spherical solution tank	9.97	245.2
LEU-SOL-THERM-010-001	Spherical solution tank	9.97	242.1

Table 4-11 (continued)

Identification	Type	Enrichment (wt %)	Uranium concentration (g/l)
LEU-SOL-THERM-010-002	Spherical solution tank	9.97	242.5
LEU-SOL-THERM-010-003	Spherical solution tank	9.97	242.8
LEU-SOL-THERM-010-004	Spherical solution tank	9.97	243.3
LEU-SOL-THERM-016-001	Slab solution tank	9.97	464.2
LEU-SOL-THERM-016-002	Slab solution tank	9.97	429.9
LEU-SOL-THERM-016-003	Slab solution tank	9.97	371.9
LEU-SOL-THERM-016-004	Slab solution tank	9.97	350.8
LEU-SOL-THERM-016-005	Slab solution tank	9.97	328.9
LEU-SOL-THERM-016-006	Slab solution tank	9.97	311.4
LEU-SOL-THERM-016-007	Slab solution tank	9.97	299.6
LEU-SOL-THERM-017-001	Slab solution tank	9.97	464.2
LEU-SOL-THERM-017-002	Slab solution tank	9.97	432.4
LEU-SOL-THERM-017-003	Slab solution tank	9.97	369.7
LEU-SOL-THERM-017-004	Slab solution tank	9.97	350.6
LEU-SOL-THERM-017-005	Slab solution tank	9.97	328.9
LEU-SOL-THERM-017-006	Slab solution tank	9.97	315.3
LEU-SOL-THERM-018-001	Slab solution tank	9.97	308.1
LEU-SOL-THERM-018-002	Slab solution tank	9.97	312.2
LEU-SOL-THERM-018-003	Slab solution tank	9.97	312.7
LEU-SOL-THERM-018-004	Slab solution tank	9.97	313.2
LEU-SOL-THERM-018-005	Slab solution tank	9.97	313.8
LEU-SOL-THERM-018-006	Slab solution tank	9.97	314.6
LEU-SOL-THERM-019-001	Slab solution tank	9.97	317.1
LEU-SOL-THERM-019-002	Slab solution tank	9.97	315.8
LEU-SOL-THERM-019-003	Slab solution tank	9.97	316.3
LEU-SOL-THERM-019-004	Slab solution tank	9.97	317.1
LEU-SOL-THERM-019-005	Slab solution tank	9.97	317.7
LEU-SOL-THERM-019-006	Slab solution tank	9.97	318.4
LEU-SOL-THERM-020-001	Cylindrical solution tank	9.97	243.1
LEU-SOL-THERM-020-002	Cylindrical solution tank	9.97	225.5
LEU-SOL-THERM-020-003	Cylindrical solution tank	9.97	204.7
LEU-SOL-THERM-020-004	Cylindrical solution tank	9.97	193.7
LEU-SOL-THERM-021-001	Cylindrical solution tank	9.97	243.1
LEU-SOL-THERM-021-002	Cylindrical solution tank	9.97	225.7
LEU-SOL-THERM-021-003	Cylindrical solution tank	9.97	204.7
LEU-SOL-THERM-021-004	Cylindrical solution tank	9.97	193.7

4.4.3 S/U Results with Existing Experiments

Initially, the S/U correlation coefficient, c_k, was used to assess the applicability of benchmark experiments to the commercial design systems. The parameter c_k gives a measure of the shared variance, due to cross-section-data uncertainties, between a design system and an experiment. The higher the correlation of the variance (higher c_k value), the greater the similarity of the two systems. However, the c_k parameter requires cross-section covariance data for each nuclide-reaction pair in the design system for which the applicability of the experiments is to be assessed. If the covariance data is not available, the nuclide-reaction pair is simply ignored. The value of c_k could be artificially inflated by the absence of nuclide-reaction pairs that are not well covered by the experiments and could be artificially reduced if well-covered nuclide-reaction pairs are omitted.

An alternative parameter to c_k is E_{sum}, which is used to assess similarity based only on the sensitivity data. Of significance to these commercial design systems is the absence of covariance data for gadolinium and zirconium. Thus, the E_{sum} parameter is expected to give a more accurate measure of the similarity for these systems.

In this analysis, the values of both c_k and E_{sum} are reported for comparison purposes. However, only the E_{sum} values will be used to assess the applicability of the experiments for the code validation of the design systems. Current guidance states that an experiment is applicable for the code validation of a design system its c_k or E_{sum} value is 0.8 or greater. Another guideline is that 15–20 systems with c_k or E_{sum} ≥ 0.8 are needed to produce an accurate trending analysis to predict any computational bias. The numbers of the 142 analyzed experiments with c_k and E_{sum} values of 0.8 or greater are given in Table 4-12 through 4-15 for 4, 6, 7 and 10 wt-% enriched design systems, respectively.

For the 4 wt-% systems, sufficient numbers of existing benchmarks with E_{sum} values exceeding 0.8 are available for validation of the low temperature design systems. The number of applicable benchmarks is reduced for the high temperature systems, but is still above the recommended number of 15–20. As stated previously, the only experimental benchmarks considered here have enrichments in the range of 5–10%. Had lower enrichments been considered, more experiments would likely have exceeded the S/U criterion for applicability.

For design applications with 6% enrichments, the number of applicable systems is reduced for the B&W assemblies at low temperature conditions. At high temperature conditions, the limited numbers of applicable benchmarks is fairly constant for all assembly types as compared to the 4 wt-% enriched assemblies. For the low temperature B&W simulated core with 1/3 loading of BP assemblies, the number of applicable benchmarks, 30, is less than half that of the other low

temperature B&W configurations. Recall from the description of these design systems that this configuration contains 500-ppm boron, where the other low temperature configurations have no soluble boron. For the other assembly types, the numbers of applicable benchmarks are fairly constant compared with the 4% systems.

With the enrichment increased to 7%, the numbers of applicable benchmarks are reduced as compared to the 6% systems. However, sufficient numbers of benchmarks are available for all low temperature systems. The numbers of applicable benchmarks for the high temperature configurations are still acceptable, but only by a small margin.

With the enrichment increased to 10%, the number of systems matching the low temperature BWR system is essentially unchanged from the previous enrichments. However, the numbers of applicable systems for the low temperature PWR systems are reduced. For the 1/3 BP configuration of the B&W assembly and all of the high temperature configurations, the numbers of applicable benchmarks just meet the S/U criterion.

From a criticality safety perspective, based on this S/U analysis, there appear to be adequate benchmarks to validate the selected design systems. However, of the 30 systems that exceeded S/U criterion for the 7 wt-% enriched low temperature B&W core with 1/3 BP loading, 10 are hexagonally-pitched arrays of fuel rods, 2 are square-pitched arrays with an irregular number of fuel rods along one edge of the critical assembly and 18 are not rod-arrays but are stacked arrays of LEU compacts with a polyethylene reflector. None of these systems is suitable for validation of the commercial reactor physics codes, which require square-pitched symmetric assemblies. However, these experiments are suitable from a criticality safety perspective.

Table 4-12: Numbers of 142 Existing Experiments with c_k and E_{sum} ≥ 0.8 for 4 wt-% ^{235}U Commercial Assemblies

Temperature	Low			High		
Poison	**BP**	**1/3 BP**	**No BP**	**BP**	**1/3 BP**	**No BP**
BWR 8×8						
c_k	131			41		
E_{sum}	131			29		
B&W 15×15						
c_k	26	39	53	34	38	38
E_{sum}	134	46	131	24	25	27
Westinghouse 17×17						
c_k			91	36		43
E_{sum}			131	27		33

Table 4-13: Numbers of 142 Existing Experiments with c_k and E_{sum} ≥ 0.8 for 6 wt-% ^{235}U Commercial Assemblies

Temperature	Low			High		
Poison	**BP**	**1/3 BP**	**No BP**	**BP**	**1/3 BP**	**No BP**
BWR 8×8						
c_k	113			37		
E_{sum}	118			27		
B&W 15×15						
c_k	41	35	42	33	34	35
E_{sum}	71	30	69	24	24	27
Westinghouse 17×17						
c_k			55	35		40
E_{sum}			132	25		27

Table 4-14: Numbers of 142 Existing Experiments with c_k and $E_{sum} \geq 0.8$ for 7 wt-% ^{235}U Commercial Assemblies

Temperature	Low			High		
Poison	**BP**	**1/3 BP**	**No BP**	**BP**	**1/3 BP**	**No BP**
BWR 8×8						
c_k	91			35		
E_{sum}	120			27		
B&W 15×15						
c_k	40	35	41	32	30	35
E_{sum}	45	30	48	23	19	24
Westinghouse 17×17						
c_k			49	35		37
E_{sum}			115	24		27

Table 4-15: Numbers of 142 Existing Experiments with c_k and $E_{sum} \geq 0.8$ for 10 wt-% ^{235}U Commercial Assemblies

Temperature	Low			High		
Poison	**BP**	**1/3 BP**	**No BP**	**BP**	**1/3 BP**	**No BP**
BWR 8×8						
c_k	55			34		
E_{sum}	117			24		
B&W 15×15						
c_k	35	30	36	29	30	30
E_{sum}	33	19	36	20	15	20
Westinghouse 17×17						
c_k			40	30		31
E_{sum}			43	20		24

The preceding discussion addressed the system-wide S/U parameters that assess the overall applicability of an experiment to a design system. These parameters may show that an experiment is applicable for the validation of a

design system if a majority of the important nuclide-reaction pairs in the design system is well covered by the experiment.

However, the 0.8 criterion may be met by experiments that show a similar response to certain nuclide-reaction pairs and a dissimilar response to others. It is also possible for the 0.8 criterion to be met by an experiment that does not include certain nuclides important to the design system. To address these concerns, a more detailed application of the S/U methodologies can reveal which nuclide-reaction pairs are well covered by the chosen experimental benchmarks and which nuclide-reaction pairs may need additional data for validation.

The *T(E)* parameter gives a measure of the relative importance of a particular nuclide-reaction pair in the experiment as compared to the relative importance of the same nuclide-reaction pair in the design system. For this study, a *T(E)* value of 0.9 or greater indicates that the nuclide-reaction pair is well covered by the experimental benchmark. A previous study indicated that 5–10 systems with *T(E)* values 0.95 or greater are necessary to validate a particular nuclide-reaction pair.

For the nuclide-reaction specific analysis, only the B&W assembly models were considered. The numbers of the 142 experimental benchmarks that exceed the 0.9 criterion for each important nuclide reaction for each assembly model are shown in Tables 17–20 for 4, 6, 7 and 10% enriched assemblies, respectively.

For the 4% assemblies, data is lacking for ^{1}H scatter, ^{10}B capture, and ^{157}Gd capture. Because ^{1}H scatter has a well-known cross section that is a smooth function of energy, the lack of systems with high *T(E)* values is not a source of significant concern. The lack of data for the poisons, ^{10}B and ^{157}Gd, reflects the absence of these nuclides in most of the selected experimental benchmarks. Other important nuclide-reaction pairs such as ^{235}U fission and ^{1}H capture are well covered by the selected experiments. ^{238}U fission is also adequately covered and ^{238}U capture is covered almost exclusively by the 18 configurations of the LCT-049 series of LEU compact experiments.

Increasing the enrichment of the commercial assemblies to 6%, there are few or no benchmarks that validate the poisons. ^{235}U and ^{238}U fission, ^{238}U capture and ^{1}H capture are still adequately covered. However, the numbers of systems that validate ^{235}U capture is less than those for the 4% assemblies.

With the enrichment of the commercial assemblies increased to 7%, the coverage for ^{235}U capture is further decreased and the number of systems validating ^{235}U fission for the low temperature 1/3 BP core, although still substantial, is nearly half that for the 6% assemblies. The coverage for other nuclides changes little from 6 to 7%.

For the 10 wt-% enriched assemblies, the coverage for ^{235}U capture is reduced to few or no benchmarks. In addition, the number of benchmarks providing coverage for ^{235}U fission greatly reduced. For the high temperature systems, little coverage is provided for any nuclide-reaction pairs except ^{1}H capture and ^{238}U fission and capture.

Thus, for all configurations, additional data is needed to validate the gadolinium and boron poisons. For enrichments ≥ 6 wt %, the selected benchmarks with enrichments of 5–10 wt % do not provide adequate coverage for ^{235}U capture. The addition of data validating ^{235}U fission for the high temperature assemblies with enrichments ≥ 6 wt % would also be useful.

Table 4-16: Numbers of 142 Existing Experiments with *T(E)* ≥ 0.9 for 4 wt-% ^{235}U Commercial Assemblies

Temperature	Low			High		
Poison	**BP**	**1/3 BP**	**No BP**	**BP**	**1/3 BP**	**No BP**
H-1 capture	114	120	114	122	122	119
H-1 scatter	0	0	0	0	0	0
U-235 fission	125	130	122	14	19	23
U-235 capture	22	31	18	35	35	24
U-238 fission	33	31	34	27	29	29
U-238 capture	22	20	22	19	20	20
B-10 capture		6		1	6	
Gd-157 capture	0	0		0	0	

Table 4-17: Numbers of 142 Existing Experiments with *T(E)* ≥ 0.9 for 6 wt-% ^{235}U Commercial Assemblies

Temperature	Low			High		
Poison	**BP**	**1/3 BP**	**No BP**	**BP**	**1/3 BP**	**No BP**
H-1 capture	117	122	117	122	122	122
H-1 scatter	0	0	0	0	0	0
U-235 fission	131	133	126	12	13	14
U-235 capture	9	14	6	20	9	8
U-238 fission	31	30	33	27	27	27
U-238 capture	27	24	27	19	20	20
B-10 capture		6		6	6	
Gd-157 capture	0	0		0	0	

Table 4-18: Numbers of 142 Existing Experiments with *T(E)* ≥ 0.9 for 7 wt-% ^{235}U Commercial Assemblies

Temperature	Low			High		
Poison	**BP**	**1/3 BP**	**No BP**	**BP**	**1/3 BP**	**No BP**
H-1 capture	118	122	118	122	12	122
H-1 scatter	0	0	0	0	0	0
U-235 fission	131	73	130	11	12	13
U-235 capture	7	10	6	9	7	6
U-238 fission	30	27	32	27	27	27
U-238 capture	27	25	27	20	21	21
B-10 capture		6		6	6	
Gd-157 capture	0	0		0	0	

Table 4-19: Numbers of 142 Existing Experiments with *T(E)* ≥ 0.9 for 10 wt-% ^{235}U Commercial Assemblies

Temperature	Low			High		
Poison	**BP**	**1/3 BP**	**No BP**	**BP**	**1/3 BP**	**No BP**
H-1 capture	120	122	120	123	123	123
H-1 scatter	0	0	0	0	0	0
U-235 fission	43	46	88	5	8	10
U-235 capture	5	6	0	5	3	3
U-238 fission	30	27	30	27	27	27
U-238 capture	27	25	27	21	22	22
B-10 capture		6		6	6	
Gd-157 capture	0	0		0	0	

4.4.4 S/U Results for the Proposed Experiments

Sensitivity data has been generated for the originally proposed configurations. The proposed experiments modeled are the eight configurations of the square core design, representative of a 3×3 array of 15×15 fuel assemblies. Each core design was modeled with fuel-rod pitches of 0.8 cm and 0.855 cm, at 20°C and 60°C and with and without 20 Gd_2O_3-UO_2 BP rods replacing fuel rods in the central assembly. Critical boron searches were performed for each configuration, and then the sensitivity data were generated for the critical configurations. A summary of the eighteen modeled configurations is provided in Table 4-20.

Table 4-20: Design Parameters of New Experiments Modeled with SEN3/KENO

Identifier	Configuration	Pitch (cm)	Temperature (°C)	Poison Rods in Center Assembly	Critical Boron Concentration (ppm)
1a	Square	0.8	20	0	697
1b	Square	0.8	60	0	649
2a	Square	0.8	20	20	338
2b	Square	0.8	60	20	305
3a	Square	0.855	20	0	1127
3b	Square	0.855	60	0	1101
4a	Square	0.855	20	20	738
4b	Square	0.855	60	20	714

The numbers of the 8 square-design experiments with c_k and E_{sum} values ≥ 0.8 for each commercial assembly system are given in Tables 4-21 through 4-24 for ^{235}U enrichments of 4, 6, 7 and 10 wt %, respectively.

For the 4% commercial systems, the new experiments are generally applicable to the design systems with the exception of the high temperature cases for the B&W assembly. Here, the difference in the c_k and E_{sum} parameters is evident for the high temperature B&W configuration with BP rods. The c_k parameter indicates that all experiments are applicable to the design system, but the E_{sum} parameter indicates that only two systems are applicable. The applicable experiments are the 60°C experiments with 20 BP rods and pitches 0.8 and 0.855 cm. Each of these experiments just exceeds the 0.8 cutoff with E_{sum} values 0.8085 and 0.8031, respectively.

For the 6% systems, all of the experiments are applicable for the low temperature configurations. However, few of the experiments are applicable for the high temperature configurations. The same conditions exist for the 7% systems, where all experiments are shown to be applicable to the low temperature configurations of the design systems.

For the 10% systems, all experiments are applicable to each of the low temperature configurations, with one exception. No experiments are applicable to the B&W 1/3 BP low temperature configuration. In addition, no experiments are applicable for any of the high temperature configurations.

Thus, these experiments provide additional data for criticality safety code validation for the low temperature configurations of the commercial assemblies with ^{235}U enrichments in the range of 4–10 wt %. In addition, because the experiment core is a symmetric square-pitched design, the data generated from these experiments will be applicable to the validation of reactor physics codes. However, the applicability of these experiments to commercial fuels at operating conditions is limited.

The E_{sum} values calculated for each of the design systems with square-design experiments are given below in Tables 4-25 through 4-28 for assembly enrichments of 4, 6, 7 and 10 wt-% ^{235}U, respectively. These are the values used to generate Tables 4-21 through 4-24.

Table 4-21: Numbers of 8 Square-Design Experiments with c_k and E_{sum} ≥ 0.8 for 4 wt-% ^{235}U Commercial Assemblies

Temperature	Low			High		
Poison	**BP**	**1/3 BP**	**No BP**	**BP**	**1/3 BP**	**No BP**
BWR 8×8						
c_k	8			8		
E_{sum}	7			8		
B&W 15×15						
c_k	8	8	8	8	8	8
E_{sum}	8	8	8	2	7	6
Westinghouse 17×17						
c_k			8	8		8
E_{sum}			8	7		8

Table 4-22: Numbers of 8 Square-Design Experiments with c_k and E_{sum} ≥ 0.8 for 6 wt-% ^{235}U Commercial Assemblies

Temperature	Low			High		
Poison	**BP**	**1/3 BP**	**No BP**	**BP**	**1/3 BP**	**No BP**
BWR 8×8						
c_k	8			8		
E_{sum}	8			3		
B&W 15×15						
c_k	8	8	8	8	8	8
E_{sum}	8	8	8	0	0	2
Westinghouse 17×17						
c_k			8	8		8
E_{sum}			8	1		5

Table 4-23: Numbers of 8 Square-Design Experiments with c_k and E_{sum} ≥ 0.8 for 7 wt-% ^{235}U Commercial Assemblies

Temperature	Low			High		
Poison	**BP**	**1/3 BP**	**No BP**	**BP**	**1/3 BP**	**No BP**
BWR 8×8						
c_k	8			8		
E_{sum}	8			2		
B&W 15×15						
c_k	8	8	8	8	8	8
E_{sum}	8	8	8	0	0	0
Westinghouse 17×17						
c_k			8	8		8
E_{sum}			8	1		5

Table 4-24: Numbers of 8 Square-Design Experiments with ck and E_{sum} ≥ 0.8 for 10 wt-% ^{235}U Commercial Assemblies

Temperature	Low			High		
Poison	**BP**	**1/3 BP**	**No BP**	**BP**	**1/3 BP**	**No BP**
BWR 8×8						
c_k	8			8		
E_{sum}	8			0		
B&W 15×15						
c_k	8	8	8	8	8	8
E_{sum}	8	0	8	0	0	0
Westinghouse 17×17						
c_k			8	8		8
E_{sum}			8	0		0

Table 4-25: Values of E_{sum} for 4% Enriched Assembly Models with 8 Square-Design Experiments

Experiment→ Assembly↓	1a	1b	2a	2b	3a	3b	4a	4b
Low Temperature								
BWR	0.8444	0.8654	0.8357	0.8611	0.8447	0.8712	0.8420	0.8618
B&W BP	0.8625	0.8784	0.8561	0.8762	0.8549	0.8776	0.8537	0.8720
B&W 1/3 BP	0.8575	0.8577	0.8544	0.8616	0.8614	0.8734	0.8590	0.8684
B&W No BP	0.8672	0.8796	0.8599	0.8764	0.8529	0.8775	0.8488	0.8690
West. No BP	0.8614	0.8773	0.8521	0.8697	0.8527	0.8771	0.8438	0.8648
High Temperature								
BWR	0.8283	0.8318	0.8406	0.8525	0.7996	0.8165	0.8136	0.8301
B&W BP	0.7912	0.7872	0.7999	0.8085	0.7805	0.7903	0.7954	0.8031
B&W 1/3 BP	0.8069	0.8009	0.8152	0.8159	0.7952	0.8038	0.8086	0.8135
B&W No BP	0.8113	0.8184	0.8227	0.8341	0.7862	0.8033	0.7987	0.8148
West. BP	0.8010	0.8095	0.8121	0.8258	0.7841	0.8017	0.8008	0.8131
West. No BP	0.8368	0.8427	0.8474	0.8562	0.8121	0.8308	0.8243	0.8408

Table 4-26: Values of E_{sum} for 6% Enriched Assembly Models with 8 Square-Design Experiments

Experiment→ Assembly↓	1a	1b	2a	2b	3a	3b	4a	4b
Low Temperature								
BWR	0.8370	0.8571	0.8323	0.8557	0.8342	0.8591	0.8319	0.8560
B&W BP	0.8638	0.8794	0.8610	0.8769	0.8473	0.8708	0.8498	0.8694
B&W 1/3 BP	0.8332	0.8279	0.8304	0.8359	0.8296	0.8340	0.8278	0.8355
B&W No BP	0.8648	0.8769	0.8631	0.8769	0.8445	0.8687	0.8436	0.8620
West. No BP	0.8695	0.8848	0.8639	0.8803	0.8538	0.8791	0.8497	0.8708
High Temperature								
BWR	0.7980	0.8063	0.8153	0.8220	0.7668	0.7834	0.7814	0.7985
B&W BP	0.7762	0.7758	0.7889	0.7942	0.7566	0.7662	0.7743	0.7832
B&W 1/3 BP	0.7733	0.7761	0.7858	0.7898	0.7571	0.7704	0.7696	0.7814
B&W No BP	0.7924	0.7923	0.8073	0.8157	0.7586	0.7750	0.7738	0.7887
West. BP	0.7835	0.7899	0.7976	0.8072	0.7589	0.7767	0.7773	0.7900
West. No BP	0.8027	0.8127	0.8167	0.8252	0.7734	0.7915	0.7897	0.8043

Table 4-27: Values of E_{sum} for 7% Enriched Assembly Models with 8 Square-Design Experiments

Experiment→ Assembly↓	1a	1b	2a	2b	3a	3b	4a	4b
Low Temperature								
BWR	0.8393	0.8642	0.8360	0.8592	0.8279	0.8620	0.8316	0.8598
B&W BP	0.8552	0.8695	0.8548	0.8721	0.8389	0.8584	0.8410	0.8593
B&W 1/3 BP	0.8295	0.8296	0.8309	0.8363	0.8166	0.8300	0.8274	0.8398
B&W No BP	0.8558	0.8660	0.8544	0.8704	0.8343	0.8584	0.8359	0.8540
West. No BP	0.8760	0.8918	0.8727	0.8881	0.8567	0.8823	0.8557	0.8765
High Temperature								
BWR	0.7920	0.7984	0.8095	0.8180	0.7544	0.7756	0.7738	0.7916
B&W BP	0.7602	0.7595	0.7779	0.7806	0.7415	0.7499	0.7605	0.7675
B&W 1/3 BP	0.7218	0.7212	0.7346	0.7379	0.6990	0.7133	0.7218	0.7281
B&W No BP	0.7724	0.7734	0.7876	0.7962	0.7381	0.7551	0.7561	0.7698
West. BP	0.7805	0.7792	0.7944	0.8041	0.7505	0.7648	0.7688	0.7844
West. No BP	0.8032	0.8056	0.8162	0.8235	0.7700	0.7863	0.7862	0.8022

Table 4-28: Values of E_{sum} for 10% Enriched Assembly Models with 8 Square-Design Experiments

Experiment→ Assembly↓	1a	1b	2a	2b	3a	3b	4a	4b
Low Temperature								
BWR	0.8333	0.8490	0.8309	0.8508	0.8200	0.8441	0.8162	0.8352
B&W BP	0.8348	0.8483	0.8401	0.8546	0.8132	0.8357	0.8207	0.8397
B&W 1/3 BP	0.7560	0.7493	0.7632	0.7662	0.7421	0.7559	0.7501	0.7640
B&W No BP	0.8365	0.8506	0.8359	0.8513	0.8088	0.8343	0.8151	0.8355
West. No BP	0.8617	0.8703	0.8612	0.8799	0.8360	0.8631	0.8400	0.8607
High Temperature								
BWR	0.7656	0.7677	0.7842	0.7919	0.7232	0.7415	0.7442	0.7612
B&W BP	0.7281	0.7252	0.7423	0.7446	0.6990	0.7078	0.7164	0.7220
B&W 1/3 BP	0.7029	0.6974	0.7222	0.7202	0.6713	0.6805	0.6879	0.7017
B&W No BP	0.7284	0.7275	0.7437	0.7521	0.6899	0.7040	0.7089	0.7209
West. BP	0.7272	0.7334	0.7415	0.7474	0.6934	0.7125	0.7116	0.7259
West. No BP	0.7586	0.7578	0.7741	0.7798	0.7195	0.7372	0.7399	0.7531

A nuclide-reaction specific analysis was performed to assess the applicability of the square-design experiments to the B&W commercial assemblies. The numbers of the

square-design experiments with *T(E)* values exceeding 0.9 are shown in Table 4-29 through 4-32 for B&W assemblies with enrichments of 4, 6, 7, and 10 wt-% ^{235}U, respectively.

The new experiments provide good coverage for the 4% systems for ^{235}U fission and capture for both low and high temperature conditions. They also provide good coverage for ^{238}U fission for the low temperature configurations. The 0.8-cm pitched experiments provide good coverage for ^{238}U fission for the high temperature assembly configurations.

The poisoned experiments provide good coverage for ^{157}Gd capture for the 1/3 BP low temperature configuration but not for any other BP containing configuration of the commercial assemblies. ^{10}B capture is well covered by the 6 of the 8 experiments, excluding only the 0.8-cm pitched configurations with BP rods.

The experiments do not provide coverage for ^{1}H scattering for any of the 4 wt % configurations. Coverage for ^{1}H capture is provided for only one low temperature configuration by the BP containing experiments.

For the high temperature configurations, all experiments provide coverage for ^{1}H capture for the design systems containing BPs. For the high temperature configuration with no BPs, only the BP containing experiments provide coverage for ^{1}H capture. The presence of boron and/or poison rods and the moderator density in the experiments or design systems has a strong effect on the sensitivity profiles for ^{1}H capture. With increased boron concentrations or decreased moderator densities, the sensitivity of k_{eff} to ^{1}H capture is reduced. Thus, for the low temperature design systems, only the 1/3 BP configuration, which contains 500-ppm boron, is covered by the experiments that contain BPs, which have lower boron concentrations.

The new experiments also provide good coverage for the 6 wt-% ^{235}U commercial assemblies. Each of the 8 experiments provides good coverage for ^{235}U fission for all of the commercial configurations with the exception of the high temperature configuration with BPs. Neither the 0.8-cm pitched experiments with BPs at 20°C nor the 0.855-cm pitched experiments without BPs provide coverage for ^{235}U fission for this configuration. Most of the experiments provide coverage for ^{235}U capture, with the exception of some of the 0.855-cm pitched configurations. The only experiments that validate ^{238}U capture are the 0.8-cm pitched configurations. These only validate ^{238}U capture for the low temperature configurations with no boron (BP and no BP configurations).

Table 4-29: Numbers of 8 Square-Design Experiments with *T(E)* Parameters ≥ 0.9 for B&W 15x15 Assemblies with 4 wt-% ^{235}U

Temperature	Low			High		
Poison	**BP**	**1/3 BP**	**No BP**	**BP**	**1/3 BP**	**No BP**
H-1 capture	0	4	0	8	8	4
H-1 scatter	0	0	0	0	0	0
U-235 fission	8	8	8	8	8	8
U-235 capture	8	8	8	8	8	8
U-238 fission	8	8	8	4	4	6
U-238 capture	0	0	0	0	0	8
B-10 capture		6		6	6	
Gd-157 capture	0	4		0	0	

Table 4-30: Numbers of 8 Square-Design Experiments with *T(E)* Parameters ≥ 0.9 for B&W 15x15 Assemblies with 6 wt-% ^{235}U

Temperature	Low			High		
Poison	**BP**	**1/3 BP**	**No BP**	**BP**	**1/3 BP**	**No BP**
H-1 capture	0	8	0	8	8	8
H-1 scatter	0	0	0	0	0	0
U-235 fission	8	8	8	5	8	8
U-235 capture	6	6	6	7	6	4
U-238 fission	8	6	8	4	4	4
U-238 capture	4	0	4	0	0	0
B-10 capture		6		8	7	8
Gd-157 capture	0	4		0	3	

Table 4-31: Numbers of 8 Square-Design Experiments with *T(E)* Parameters ≥ 0.9 for B&W 15x15 Assemblies with 7 wt-% ^{235}U

Temperature	Low			High		
Poison	**BP**	**1/3 BP**	**No BP**	**BP**	**1/3 BP**	**No BP**
H-1 capture	3	8	3	8	8	8
H-1 scatter	0	0	0	0	0	0
U-235 fission	8	8	8	4	5	8
U-235 capture	6	6	4	6	4	3
U-238 fission	8	6	8	4	4	4
U-238 capture	4	0	5	0	0	0
B-10 capture		6		8	8	8
Gd-157 capture	0	4		0	2	

Table 4-32: Numbers of 8 Square-Design Experiments with *T(E)* Parameters ≥ 0.9 for B&W 15x15 Assemblies with 10 wt-% ^{235}U

Temperature	Low			High		
Poison	**BP**	**1/3 BP**	**No BP**	**BP**	**1/3 BP**	**No BP**
H-1 capture	8	8	8	8	8	8
H-1 scatter	0	0	0	0	0	0
U-235 fission	8	8	8	0	0	1
U-235 capture	3	4	2	1	0	0
U-238 fission	8	4	8	4	4	4
U-238 capture	5	0	6	0	0	0
B-10 capture		8		8	8	
Gd-157 capture	0	4		0	3	

The experiments provide coverage for ^{157}Gd capture for the low temperature and high temperature 1/3 BP configurations except for the 0.855-cm pitched case at 60°C which does not provide coverage for the high temperature configuration. The configurations with only BP assemblies are not covered by the experiments.

As with the 4 wt-% cases, coverage for ^{1}H capture is only provided for the design systems that contain boron.

For the 7 wt-% assemblies, the square-design experiments provide similar coverage as for the 6% assemblies. Three experiments provide ^{1}H capture coverage for the low temperature configurations of the 7 wt-% assemblies. As the enrichment is increased, the importance of ^{1}H capture in the design systems is decreased.

For the 10 wt-% assemblies, the nuclide-reaction specific coverage is somewhat reduced as compared to the lower enriched assemblies. For the low temperature configurations, the coverage is still adequate. For the nuclide-reaction pairs with reduced coverage, the 0.855-cm pitched arrays have been excluded from the coverage. The 0.8-cm pitched arrays still provide good coverage. The experiments provide little coverage for the high temperature configurations at 10% enrichment.

None of the new experiments provide coverage for ^{1}H scatter for any of the design applications. The reason for this is the high neutron leakage caused by the small core size of the experiment design.

The sensitivity profiles for the B&W 15×15 assembly at 7 wt-% ^{235}U at 20°C with no BPs and for the square-design experiment with 0.8-cm pitch at 20°C with no BPs are shown in Figure 4-6. It can be seen from this figure that the sensitivity for ^{1}H scatter for the B&W assembly (red line) is actually negative above resonance energies. In the infinite array geometry, if neutrons are scattered from fission energies into the ^{238}U resonances the scattering will have a negative effect on k_{eff}, especially if the neutrons are scattered below the fast fission cross section for ^{238}U. For the experiment, the reflector creates a strongly positive sensitivity for ^{1}H scatter above the resonance region. If fast neutrons leak from the fuel into the reflector, then are scattered and return to the core, the effect on k_{eff} is positive. Because of these contrary effects, the *T(E)* value relating ^{1}H scatter for these two systems is 0.3798, well below criteria of 0.9. This result is typical for each of these experiments as compared to the infinite array models of the commercial design systems.

Figure 4-7 displays the sensitivity profiles for ^{238}U capture for the B&W assemblies at 7 wt-% ^{235}U with 20 BPs at high and low temperature conditions and the square-design experiment with 0.8-cm pitch at 60°C with 20 BPs. The *T(E)* values for the experiment with these design systems are 0.9522 and 0.7451 for the low and high temperature assemblies, respectively. Because the high temperature assembly contains 500-ppm boron, where the low temperature system contains no boron, and the experiment contains 305-ppm boron, there is a difference in the profiles at thermal energies. At

resonance energies and above, the high temperature assembly (dark blue line) displays a higher (more negative) sensitivity than do the other systems because of the Doppler broadening of the ^{238}U capture resonances.

Figure 4-8 displays the sensitivity profiles for ^{235}U fission for the B&W assemblies at 7 wt-% ^{235}U with 20 BPs at low and high temperature conditions and the square-design experiment with 0.8-cm pitch at 60°C with 20 BPs. The *T(E)* values for the experiment with these design systems are 0.9849 and 0.9095 for the low and high temperature assemblies, respectively. Thus, the *T(E)* value for this experiment when compared to the high temperature assembly just exceeds the criteria of 0.9 used here. It fails the 0.95 criteria used in previous studies.

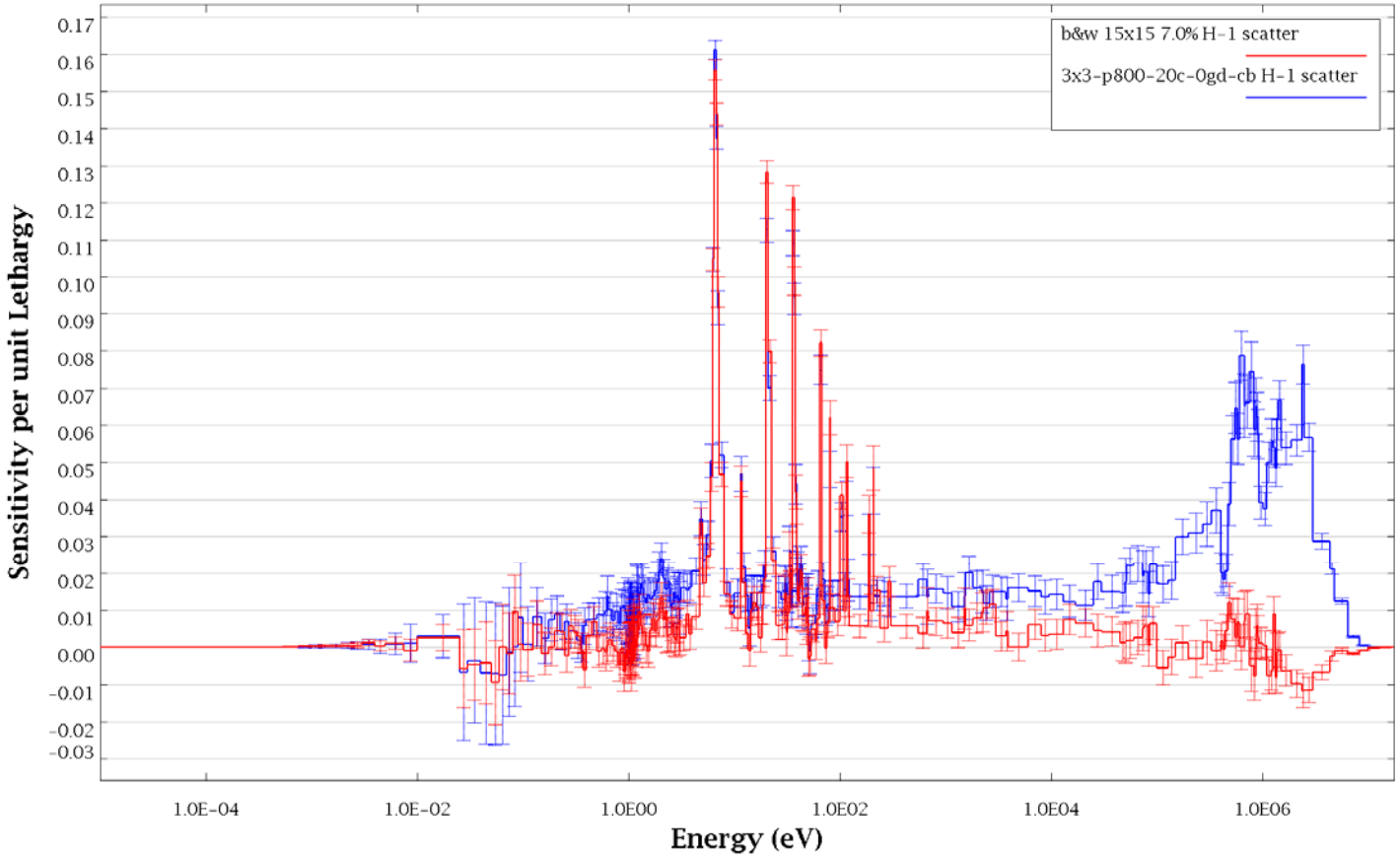

Figure 4-6: Sensitivity Profiles for ^{1}H Scattering for B&W Assembly at 7 wt-% Enrichment at 20°C with no BPs and Square-Design Experiment with 0.8-cm pitch at 20°C with no BPs

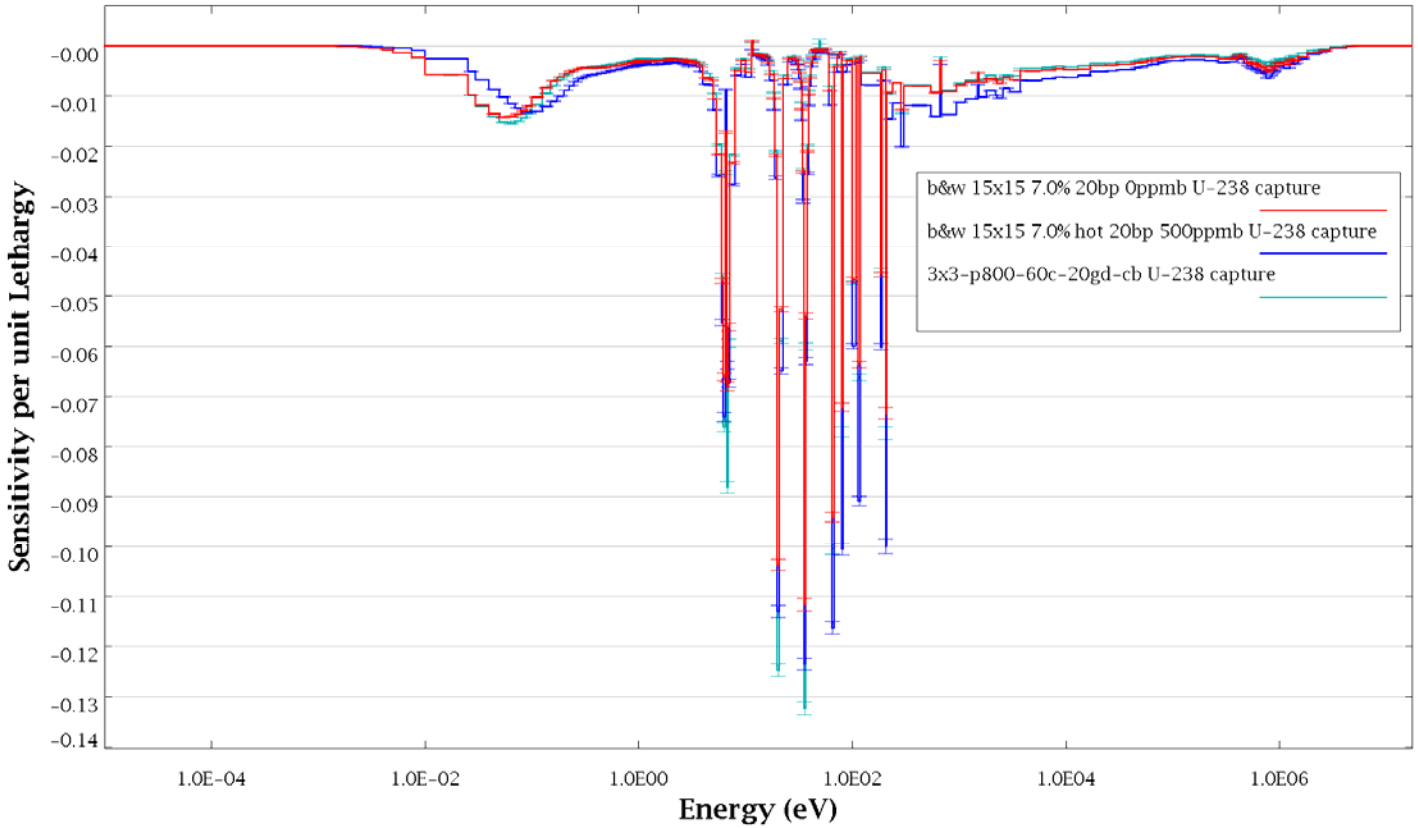

Figure 4-7: Sensitivity Profiles for ^{238}U capture for B&W Assemblies with 7wt-% ^{235}U and 20 BPs at Low and High Temperature Conditions and Square-Design Experiment with 0.8-cm Pitch at 60°C and 20 BPs

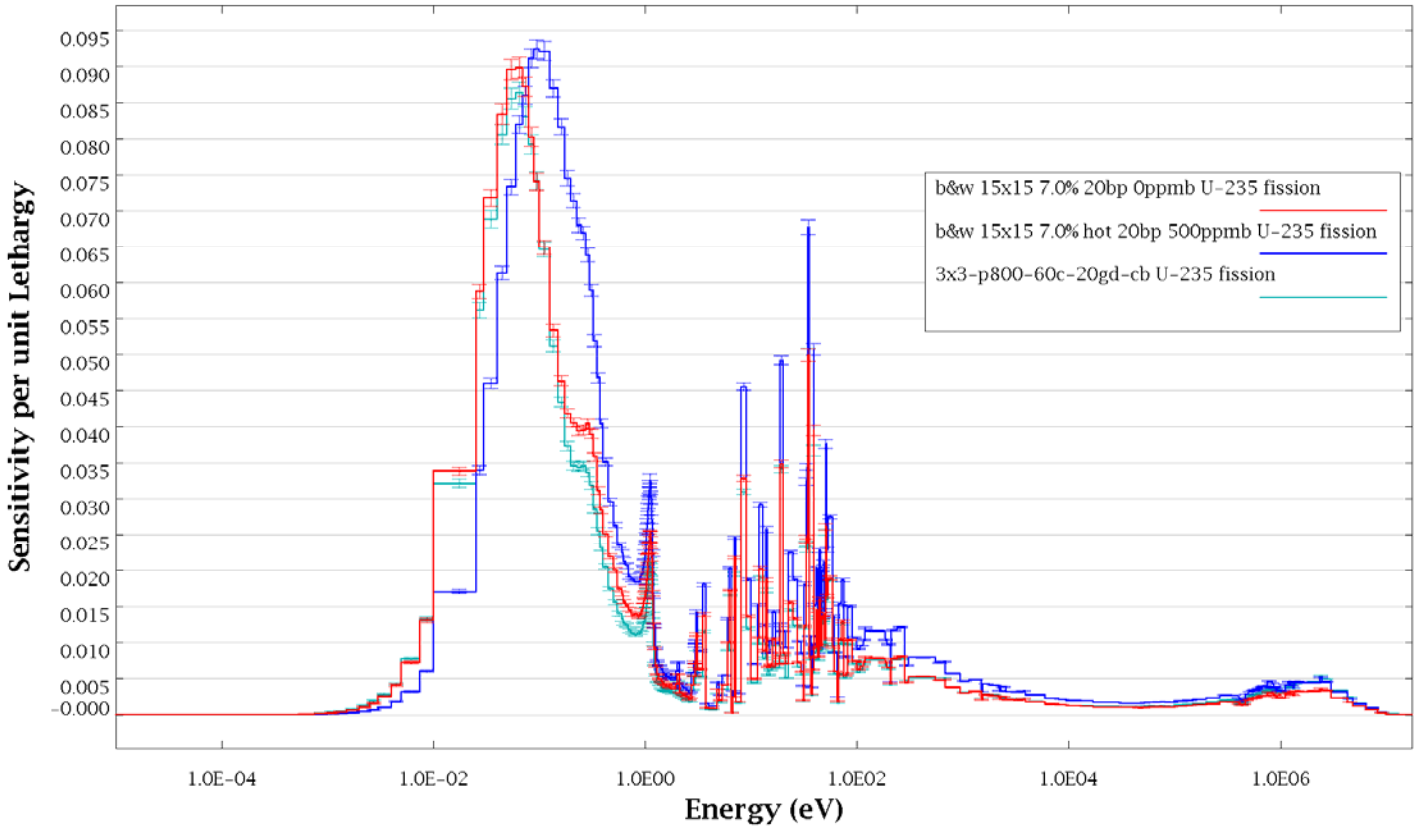

Figure 4-8: Sensitivity Profiles for ^{235}U fission for B&W Assemblies with 7wt-% ^{235}U and 20 BPs at Low and High Temperature Conditions and Square-Design Experiment with 0.8-cm Pitch at 60°C and 20 BPs

5. Fuel Facility Scoping Analysis

In addition to the experiment program, this project included an evaluation of typical fuel-processing operations to determine the limits and restrictions required for fabricating higher-enriched fuel. The team used MCNP to determine these limits.

Under the NERI program, research is being funded to develop innovative nuclear fuel and plant designs. Some of these designs proposed uranium fuel enrichments greater than the 5-wt% enrichment level currently approved for the commercial nuclear industry. The research programs on thoria fuel designs have proposed uranium enrichments up to 19.9-wt%. Similarly, cermet fuel designs have been proposed as high as 10-wt% uranium or higher. Some gas-cooled reactors being proposed would operate with nuclear fuel in the range of 8 to 10-wt% enriched uranium. In addition, the current generation of light water reactors (LWRs) is considering using fuel above the 5-wt% limit for their multi-year fuel cycles at up-rated powers.

Battelle Columbus[5,6] documented a study for the Department of Energy on the nuclear safety of the 30B and 48X UF_6 shipping container for enrichments to 20% ^{235}U. The study included the associated processes and equipment at the gaseous diffusion plant formerly located in Portsmouth, Ohio. The study concluded that the 30B cylinders are subcritical both individually and in infinite storage array filled with UF_6 when stacked one high under moderation control at a ^{235}U enrichment of 10%. The study also concluded that only minor modifications were necessary to the Portsmouth facility to handle the enriched fuel.

For this evaluation, the team performed MCNP scoping calculations to review the sizing of criticality safe processing equipment. For purposes of this study, the team used the traditional criticality safety analysis criteria that configurations are considered safe if the predicted value of k_{eff} is less than 0.95 with a 95 percent confidence level.

A diagram of the fuel cycle is shown in Figure 5-1. The project focused on each of the steps from shipment of UF_6 to storage of the spent fuel in the spent fuel storage pool.

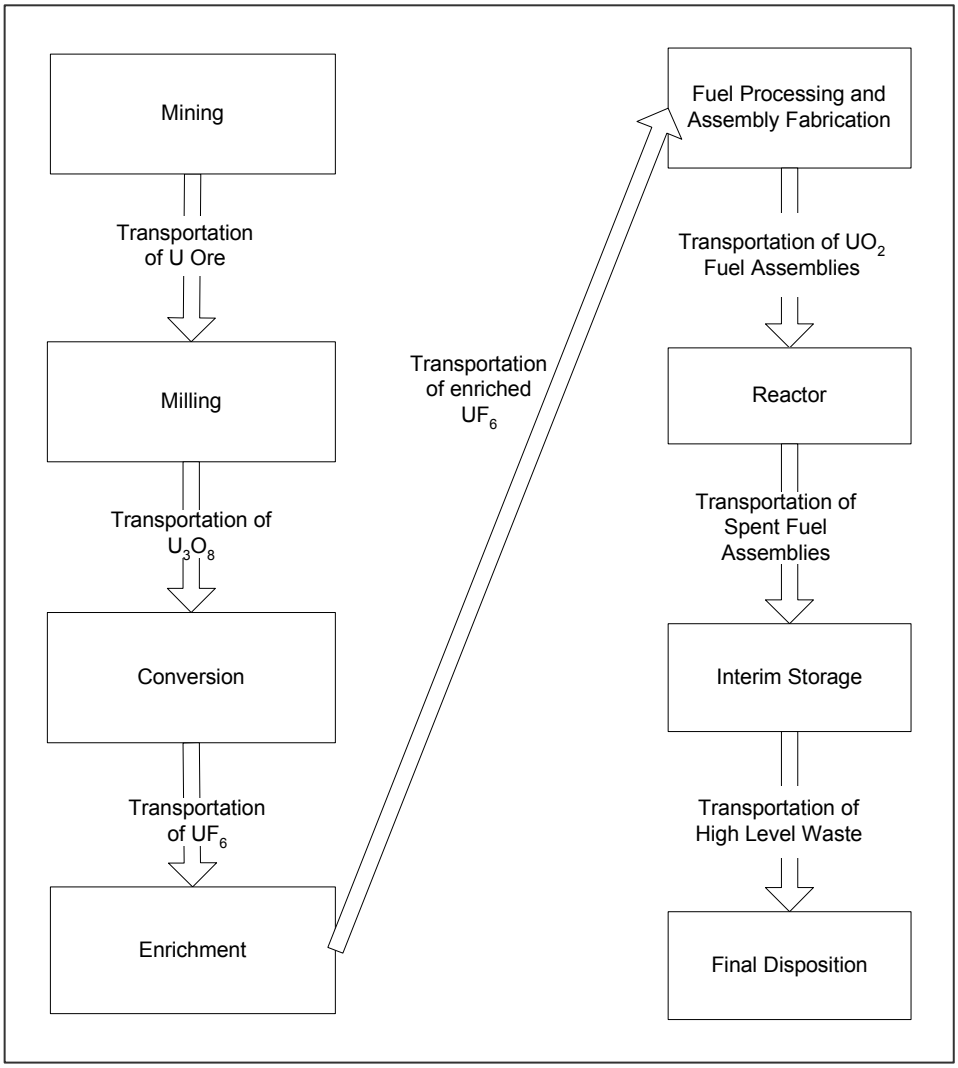

Figure 5-1: The once-through nuclear fuel cycle.

5.1 Fuel Cycle Analysis

The initial fuel processing operation is the enriching of the uranium either in a gaseous diffusion plant or a gaseous centrifuge plant. The uranium is processed as UF_6 and is stored and shipped to the commercial nuclear fuel processing as UF_6.

5.1.1 Receipt of Fuel in 30B Cylinders

The effects of enrichment on the storage and shipping of LEU material has been covered adequately in Reference 5 and 6.

Commercial fuel fabricators typically receive UF_6 in 30B cylinders. A 30B cylinder has a nominal diameter of 30 inches and a nominal length of 81.5 inches. A steel skirt extends 5 inches from the cylinder head to protect the cylinder and the valve. Only 76 inches of the 81.5-inch nominal length of the cylinder contain UF_6.

For the purposes of this analysis, the cylinder is modeled as a right circular cylinder. The maximum permissible cylinder fill weight of UF_6 is 2,277 kg. More material can be physically placed in the cylinder during filling, but adding material beyond this weight limit increases the possibility of hydraulically rupturing the cylinder on subsequent reheating.

During the withdrawal of UF_6, operating procedures require that condenser pressures and temperatures be near those of saturated UF_6 to assure that impurities are not present. The gaseous diffusion cascade consistently produces high-purity UF_6 (i.e. greater than 99.5 weight percent UF_6). For nuclear criticality safety purposes, all impurities are conservatively assumed to be HF. Assuming that UF_6 is 99.5 pure weight percent and that the other 0.5 weight percent is HF, an H/U atomic ratio of 0.088 is obtained.

A worst case scenario was modeled in which solid UF_6, moderated by HF (at an H/U ratio of 0.088), filled the cylinder to the top. The model included a 2-foot water reflector around the cylinder. The results of this analysis are shown in Table 5-1. These results indicate that the 30B container can carry enriched UF_6 up to at least 15-wt% ^{235}U.

Table 5-1: Results of MCNP4c2 Calculations of UF_6 in a 30B cylinder with 2 ft water Reflector

wt% ^{235}U	k_{eff}	σ
5	0.57460	0.00031
7	0.65893	0.00033
10	0.75998	0.00038
12	0.81805	0.00038
15	0.89126	0.00041
17	0.93369	0.00037
20	0.99295	0.00043

A worst-case scenario in which the 30B container was filled to the top with solid UF_6, moderated by HF (at an H/U ratio of 0.088) was evaluated. A 2-foot water reflector was modeled around the cylinder. The results from this analysis are shown in Table 5-5. The results for this accident scenario would limit the 30B container to carrying UF_6 enriched to a maximum of 18.25-wt% ^{235}U, for a maximum H/U ratio of 0.088. A loss of moderation control in the enriching process would increase this ratio and further limit the allowable ^{235}U enrichment.

Table 5-2: Results of MCNP4c2 Calculations of a 30B Container Completely Filled with UF_6 with 2-ft Water Reflector

Filename	wt% ^{235}U	k_{eff}	σ
b305	5	0.57031	0.00033
b306	6	0.61327	0.00049
b307	7	0.65232	0.00053
b308	8	0.68847	0.00060
b309	9	0.72363	0.00058
b3010	10	0.75389	0.00058
b3011	11	0.78333	0.00054
b3012	12	0.80948	0.00056
b3013	13	0.83408	0.00057
b3014	14	0.85927	0.00063
b3015	15	0.88431	0.00058
b3016	16	0.90482	0.00062
b3017	17	0.92582	0.00061
b3018	18	0.94547	0.00064
b3018b	18.25	0.95025	0.00066
b3019	19	0.96506	0.00063
b3020	20	0.99098	0.00063

Additional models were developed to represent a completely full 30B container on its side, lying on a 1-ft concrete slab, surrounded by 2 feet of air, water, or water vapor of

varying densities. The results of these calculations are shown in Tables 5-3 through 5-12.

Table 5-3: Results of MCNP4c2 Calculations of a 30B Container Completely Filled with UF_6 on a Concrete Slab with 20 ºC Water Reflector

Filename	wt% ^{235}U	k_{eff}	σ
b305d	5	0.57194	0.00049
b306d	6	0.61519	0.00048
b307d	7	0.65424	0.00049
b308d	8	0.69178	0.00052
b309d	9	0.72532	0.00055
b3010d	10	0.75582	0.00051
b3011d	11	0.78486	0.00055
b3012d	12	0.81114	0.00060
b3013d	13	0.83859	0.00052
b3014d	14	0.86272	0.00062
b3015d	15	0.88543	0.00057
b3016d	16	0.90797	0.00065
b3017d	17	0.92859	0.00064
b3018d	18	0.95029	0.00064
b3019d	19	0.96750	0.00058
b3020d	20	0.98585	0.00062

Table 5-4: Results of MCNP4c2 Calculations of a 30B Container Completely Filled with UF_6 on a Concrete Slab with 0.8 g/cm^3 Water Vapor Reflector

Filename	wt% ^{235}U	k_{eff}	σ
b305e	5	0.57022	0.00045
b306e	6	0.61421	0.00049
b307e	7	0.65359	0.00055
b308e	8	0.69038	0.00053
b309e	9	0.72460	0.00052
b3010e	10	0.75550	0.00053
b3011e	11	0.78455	0.00059
b3012e	12	0.81088	0.00060
b3013e	13	0.83649	0.00057
b3014e	14	0.86129	0.00058
b3015e	15	0.88374	0.00063
b3016e	16	0.90825	0.00066
b3017e	17	0.92868	0.00057
b3018e	18	0.94838	0.00064
b3019e	19	0.96720	0.00059
b3020e	20	0.98665	0.00061

Table 5-5: Results of MCNP4c2 Calculations of a 30B Container Completely Filled with UF_6 on a Concrete Slab with 0.6 g/cm^3 Water Vapor Reflector

Filename	wt% ^{235}U	k_{eff}	σ
b305f	5	0.56753	0.00052
b306f	6	0.61223	0.00053
b307f	7	0.65269	0.00052
b308f	8	0.68878	0.00052
b309f	9	0.72280	0.00052
b3010f	10	0.75374	0.00057
b3011f	11	0.78172	0.00058
b3012f	12	0.81103	0.00056
b3013f	13	0.83639	0.00058
b3014f	14	0.86020	0.00063
b3015f	15	0.88394	0.00058
b3016f	16	0.90547	0.00059
b3017f	17	0.92740	0.00058
b3018f	18	0.94607	0.00071
b3019f	19	0.96644	0.00060
b3020f	20	0.98594	0.00058

Table 5-6: Results of MCNP4c2 Calculations of a 30B Container Completely Filled with UF_6 on a Concrete Slab with 0.5 g/cm^3 Water Vapor Reflector

Filename	wt% ^{235}U	k_{eff}	σ
b305g	5	0.56697	0.00051
b306g	6	0.61071	0.00050
b307g	7	0.65055	0.00054
b308g	8	0.68846	0.00057
b309g	9	0.72135	0.00053
b3010g	10	0.75312	0.00058
b3011g	11	0.78243	0.00053
b3012g	12	0.81000	0.00058
b3013g	13	0.83389	0.00058
b3014g	14	0.85925	0.00061
b3015g	15	0.88134	0.00062
b3016g	16	0.90409	0.00065
b3017g	17	0.92588	0.00057
b3018g	18	0.94822	0.00057
b3019g	19	0.96546	0.00069
b3020g	20	0.98390	0.00065

Table 5-7: Results of MCNP4c2 Calculations of a 30B Container Completely Filled with UF_6 on a Concrete Slab with 0.4 g/cm^3 Water Vapor Reflector

Filename	wt% ^{235}U	k_{eff}	σ
b305h	5	0.56520	0.00050
b306h	6	0.60901	0.00051
b307h	7	0.64947	0.00047
b308h	8	0.68634	0.00051
b309h	9	0.71908	0.00058
b3010h	10	0.74943	0.00054
b3011h	11	0.78008	0.00061
b3012h	12	0.80628	0.00056
b3013h	13	0.83277	0.00062
b3014h	14	0.85763	0.00055
b3015h	15	0.88040	0.00063
b3016h	16	0.90215	0.00061
b3017h	17	0.92373	0.00063
b3018h	18	0.94521	0.00065
b3019h	19	0.96361	0.00065
b3020h	20	0.98267	0.00063

Table 5-8: Results of MCNP4c2 Calculations of a 30B Container Completely Filled with UF_6 on a Concrete Slab with 0.3 g/cm^3 Water Vapor Reflector

Filename	wt% ^{235}U	k_{eff}	σ
b305i	5	0.56149	0.00047
b306i	6	0.60533	0.00050
b307i	7	0.64562	0.00052
b308i	8	0.68399	0.00049
b309i	9	0.71593	0.00052
b3010i	10	0.74657	0.00053
b3011i	11	0.77722	0.00052
b3012i	12	0.80469	0.00058
b3013i	13	0.82981	0.00061
b3014i	14	0.85444	0.00063
b3015i	15	0.87856	0.00063
b3016i	16	0.90016	0.00055
b3017i	17	0.92129	0.00057
b3018i	18	0.94043	0.00062
b3019i	19	0.96199	0.00058
b3020i	20	0.98050	0.00070

Table 5-9: Results of MCNP4c2 Calculations of a 30B Container Completely Filled with UF_6 on a Concrete Slab with 0.2 g/cm^3 Water Vapor Reflector

Filename	wt% ^{235}U	k_{eff}	σ
b305j	5	0.55457	0.00046
b306j	6	0.59920	0.00051
b307j	7	0.64016	0.00051
b308j	8	0.67693	0.00053
b309j	9	0.71010	0.00058
b3010j	10	0.74272	0.00054
b3011j	11	0.77189	0.00058
b3012j	12	0.79945	0.00059
b3013j	13	0.82437	0.00064
b3014j	14	0.84929	0.00060
b3015j	15	0.87289	0.00064
b3016j	16	0.89573	0.00058
b3017j	17	0.91785	0.00060
b3018j	18	0.93828	0.00062
b3019j	19	0.95698	0.00062
b3020j	20	0.97530	0.00065

Table 5-10: Results of MCNP4c2 Calculations of a 30B Container Completely Filled with UF_6 on a Concrete Slab with 0.1 g/cm^3 Water Vapor Reflector

Filename	wt% ^{235}U	k_{eff}	σ
b305k	5	0.54037	0.00045
b306k	6	0.58501	0.00053
b307k	7	0.62553	0.00049
b308k	8	0.66298	0.00053
b309k	9	0.69705	0.00050
b3010k	10	0.73027	0.00055
b3011k	11	0.75872	0.00053
b3012k	12	0.78718	0.00055
b3013k	13	0.81271	0.00063
b3014k	14	0.83904	0.00059
b3015k	15	0.86154	0.00059
b3016k	16	0.88434	0.00058
b3017k	17	0.90487	0.00063
b3018k	18	0.92660	0.00062
b3019k	19	0.94577	0.00067
b3020k	20	0.96504	0.00065

Table 5-11: Results of MCNP4c2 Calculations of a 30B Container Completely Filled with UF_6 on a Concrete Slab with 0.01 g/cm^3 Water Vapor Reflector

Filename	wt% ^{235}U	k_{eff}	σ
b305l	5	0.50122	0.00041
b306l	6	0.54693	0.00042
b307l	7	0.58779	0.00050
b308l	8	0.62545	0.00051
b309l	9	0.65959	0.00048
b3010l	10	0.69221	0.00050
b3011l	11	0.72277	0.00055
b3012l	12	0.75150	0.00057
b3013l	13	0.77727	0.00056
b3014l	14	0.80371	0.00059
b3015l	15	0.82810	0.00052
b3016l	16	0.85028	0.00062
b3017l	17	0.87134	0.00063
b3018l	18	0.89460	0.00058
b3019l	19	0.91325	0.00058
b3020l	20	0.93398	0.00068

One further model was developed in which the 30B container was only filled to the allowable limit and was on its side lying on a 1-ft concrete slab surrounded by 2 feet of air. The result of this analysis is shown in Table 5-12.

Table 5-12: Results of MCNP4c2 Calculations of a 30B Container Completely Filled with UF_6 on a Concrete Slab with Air Reflector

Filename	wt% ^{235}U	k_{eff}	σ
b305b	5	0.38112	0.00039
b306b	6	0.41535	0.00041
b307b	7	0.44641	0.00042
b308b	8	0.47495	0.00045
b309b	9	0.50156	0.00049
b3010b	10	0.52742	0.00049
b3011b	11	0.55098	0.00050
b3012b	12	0.57327	0.00050
b3013b	13	0.59567	0.00053
b3014b	14	0.61516	0.00055
b3015b	15	0.63498	0.00053
b3016b	16	0.65465	0.00057
b3017b	17	0.67282	0.00057
b3018b	18	0.69094	0.00057
b3019b	19	0.70846	0.00057
b3020b	20	0.72535	0.00062

Figure 5-2 clearly shows the full UF_6 30B container bounds the partially filled container and is conservative to use in future cases. As shown in Figure 5-3, for the case of a single container on a concrete slab the bounding case is the use of a water reflector at 20 ºC. This limits the 30B container to carrying enriched UF_6 to just under 18-wt% ^{235}U.

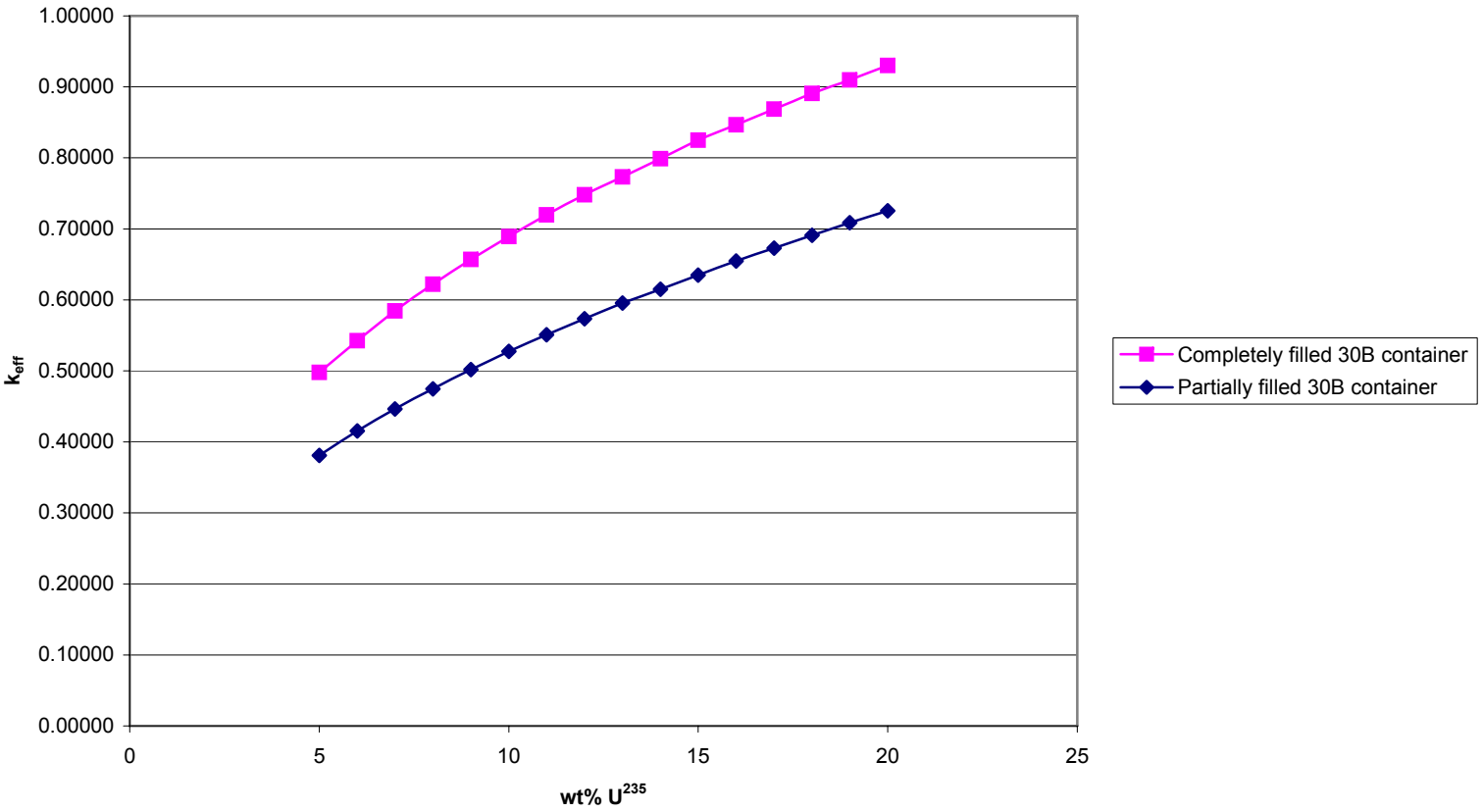

Figure 5-2: Comparison of k_{eff} vs wt% ^{235}U of Full and Partially Filled 30B UF_6 Container on a Concrete Slab with Air Reflector

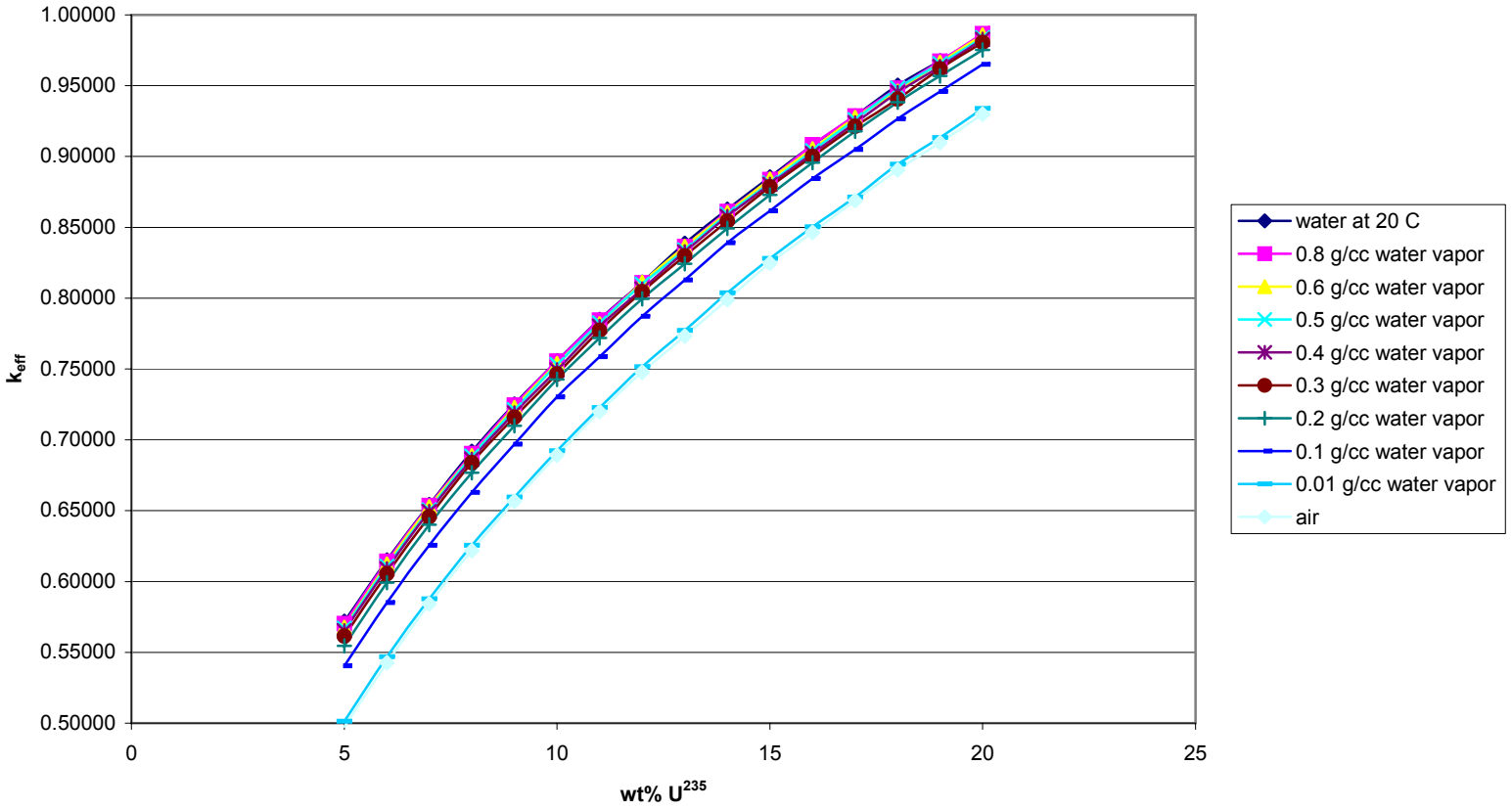

Figure 5-3: Comparison of k_{eff} vs wt% ^{235}U of Full and Partially Filled 30B UF_6 Container on a Concrete Slab with Varying Reflectors

The previous models considered a single 30B UF_6 container, used to store and ship enriched UF_6. The following discussion addresses an infinite horizontal array, stacked two high in a triangular pitch, placed on a 1 ft concrete slab and are shown in Figure 5-4. Various moderators consisting of air, water, or water vapor of varying densities were modeled.

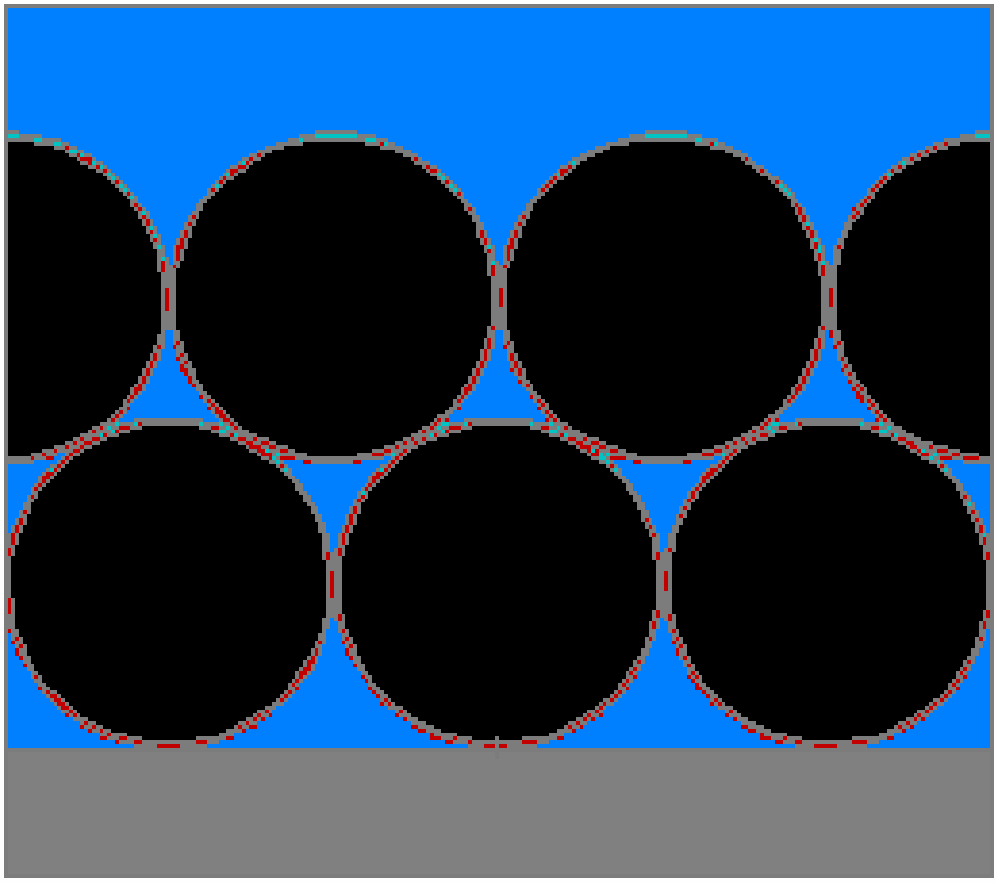

Figure 5-4: Side View of Triangular Pitch Array of UF_6 Filled 30B Containers

Figure 5-5 shows the results of the infinite triangular pitch array of 30B containers. The most limiting moderators were the 0.2 and 0.3 g/cm^3 vapor cases. At lower enrichments (below 10 wt% ^{235}U) the 0.2 g/cm^3 case is more limiting. At the higher enrichments the 0.3 g/cm^3 case becomes more limiting. These cases show that the 30B container would be limited to carrying enriched UF_6 of 10 wt% or less of ^{235}U which would be enough for

the commercial gas centrifuge uranium enrichment the United States Enrichment Corporation (USEC) plans to develop and build.

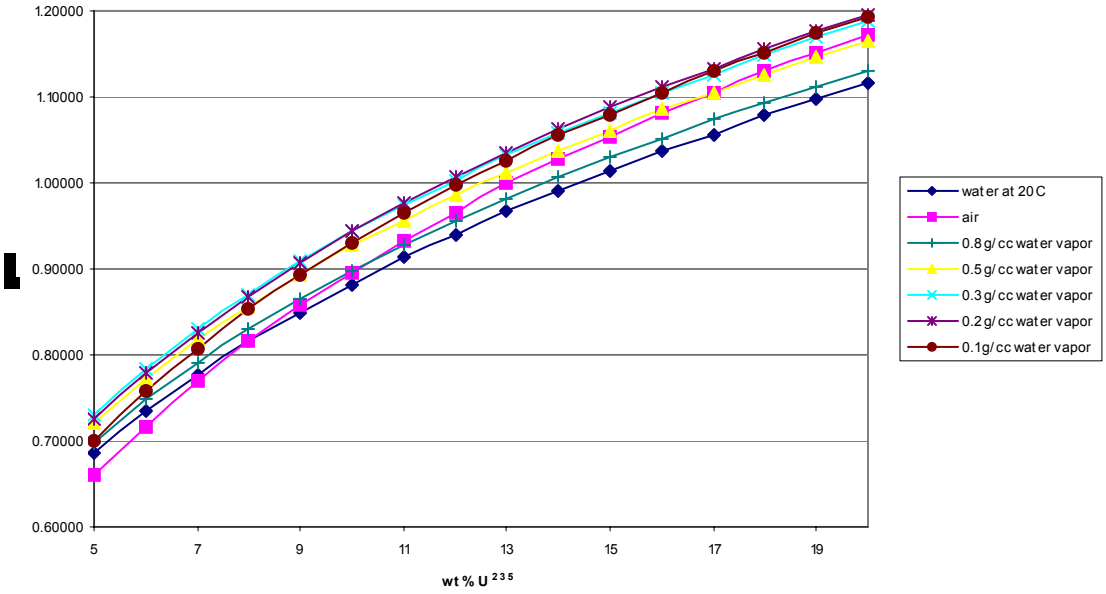

Figure 5-5: Infinite Triangular Pitch Array

5.1.2 Conversion Facility

Currently, in the United States, there are three fuel fabrication facilities, which are capable of converting the UF_6 gas to solid UO_2. These facilities and their processes licensed are:

(1) Westinghouse Electric Company LLC – Columbia Fuel Fabrication Facility located in Columbia, South Carolina. Two processes are installed at the CFF for converting UF_6 to UO_2 powder: the ammonium diuranate (ADU) process and the integrated dry route process. However, the integrated dry route process has been mothballed. The CFFF holds a license from the U.S. Nuclear Regulatory Commission (NRC) (SNM-1107; Docket No. 70-1151).

(2) AREVA NP Inc. – Engineering and Manufacturing Facility located in Richland, Washington. The AREVA facility processes uranium using dry conversion. The Engineering and Manufacturing Facility holds a license from the NRC (SNM-1227; Docket No. 70-1257).

(3) Global Nuclear Fuel – Americas (GNF-A) LLC located in Wilmington, North Carolina. The GNF-A holds a license from the NRC (SNM-1097; Docket No. 70-1113).

Figure 5-6 shows a flow chart of the ADU process used by Westinghouse and Global Nuclear Fuel for UF_6 conversion to UO_2.

For this evaluation, the models of the ADU process equipment used typical plant processing equipment dimensions, which will ensure nuclear criticality safety in the wet processing of 20-wt% ^{235}U uranium regardless of the values of any other parameters in the system. A pipe is modeled conservatively as a cylinder of infinite length. Further conservatism is introduced by assuming that the pipe is surrounded by an annular thickness of 1 foot of water, providing moderation and reflection of neutrons that leak out the side of the pipe. The material assumed will be a homogeneous slurry of UO_2 + H_2O. In a system which does not process elemental uranium, a slurry of uranium dioxide provides maximum reactivity.

Tables 5-13 through 5-15 present the cases analyzed using MCNP4c2, to determine the values of k_{eff} for 6, 8, and 10-inch (where applicable) diameter schedule 40ST SS piping of infinite length surrounded by one foot of water. These results are presented graphically in Figures 5-7 through 5-9. The results show that without moderation control, up to 10-wt% ^{235}U can be processed in an 8-inch pipe and 20-wt% ^{235}U can be processed in a 6-inch pipe.

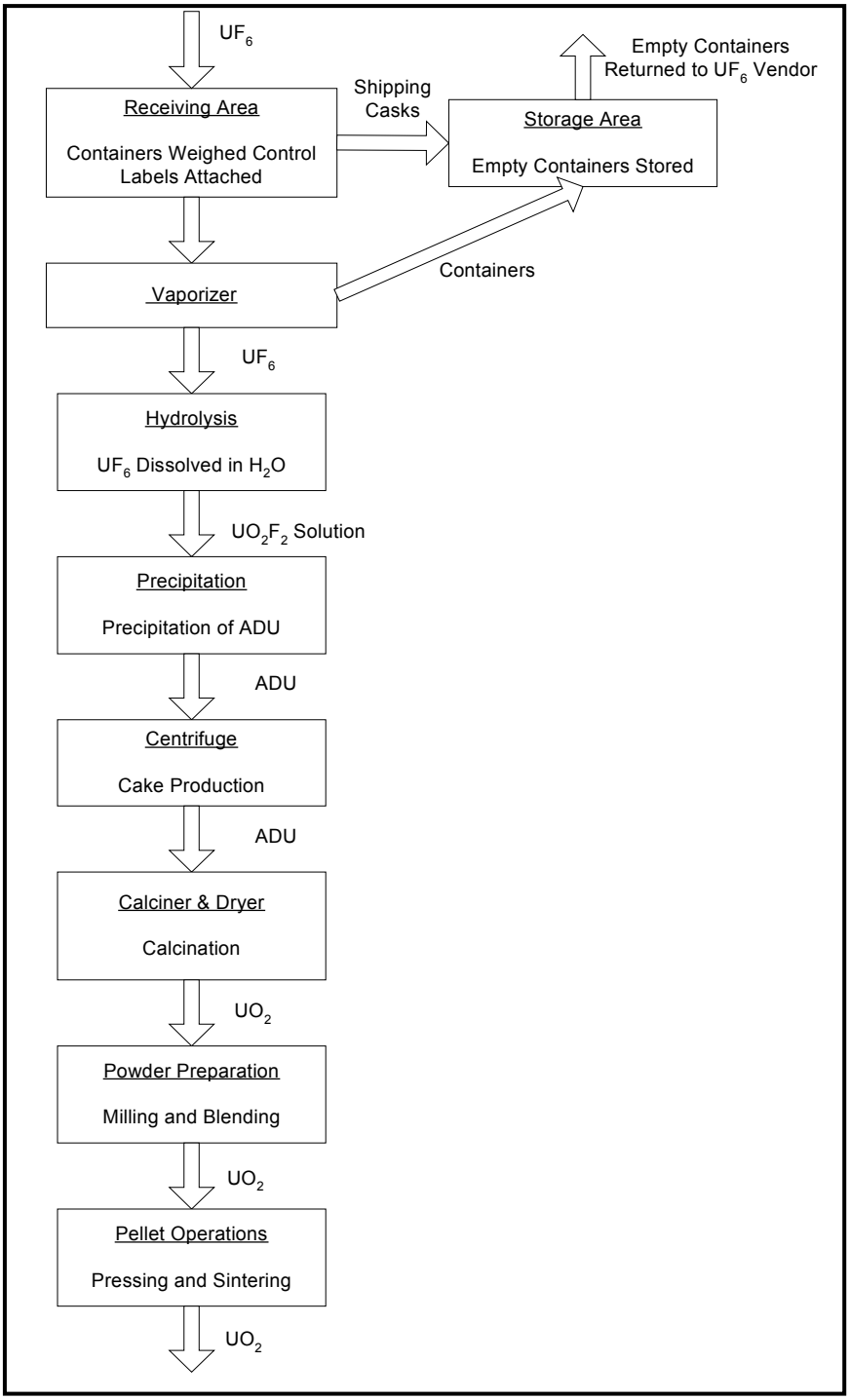

Figure 5-6: ADU Process Flowchart

Table 5-13: Results of MCNP4c2 Calculations for Water/UO_2 Slurry in a 6-inch Pipe

Density	5 wt%		7 wt%		10 wt%		15 wt%		20 wt%	
(gU/cm^3)	k_{eff}	σ	k_{eff}	σ	k_{eff}	σ	k_{eff}	σ	k_{eff}	σ
2.054	0.6855	0.0005	0.7376	0.0005	0.7837	0.0006	0.8294	0.0006	0.8572	0.0006
1.880	0.6815	0.0005	0.7364	0.0005	0.7861	0.0005	0.8322	0.0006	0.8606	0.0008
1.700	0.6758	0.0005	0.7342	0.0005	0.7866	0.0006	0.8345	0.0006	0.8638	0.0006
1.500	0.6668	0.0005	0.7277	0.0005	0.7827	0.0005	0.8366	0.0005	0.8664	0.0006
1.400	0.6609	0.0005	0.7238	0.0005	0.7814	0.0005	0.8353	0.0006	0.8678	0.0006
1.280	0.6510	0.0005	0.7158	0.0005	0.7762	0.0006	0.8336	0.0006	0.8676	0.0006
1.200	0.6436	0.0005	0.7111	0.0005	0.7729	0.0005	0.8327	0.0005	0.8676	0.0005
1.014	0.6207	0.0004	0.6926	0.0005	0.7600	0.0005	0.8239	0.0006	0.8621	0.0006
0.900	0.6017	0.0004	0.6775	0.0005	0.7476	0.0005	0.8163	0.0005	0.8570	0.0006
0.800	0.5828	0.0004	0.6603	0.0005	0.7343	0.0005	0.8068	0.0005	0.8511	0.0006
0.701	0.5581	0.0004	0.6377	0.0005	0.7167	0.0005	0.7938	0.0005	0.8408	0.0006
0.601	0.5282	0.0004	0.6096	0.0004	0.6929	0.0005	0.7752	0.0005	0.8258	0.0006

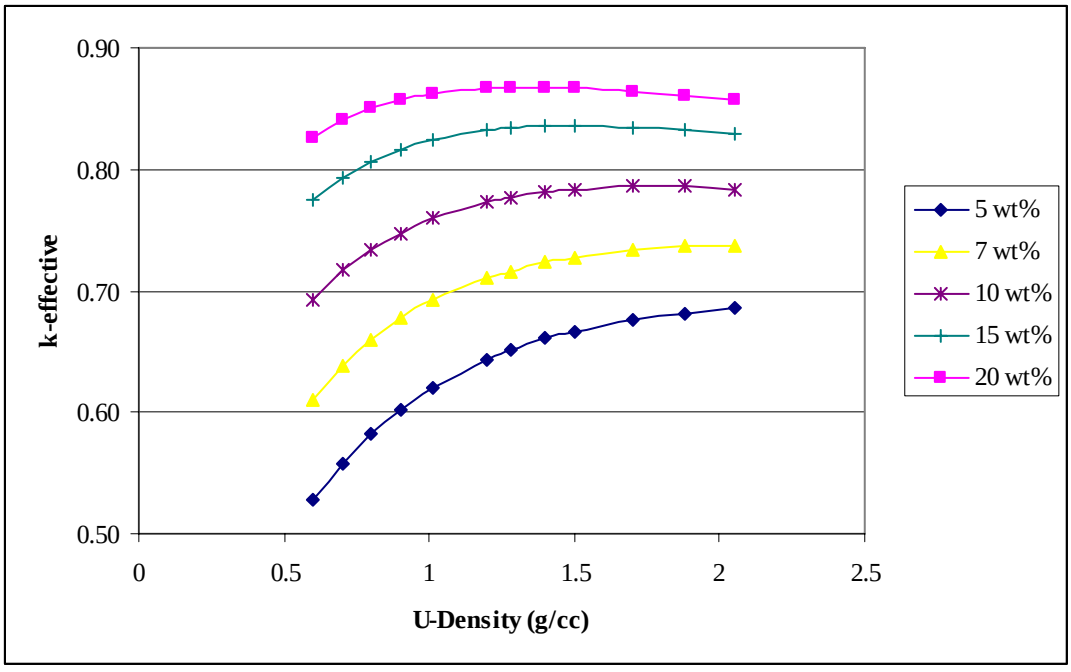

Figure 5-7: k_{eff} vs. U concentration for UO_2 in water slurry in a SS 40ST 6-inch pipe

Table 5-14: Results of MCNP4c2 Calculations for Water/UO_2 Slurry in a 8-inch Pipe

Density	5 wt%		7 wt%		10 wt%		15 wt%		20 wt%	
(gU/cm^3)	k_{eff}	σ	k_{eff}	σ	k_{eff}	σ	k_{eff}	σ	k_{eff}	σ
2.054	0.8317	0.0005	0.8871	0.0006	0.9357	0.0006	0.9803	0.0006	1.0086	0.0006
1.880	0.8303	0.0005	0.8888	0.0005	0.9388	0.0006	0.9869	0.0006	1.0134	0.0006
1.700	0.8258	0.0005	0.8864	0.0005	0.9409	0.0006	0.9907	0.0006	1.0196	0.0006
1.500	0.8173	0.0005	0.8831	0.0005	0.9413	0.0005	0.9940	0.0005	1.0247	0.0006
1.400	0.8112	0.0005	0.8797	0.0005	0.9395	0.0006	0.9948	0.0006	1.0276	0.0006
1.280	0.8022	0.0005	0.8732	0.0005	0.9374	0.0005	0.9955	0.0006	1.0271	0.0006
1.200	0.7954	0.0005	0.8683	0.0005	0.9337	0.0006	0.9949	0.0006	1.0293	0.0006
1.014	0.7711	0.0005	0.8509	0.0005	0.9221	0.0005	0.9884	0.0006	1.0277	0.0006
0.900	0.7522	0.0004	0.8346	0.0005	0.9110	0.0006	0.9817	0.0006	1.0241	0.0006
0.800	0.7301	0.0005	0.8170	0.0005	0.8970	0.0005	0.9728	0.0006	1.0178	0.0006
0.701	0.7043	0.0004	0.7944	0.0005	0.8788	0.0005	0.9606	0.0005	1.0103	0.0006
0.601	0.6702	0.0004	0.7642	0.0005	0.8552	0.0005	0.9451	0.0005	0.9960	0.0006

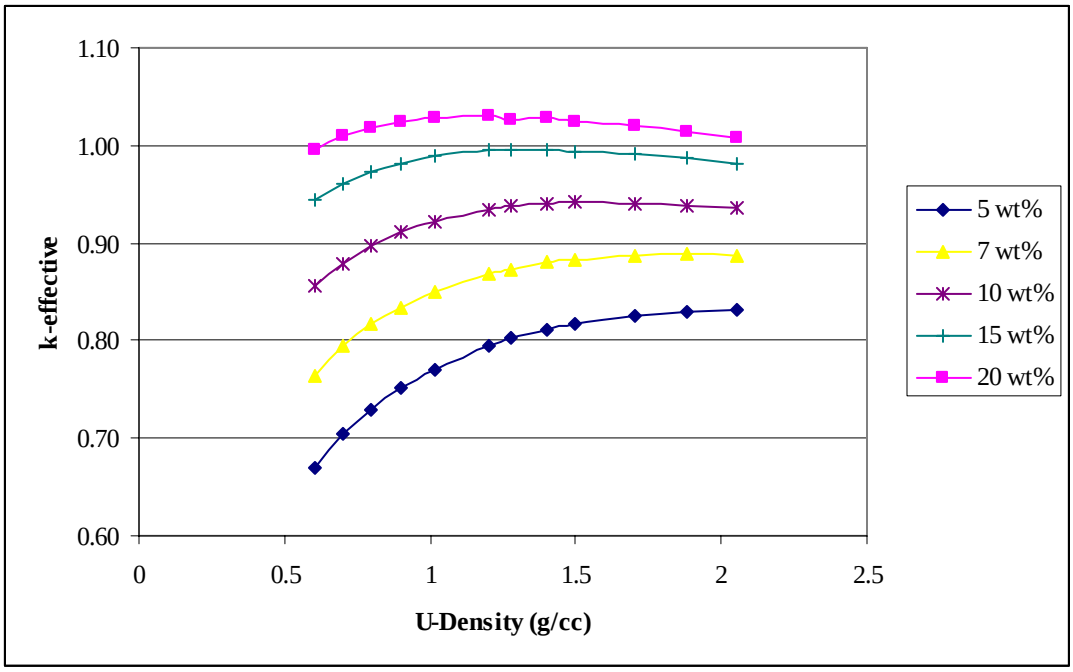

Figure 5-8: k_{eff} vs. U concentration for UO_2 in water slurry in a SS 40ST 8-inch pipe

Table 5-15: Results of MCNP4c2 Calculations for Water/UO_2 Slurry in a 10-inch Pipe

Density (gU/cm^3)	5 wt%		7 wt%	
	k_{eff}	σ	k_{eff}	σ
2.054	0.9509	0.0005	1.0075	0.0005
1.880	0.9507	0.0005	1.0103	0.0006
1.700	0.9460	0.0005	1.0091	0.0005
1.500	0.9390	0.0005	1.0074	0.0006
1.400	0.9341	0.0005	1.0050	0.0005
1.280	0.9255	0.0005	0.9983	0.0005
1.200	0.9171	0.0005	0.9938	0.0005
1.014	0.8938	0.0005	0.9768	0.0006
0.900	0.8732	0.0004	0.9607	0.0005
0.800	0.8508	0.0005	0.9428	0.0005
0.701	0.8222	0.0004	0.9196	0.0005
0.601	0.7871	0.0004	0.8884	0.0005

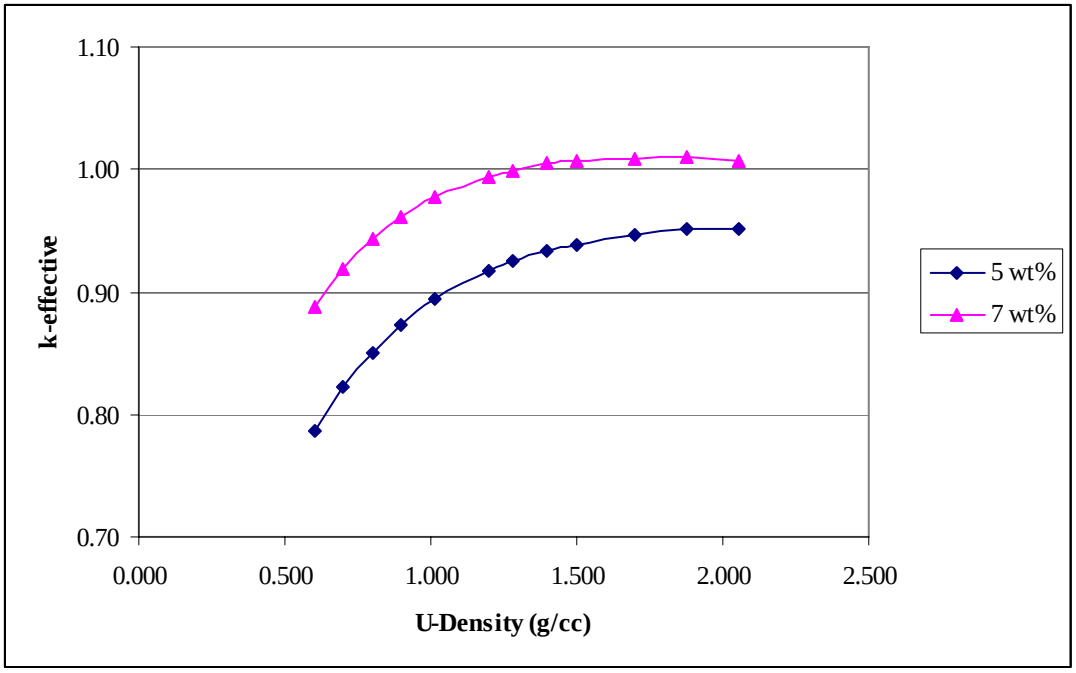

Figure 5-9: k_{eff} vs. U concentration for UO_2 in water slurry in a SS 40ST 10-inch pipe

As stated previously, Westinghouse and Global Nuclear Fuel use wet processing to convert UF_6 to UO_2. However, AREVA uses a dry conversion process. The dry process changes UF_6 into a ceramic grade uranium dioxide powder in a single stage by mixing it with steam and hydrogen in a kiln. An original KENO model of the kiln was obtained. Using this as a base model, MCNP models were developed. The results indicate that the current kiln would be limited to approximately 8-wt% ^{235}U without modifications.

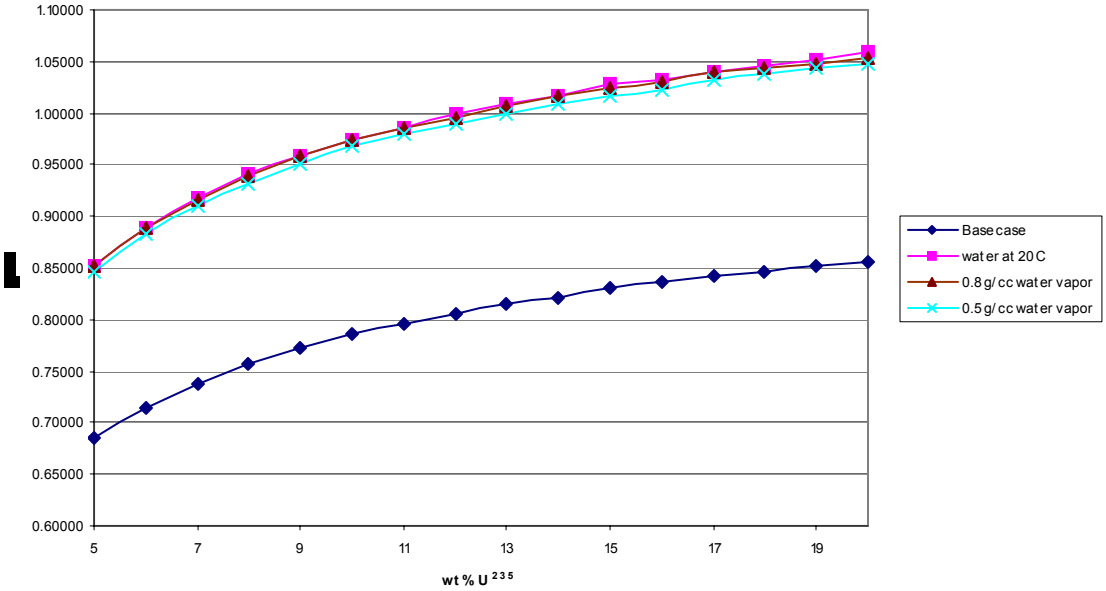

Figure 5-10: Results of MCNP Models of Dry Conversion Kiln

After the UF_6 is converted to UO_2 in the kiln, the UO_2 flows through a calciner where it is heated and excess water is removed. Using an original KENO model for the calciner from a representative vendor, an MCNP model was developed using 5-wt% ^{235}U fuel and an accident situation using water moderator. No further models were developed as this case showed that the current calciner was at the 0.95 k_{eff} limit under accident conditions. Thus for the dry conversion process it appears that for current processes, the calciner is limiting and thus enrichment above 5-wt% is expected to require capital investment.

Once the UO_2 is converted to powder it is typically stored in 45-gallon containers until it is used to form pellets. These drums are modeled as a cylinder with an inner radius of 28.575 cm, a height of 66.038 cm and with 0.1651 cm thick stainless steel walls,

bottom, and lid. The powder in the barrels was assumed to be composed of 4.0 g/cm^3 UO_2 and 0.2105 g/cm^3 water.

Models were developed of a single barrel completely filled with powder and reflected on all sides by water at 20 °C. The 45-gallon drum is modeled as a cylinder with an inner radius of 28.575 cm, a height of 66.038 cm and with 0.1651 cm thick stainless steel walls, bottom, and lid. The powder in the barrels is assumed to be composed of 4.0 g/cm^3 UO_2 and 0.2105 g/cm^3 water.

An additional model has been developed of an infinite array of these barrels containing two rings of 8 poison rods with one poison rod in the center (see Figure 5-11). Various moderator ratios consisting of air, water, or water vapor of varying densities were modeled in order to define the optimum moderation.

The results of the infinite array of UO_2 filled 45-gallon containers are shown in Figure 5-12. The most limiting moderator was the 0.3 g/cm^3 vapor case. These cases show that the current 45-gallon container would be limited to enriched UO_2 of 11-wt% or less of ^{235}U, which is sufficient for the uranium enrichment being proposed for most gas-cooled and other advanced concept reactor and cermet fuels.

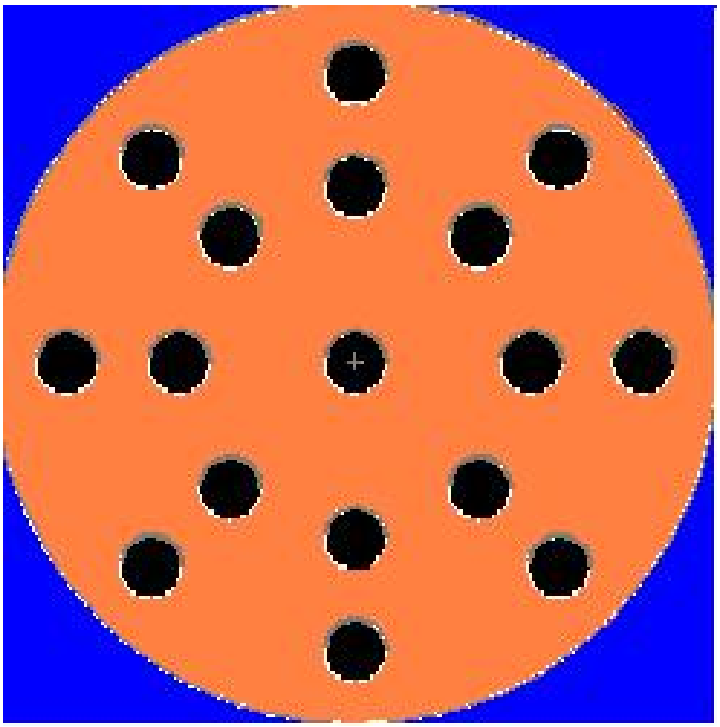

Figure 5-11: Top view of Infinite Array of UO_2 Filled 45-gallon Containers

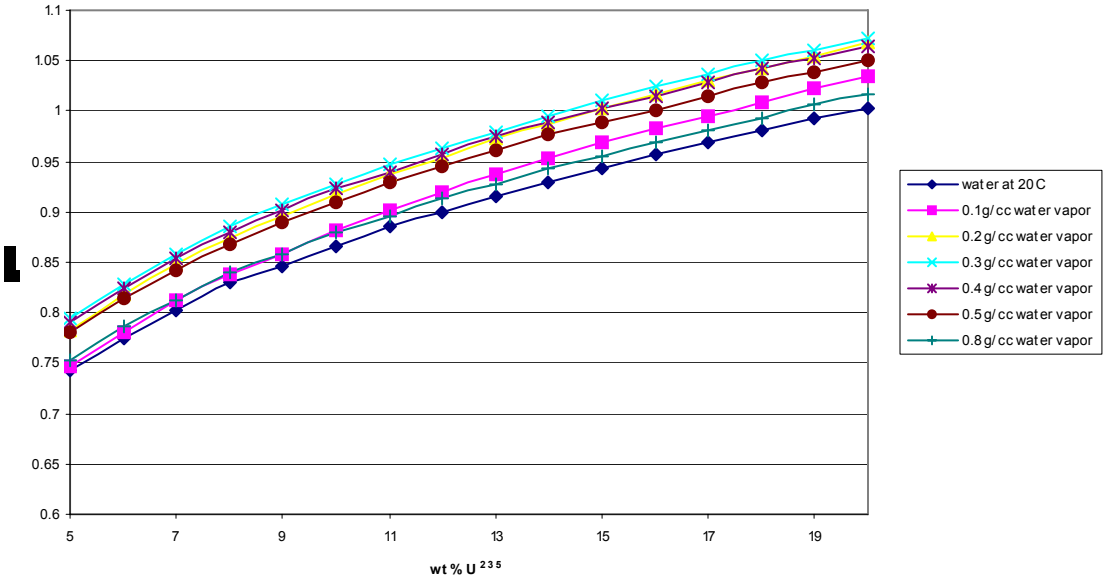

Figure 5-12: Results of MCNP Calculations of Infinite Array of UO_2 Filled 45-gallon Containers

Once the UO_2 powder is formed into pellets, they are placed into molybdenum boats and go through a sintering furnace. Afterwards the boats are typically placed on stainless steel shelves. An original KENO model of the molybdenum boats used by a representative vendor was obtained. Using this as a base model, MCNP models were developed.

The first models developed were single boats filled with UO_2 pellets and water at 20 °C. Two sets of criticality models were developed to bound the potential U/H ratio. One set assumed 9.3% water and 90.7% UO_2 by volume, the maximum amount of UO_2 that would be able to be put into a boat assuming cylindrical pellets. The 2nd set of models assumed a 2 to 1 ratio of water to UO_2. Results show that the 2nd set of models was more limiting for the single boat case.

Next, a model was developed using a 2 to 1 ratio of water to UO_2 of an infinite array of boats stacked one high on a ¼ inch stainless steel shelf, with 1 foot of water or water vapor moderator on all sides, with reflective boundaries. The results show that the boats would be limited to approximately 12-wt% ^{235}U.

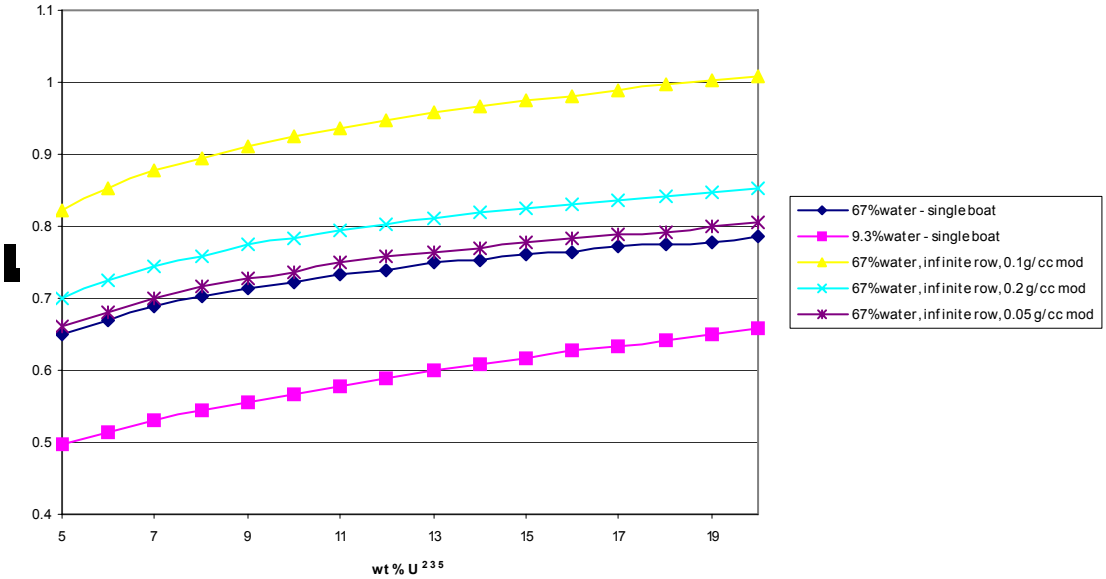

Figure 5-13: Results of MCNP Calculations of Molybdenum Pellet Boats

5.1.3 Fuel Assembly Shipping

After the UO_2 powder is formed into pellets, these pellets are loaded into rods and formed into assemblies. The assemblies are then shipped from a vendor to the nuclear plants in shipping casks.

Using the licensed specifications of one vendor cask infinite arrays of shipping casks were modeled. These casks were modeled as a cylinder with an inner radius of 50.574 cm, a height of 507.367 cm and with 0.3175 cm thick stainless steel walls, bottom, and lid. Two assemblies were placed in the center of the barrel on a steel plate, with two borated steel plates separating them. The distance between the two borated steel plates is 5.87 cm. The casks were reflected on four sides with 60.96 cm of water above and below the casks. This model is shown in Figure 5-14.

Calculations for a single assembly showed that the 15x15 assembly is slightly more reactive then the 17x17 assembly, so all cask models used the 15x15 assembly. Various moderator ratios consisting of air, water, or water vapor of varying densities were modeled in order to define the optimum moderation.

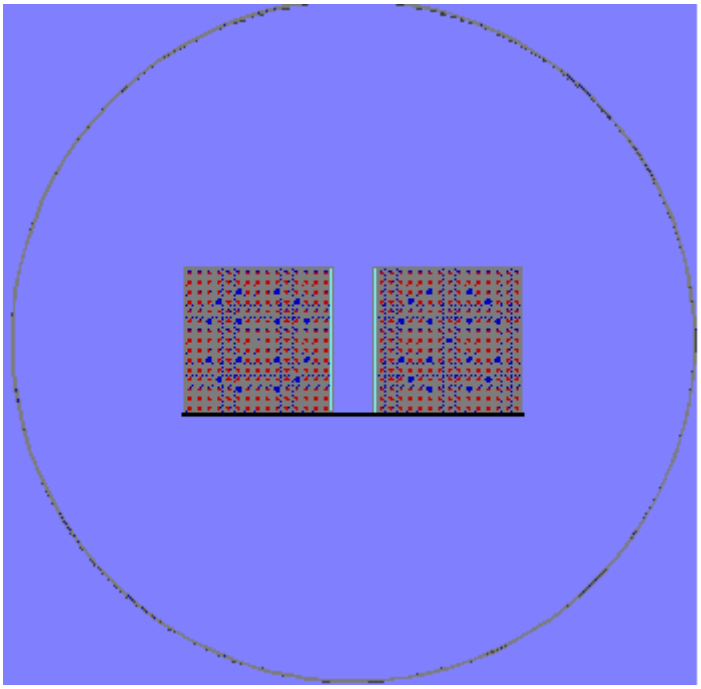

Figure 5-14: Top View of a 15x15 Assembly Shipping Container

The results of the infinite array of shipping containers are shown in Figure 5-15. The most limiting moderator was the water at 20 ºC case. These cases show that the selected cask would be limited to enriched UO_2 of 6-wt% or less of ^{235}U.

Additional models were developed with incorporating stainless steel rods or burnable poison rod assemblies (BPRAs) in the guide tubes. The results of these runs, shown in Figure 5-16, indicate that the addition of steel rods would allow shipping of fuel enriched up to 8-wt% ^{235}U and BPRAs would increase that limit up to 15-wt% ^{235}U.

Models were developed for an array of single 15x15 assemblies in water at 20 ºC. Single assembly calculations show that assemblies must have some sort of moderation control above 5-wt% ^{235}U. This would require either the addition of steel rods, BPRAs, or some other absorber when the assembly is constructed, during transportation, and placement into the spent fuel pool.

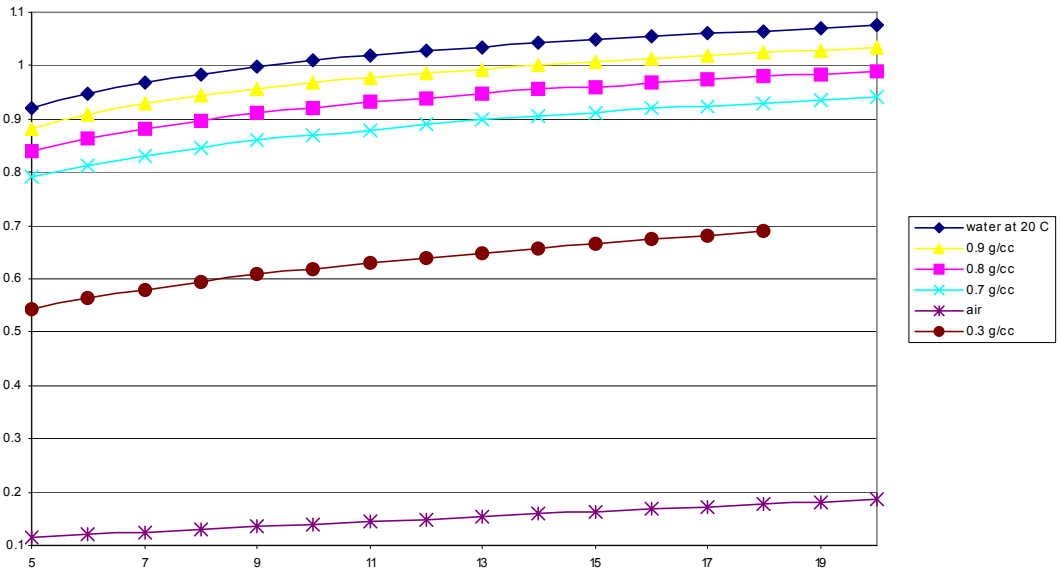

Figure 5-15: Results of MCNP Calculations for Infinite Array of 15x15 Assembly Shipping Containers

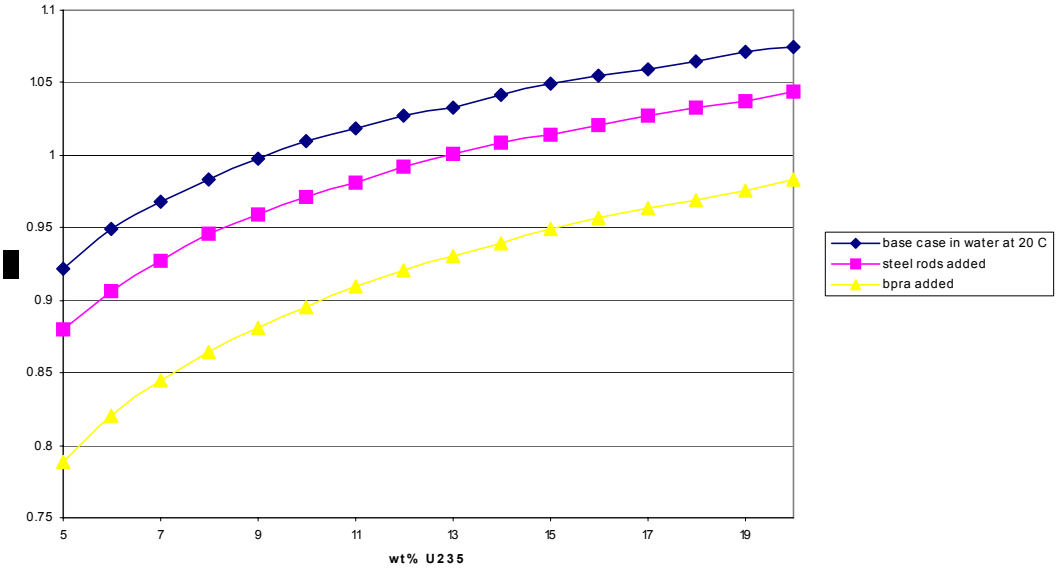

Figure 5-16: Results of MCNP Calculations for Infinite Array of 15x15 Assembly Shipping Containers in Water at 20 ºC

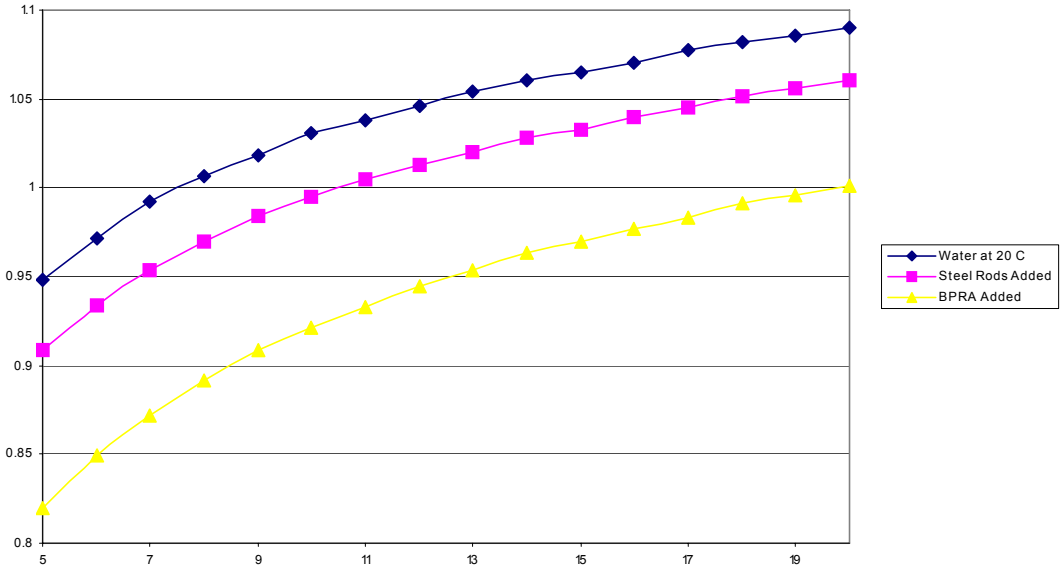

Figure 5-17: Results of MCNP Calculations for an Array of Single 15x15 Assemblies in Water at 20 ºC

5.1.4 Spent Fuel Pool

Nuclear power plants must have the ability to offload an entire core into the spent fuel pool. A typical limiting configuration for fresh fuel bundles was modeled as shown in Figure 5-18. The fresh fuel locations, shown in grey, are modeled as the 15x15 assemblies. Each assembly location is surrounded by 0.2921 cm of water, in a 0.1905 cm thick steel sheath. Each sheath is separated by 3.429 cm of water. The entire spent fuel pool rack was surrounded by 60.96 cm of water.

Two criteria are typically used in a criticality safety analysis for the spent fuel pool. The first is that the k_{eff} must be less then 1.0 with no soluble boron. The second is that k_{eff} must be less then 0.95 with soluble boron. The spent fuel pool was modeled with and without 500 ppm boron and also with and without the addition of BPRAs in the fresh fuel assemblies.

The results of the spent fuel pool calculations are shown in Figure 5-19. For the first criterion, the spent fuel pool would be limited to 8-wt% ^{235}U, or less, without the use of BPRAs. The second criterion limits the pool to 9.5-wt% ^{235}U, or less. The addition of BPRAs would increase the limits of both criteria to 20-wt% ^{235}U.

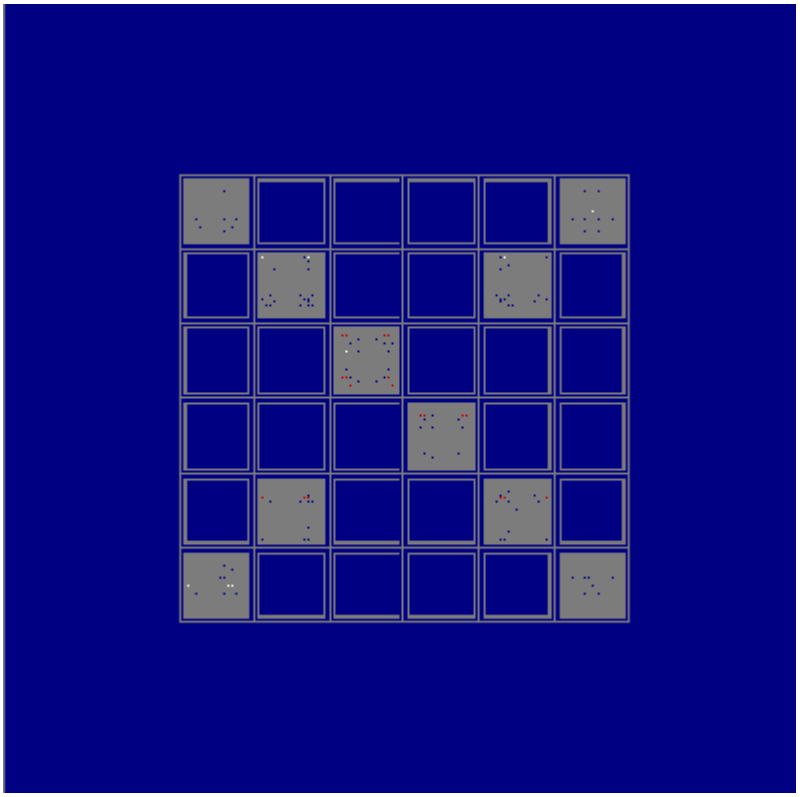

Figure 5-18: Top View of MCNP Model of a Spent Fuel Pool

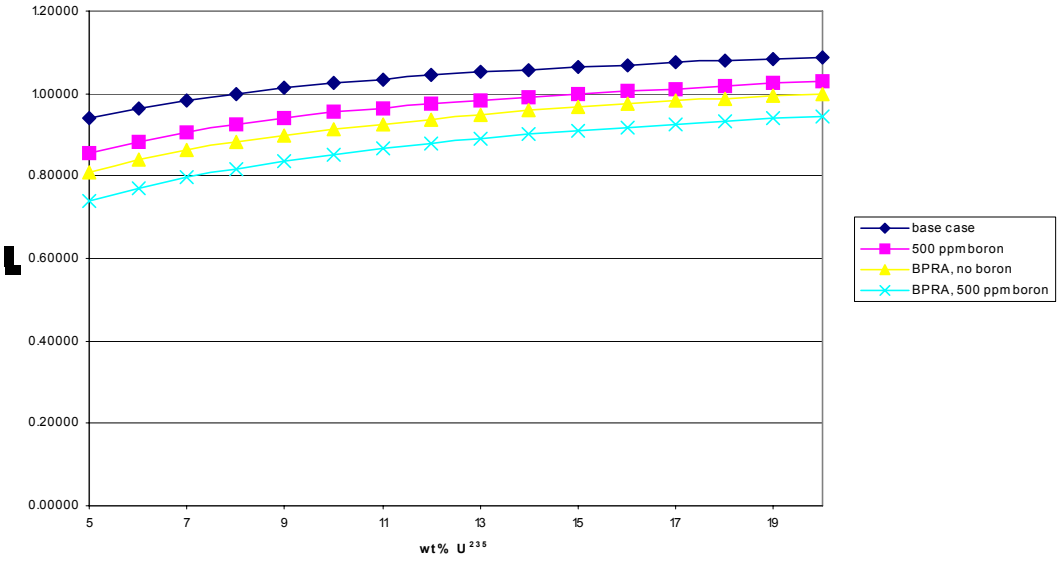

Figure 5-19: Results of MCNP Calculations for a Spent Fuel Pool

5.2 Economic Analysis

The evaluation discussed above indicates that increasing enrichments to 10.0-wt% ^{235}U is a viable option for most of today's equipment. The economic model indicates that there is little incentive for plants using an 18-month cycle to increase enrichments. For the base case models, the 24-month cycle is the most competitive. Up to 6.5-wt% is an attractive option economically for the 24-month cycle with interest rates up to 9.5%.

It is suggested that a minimum of two reactors on a 24-month cycle participate in any program to increase enrichments in order for there to be an economic incentive to do so. A single reactor developing a 30-month cycle could see significant savings in such a program.

Longer fuel cycles could only be achieved with enrichments greater than the currently licensed 5.0-wt% limit. These longer cycles would still have fuel cycle cost minimums in the range of 8.0 to 9.0-wt%, and, therefore, it is concluded that licensing and equipment modification beyond this point would be unnecessary for current PWRs in the United States. The question of inert matrix fuels (IMF) and their need for higher enrichments has not been addressed because these fuels would most likely require a new processing and fabrication line to begin with.

An increase in ore cost lowers the enrichment at which the fuel cycle has its minimum fuel cycle cost. Even with a 100% increase in ore cost there are still significant savings in going from the 5.0-wt% to higher enrichments for the 24 and 30-month cycles. Increasing conversion costs will also lower the enrichments for the fuel cycle cost minimums but because conversion is typically only one to three percent of the total fuel cycles costs, its effect on the enrichment minimums and cost savings is relatively minor.

On the other hand, changes to the SWU costs have a much greater impact on fuel cycle enrichment minimums and potential cost savings. A 100% increase in SWU price would all but eliminate the incentive for going to higher enrichments. Although the 24-month cycle would still see some savings, the 18-month cycle becomes the cheapest fuel cycle and has minimums at 5-wt% or less. With a 50% decrease in SWU costs, not only is there incentive to increase enrichments, but the longer fuel cycles become competitive.

Increases in fabrication cost also raise the cost savings from increased enrichment. If the fabrication charges are increased by 100%, the 24-month cycle with the 15-day outage remains the most competitive but the 30-day outage has a minimum fuel cycle cost, using the 30-month cycle at an enrichment of 8.0-wt%. There is only a 9% difference between the cost savings of a 24-month cycle going from 5.0-wt% to 6.5-wt% and the same plant going to the longer 30-month cycle with 8.0-wt% fuel.

Increases of dry cask storage costs have a similar effect but to a lesser degree. When the cost of dry cask storage is increased by 100% the 24-month cycle is the most cost effective for both cycle lengths, but the 30-month cycle is a very close second at 8.0-wt% fuel for the 30-day outage case. Recent court decisions requiring the Department

of Energy to reimburse Exelon for all fuel cask storage costs incurred may make cask storage costs no longer relevant.

Reload licensing variations have little effect on cost savings for higher enrichments fuel cycles. When the reload licensing costs are increased by 100% little effect is seen on the shape of the fuel cycle cost curves. What is changed is the vertical position of the cycle-lengths. As reload licensing costs are increased, the longer cycles become more competitive.

Variations of replacement power costs have a similar effect. An increase in replacement power cost also increases the potential cost savings of going to longer cycle lengths.

Variations in the disposal fee have no effect on cost savings of increasing enrichments or cycle lengths. Modification to the way this fee is assessed, in order to encourage the use of fewer assemblies, could potentially encourage the use of higher enrichments by increasing the cost savings by millions per year.

Fuel purchase interest rates are the dominate factor in determining the cost savings or loss in using higher then 5.0-wt% fuel. At fuel purchase interest rates of 6 to 7%, the economic model shows a potential savings of over 2 million dollars per year for reactors using a 24-month cycle and a cost savings of 5 to 6 million dollars per year if reactors were to develop a 30-month cycle. Increases in interest rates could result in very large cost penalties if reactors were to go to higher enrichments. As long as the participating reactors did not contract to use the higher enrichments but only to pay for the licensing and equipment upgrades for the ability to go to higher enrichments they could minimize any potential losses.

If a program is developed with 10 participating reactors, even if interest rates on purchase of fuel were raised to 20%, reactors on a 24-month cycle could go back to using 5-wt% fuel and only experience an investment loss of approximately $100,000 each year for a maximum of 5 years. Any time after that 5 year period, if the interest rates dropped and the utility purchased 6.5-wt% fuel at 7% interest then each plant could potentially save 1.4 to 1.7 million dollars a year, depending on the outage length. Fuel purchases at an interest rate of 9% would recoup the 5-year loss in less then a year.

While rising interest rates may deter participating plants from using higher enrichments, there is a potential savings of millions of dollars per year. The Federal funds interest rate, at the time of this study, was at 1%, but has been as high as 11.64% in the last 20 years and 19.10% (June, 1981) in the last 30 years.

The model indicates that achieving savings from increased enrichments in the first five years requires the interest rate on purchases of fuel be in the range of 9.5% or less. Although interest rates are volatile, the potential gain appears to out-weigh any loss that

could be seen by increased enrichments beyond the current licensing limit of 5-wt% ^{235}U.

6. Conclusions

The objective of the NERI project is to design, perform, and analyze critical benchmark experiments for validating reactor physics methods and models for fuel enrichments greater than 5-wt% ^{235}U. To demonstrate the ability of computer codes to handle the geometry and spectrum of the experiments, various codes are used to calculate k_{eff} of the materials and critical boron concentration for the proposed experiments.

Comparison of the isotopic compositions demonstrates good agreement. For the most part, the significance of the variations was observed to be minimal by comparing the k_{inf} values calculated for the assemblies.

Comparison of the calculated critical boron concentrations indicates reasonable agreement between the NEMO, KENO and MCNP calculations, but the SIMULATE calculations for the smaller pitch case resulted in significantly lower predicted boron concentrations.

Due to the nature of the nodal methodology, it was expected that the nodal codes, NEMO and SIMULATE, might exhibit difficulties with the small core configurations. NEMO uses reflector data generated by APOLLO2-F. The reflector methodology used in APOLLO2-F is more rigorous than that used in CASMO3. This may explain why NEMO appears to produce results more in-line with KENO and MCNP than those produced by SIMULATE.

The S/U analysis of the proposed experiment designs found that the experiments would serve as excellent benchmarks for the low temperature configurations of the design systems studied. However, they would provide little data for the validation of codes at reactor operating conditions. The experiments will provide reasonable benchmarks for commercial assembly configurations containing soluble boron and for ^{235}U capture. With the limitations placed on this experiment design, such as fuel enrichment and dimensions, amount of fuel pellets, finite size open core tank and symmetric arrays, the series is likely as close to commercial assemblies as can be achieved.

The fuel cycle evaluation discussed in Section 5 indicates that increasing enrichments to 10.0-wt% ^{235}U is a viable option for most of today's equipment. The economic model indicates that there is little incentive for plants using an 18-month cycle to increase enrichments. For the base case models, the 24-month cycle is the most competitive. Up to 6.5-wt% is an attractive option economically for the 24-month cycle with interest rates up to 9.5%.

7. References

1. AREVA Document, 38-5061643-00, *NERI Critical Assembly 01-124 Final Assembly Drawings*, 3/15/2005.
2. *International Handbook of Evaluated Criticality Safety Benchmark Experiments*.
3. Rearden, B. T. *, Anderson, W. J., and Harms, G. A., "*Use of Sensitivity and Uncertainty Analysis in the Design of Reactor Physics and Criticality Benchmark Experiments for Advanced Nuclear Fuel.*" **Nuclear Technology**. Vol. 151, Number 2, August 2005 (pp. 133-151).
4. Elam, K. R. and Rearden, B. T., "*Use of Sensitivity and Uncertainty Analysis to Select Benchmark Experiments for the Validation of Computer Codes and Data*." **Nucl. Sci. Eng.**, Vol. 145, 2003, (pp. 196-212).
5. Tayloe, Jr., R. W., "Nuclear Criticality Safety Analysis for Increased Limit in 10-ton (48x) Cylinders," May 1991, POEF-T-3563.
6. Tayloe, Jr., R. W., "Nuclear Criticality Safety Study for Increased Enrichment Limit in 2 1/2-Ton (30B) UF6 Cylinders," October 1992, POEF-T-3597.

8. Additional Information

8.1 Fuel Materials

Table 8-1: ORNL Sample Results from Impurities Assessment

A	Element	S1	S2	S3	S4	S5	S6	S7	S8	S9	S10
5	**B (ng/g)**	2.24E+01	6.66E+02	1.56E+03	8.47E+01	4.88E+01	3.17E+02	4.56E+02	3.50E+02	1.76E+02	9.42E+01
23	**V (ng/g)**	1.51E+02	1.28E+02	1.18E+02	1.04E+02	9.94E+01	1.56E+02	9.71E+01	1.03E+02	1.51E+02	1.09E+02
24	**Cr (ng/g)**	4.03E+04	2.37E+04	1.94E+04	1.54E+04	1.31E+04	1.53E+04	1.32E+04	1.49E+04	4.03E+04	1.52E+04
25	**Mn (ng/g)**	4.10E+03	2.58E+03	2.23E+03	1.77E+03	1.77E+03	2.95E+03	1.50E+03	1.67E+03	4.51E+03	2.10E+03
26	**Fe (ng/g)**	1.79E+05	1.02E+05	8.30E+04	6.29E+04	8.34E+04	7.20E+04	5.27E+04	6.58E+04	1.62E+05	6.85E+04
27	**Co (ng/g)**	2.37E+02	2.58E+02	3.13E+02	1.82E+02	1.27E+02	2.11E+02	1.28E+02	1.84E+02	2.24E+02	1.96E+02
28	**Ni (ng/g)**	4.59E+04	3.23E+04	3.01E+04	2.64E+04	2.31E+04	5.73E+04	2.34E+04	2.70E+04	4.09E+04	2.60E+04
29	**Cu (ng/g)**	3.01E+03	2.54E+03	3.93E+03	2.13E+03	4.34E+02	1.11E+03	2.26E+02	4.95E+03	1.28E+03	2.93E+02
42	**Mo (ng/g)**	4.35E+03	8.17E+02	8.34E+02	6.52E+02	6.41E+02	9.40E+02	5.19E+03	1.04E+03	4.16E+03	6.34E+02
47	**Ag (ng/g)**	6.63E+01	6.36E+01	5.04E+01	6.67E+02	3.87E+02	7.52E+01	2.39E+01	2.24E+01	5.76E+01	5.99E+01
48	**Cd (ng/g)**	7.53E+01	9.36E+02	2.27E+01	2.26E+01	2.26E+01	3.85E+01	5.42E+01	2.24E+01	2.21E+01	2.30E+01
62	**Sm (ng/g)**	2.24E+01	2.27E+01	5.31E+01	2.26E+01	2.26E+01	2.26E+01	2.26E+01	2.24E+01	2.21E+01	2.25E+01
63	**Eu (ng/g)**	2.24E+01	2.27E+01	2.27E+01	2.26E+01	2.26E+01	2.26E+01	2.26E+01	2.24E+01	2.21E+01	2.25E+01
64	**Gd (ng/g)**	2.24E+01	2.27E+01	2.27E+01	2.26E+01	2.26E+01	2.26E+01	2.26E+01	2.24E+01	2.21E+01	2.25E+01
66	**Dy (ng/g)**	2.24E+01	2.27E+01	2.27E+01	2.26E+01	2.26E+01	2.26E+01	2.26E+01	2.24E+01	2.21E+01	2.25E+01
74	**W (ng/g)**	1.23E+02	1.23E+02	1.12E+02	9.96E+01	1.00E+02	1.10E+02	8.53E+01	1.00E+02	1.10E+02	1.07E+02
SAMPLE WT		2.23E+00	2.20E+00	2.20E+00	2.21E+00	2.21E+00	2.21E+00	2.22E+00	2.23E+00	2.26E+00	2.22E+00

8.2 Non-fuel Materials

Table 8-2: Al 6061 Material Definition

(based on a Kaiser Aluminum Certified Test Report)

Element	A (g/mole)	wt%			Density	
		max.	min.	actual	g/cm^3	atm/b*cm
Al	26.98	Balance		96.06%	2.5955	5.7930E-02
Si	28.09	0.80%	0.40%	0.72%	0.0195	4.1713E-04
Fe	55.85	0.70%	N/A	0.62%	0.0168	1.8064E-04
Cu	63.55	0.40%	0.15%	0.31%	0.0084	7.9378E-05
Mn	54.94	0.15%	N/A	0.90%	0.0243	2.6656E-04
Mg	24.31	1.20%	0.80%	1.04%	0.0281	6.9625E-04
Cr	52.00	0.35%	0.04%	0.20%	0.0054	6.2587E-05
Zn	65.38	0.25%	N/A	0.12%	0.0032	2.9865E-05
Ti	47.90	0.15%	N/A	0.02%	0.0005	6.7939E-06
V	50.94	N/A	N/A	0.01%	0.0003	3.1941E-06
Other	*N/A*	*0.15%*	*0.05%*	*0.00%*[1]	*N/A*	*N/A*

ρ =2.702 g/cm^3

[1] Because "Other" could not be modeled it was ignored and was replaced with Aluminum.

Table 8-3: Al 3003 Material Definition

(based on ASTM B209-04)

Element	A (g/mole)	wt%			Density	
		max.	min.	actual	g/cm^3	atm/b*cm
Al	26.98	Balance		97.92%	2.6459	5.9054E-02
Si	28.09	0.60%	N/A	0.30%	0.0081	1.7381E-04
Fe	55.85	0.70%	N/A	0.35%	0.0095	1.0198E-04
Cu	63.55	0.20%	0.05%	0.13%	0.0034	3.2007E-05
Mn	54.94	1.50%	1.00%	1.25%	0.0338	3.7022E-04
Zn	65.38	0.10%	N/A	0.05%	0.0014	1.2444E-05
Other	*N/A*	*0.15%*	*N/A*	*0.00%*[1]	*N/A*	*N/A*

ρ =2.702 g/cm^3

[1] Because "Other" could not be modeled it was ignored and was replaced with Aluminum.

Table 8-4: SS 304 Material Definition

(based on the AK Steel Type 304 Specification)

Element	A (g/mole)	wt%			Density	
		max.	min.	actual	g/cm^3	atm/b*cm
Fe	55.85	Balance		69.23%[1]	5.5588	5.9940E-02
Cr	52.00	20.00%	18.00%	19.00%	1.5257	1.7670E-02
Ni	58.70	12.00%	8.00%	10.00%	0.8030	8.2379E-03
Mn	54.94	2.00%	N/A	1.00%	0.0803	8.8020E-04
Si	28.09	0.75%	N/A	0.38%	0.0301	6.4566E-04
C	12.01	0.80%	N/A	0.40%	0.0321	1.6104E-03
P	30.97	0.05%	N/A	0.02%	0.0018	3.5127E-05
S	32.06	0.03%	N/A	0.02%	0.0012	2.2625E-05
N	14.01	0.10%	N/A	0.05%	0.0040	1.7262E-04

ρ =8.03 g/cm^3

[1] The percentage of Fe used in these calculations is too great. It should be 69.14%. However, this results in an iron density increase of only 0.007 g/cm^3, which is insignificant and well within the uncertainty in these calculations.

Table 8-5: SS 304 - Springs Material Definition

(modified from AK Steel Type 304 Specification)

Element	A (g/mole)	wt%			Density	
		max.	min.	actual	g/cm^3	atm/b*cm
Fe	55.85	Balance		69.23%[1]	1.1746	1.2665E-02
Cr	52.00	20.00%	18.00%	19.00%	0.3224	3.7337E-03
Ni	58.70	12.00%	8.00%	10.00%	0.1697	1.7407E-03
Mn	54.94	2.00%	N/A	1.00%	0.0170	1.8599E-04
Si	28.09	0.75%	N/A	0.38%	0.0064	1.3643E-04
C	12.01	0.80%	N/A	0.40%	0.0068	3.4028E-04
P	30.97	0.05%	N/A	0.02%	0.0004	7.4224E-06
S	32.06	0.03%	N/A	0.02%	0.0003	4.7806E-06
N	14.01	0.10%	N/A	0.05%	0.0008	3.6475E-05

ρ =1.70 g/cm^3 (*assumes a 21.13% volume fraction for the springs in the total volume*)

[1] The percentage of Fe used in these calculations is too great. It should be 69.14%. However, this results in an iron density increase of only 0.0015 g/cm^3, which is insignificant and well within the uncertainty in these calculations.

Table 8-6: Polyethylene Material Definition

(provided by SNL)

Element	A (g/mole)	wt%			Density	
		max.	min.	actual	g/cm^3	atm/b*cm
C	12.01	N/A	N/A	85.63%	0.7964	3.9927E-02
H	1.01	N/A	N/A	14.37%	0.1337	7.9854E-02

ρ =0.93 g/cm^3